On the Interaction of Charging-Aware Mobility and Wireless Communications

by

Wanxin Gao

A thesis submitted in partial fulfillment of the requirements for the degree of

Doctor of Philosophy

Department of Computing Science

University of Alberta

Abstract

Today's mobile battery-powered communication devices require that users access chargers via wired and, recently, wireless recharging facilities. For a device departing from a location with a given energy "budget", a plausible strategy is to seek a charger location once the energy is exhausted. We present a set of charging-aware mobility models that capture the paths followed by the nodes with depleted energy seeking, possibly via a detour, to reach a charger.

Firstly, for a 1-dimensional space, we derive the location-dependent mobile node density distribution, using it to express the location-dependent congestion of a wireless network whose capacity is used by the mobile nodes. The boundaries, and the relative placement of the charger, create intriguing discontinuities in the probability density function of the nodes across space. We find that chargers are not always "hotspots" in terms of node density, and that the energy budget of the nodes determines the hotspot.

For a 2-dimensional space, the analysis shows asymmetrically spiked node density in the locality of the charger, which, counterintuitively, is encircled by relative dips in node density. We extend the probability density function derived for one-charger deployment to approximate that under multiple chargers, observing high accuracy for sparse deployment. We also study the performance of charging-aware mobiles that conduct ad hoc communication in a grid. The results show that the recharging behavior can improve energy supply and communication opportunities. The simulation further demonstrates the advantages and implications of deploying multiple distributed chargers.

Preface

This thesis comes from the original work by Wanxin Gao, under the supervision of Dr. Janelle Harms and Dr. Ioanis Nikolaidis. The contents of Chapter 3 have been published in [27], while the work of Chapters 4 and 5 is expected to be submitted (after revision) for publication in the future.

To my parents, my supervisors, and anyone else who has been believing in me.

A well-designed mathematical model, on the other hand, generalizes the particulars revealed by physical experiments, computer-based models, and interdisciplinary comparisons.

– John H. Holland, 1995.

Acknowledgements

Firstly, I would like to express heartfelt thanks to my supervisors, Dr. Janelle Harms and Dr. Ioanis (Yannis) Nikolaidis, for the tremendous help and support during my PhD study. A PhD journey is tough, but mine has been tougher for certain reasons. There were countless times I was on the verge of quiting my PhD program. It is Janelle, who, instead of giving up on me, kept supporting and guiding me till after my research came back onto the right track. Also, it is a great pleasure to work with Yannis, who has provided many invaluable insights into the resolution of my research problems. The finish of this thesis would be impossible without them. As model scientists, Janelle and Yannis have expanded my awareness of how much knowledge one can have and how rigorous one can be in doing scientific research.

Secondly, I would like to thank all the examining committee members, Dr. Ehab Elmallah, Burak Kantarci, Chinthananda Tellambura, and Abram Hindle. I greatly appreciate the effort they have put into my thesis examination. Their reviews and comments brought notable improvements to my thesis and a deeper understanding of the subject.

Last but not least, I want to say I owe my parents a debt of gratitude that is too much to be paid off for life. They have genuine and firm belief in any decision of mine, constantly and unconditionally. I hope to make it up to them in the future for my absence from home in the past years especially during the festivities when I should have been around them.

Contents

List of Tables

List of Figures

Chapter 1

Introduction

1.1 Overview

The continuous development of new types of mobile wireless networks, e.g. IoT (Internet of Things), 5G networks, delay-tolerant networks etc, together with the proliferation of bandwidth-hungry, CPU-hungry applications, e.g. online gaming, live broadcasting, augmented reality etc, puts great pressure on energy provisioning for modern mobile computing systems. On the one hand, the development of portable high-capacity batteries is not happening fast enough to cope with energy-hungry devices and applications. On the other hand, despite the increased popularity of wireless charging technologies, because of their limitations in efficiency and workable ranges, the charging behavior of mobile users has hardly changed. The users may need to "serve" as carriers and forage for energy sources en route to sustain/restore operation of their fast-draining mobile devices. Such charging-aware mobility and its implications for wireless communications are the subject matter of this thesis.

Conceptually, regardless of whether we are interested in plugging laptops into power outlets or wireless charging of smartphones, we can identify two characteristics of the underlying system:

1) an influence exerted on a mobile agent to deviate from its original path in order to recharge, measured against the inability to communicate if no recharging is performed, and,

2) an increase of density of the mobile agents near chargers, resulting in

increase of communication congestion especially if they are, as often assumed, wireless spectrum users.

As we are primarily interested in systems akin to smartphone and wearable devices carried by "human" agents, depletion of energy does not imply inability to move—as opposed to the case of electric vehicles, which is outside the scope of the thesis.

This thesis provides both an analytical and numerical investigation of the interaction between recharging and capacity resulting from (1) and (2). Notably, we have attempted to explore such interaction in our previous work [26], where we devise different possible strategies for the charger-aware mobility and compare the induced network performance (in terms of packet delays and delivery ratios) through simulations. The settings assumed in [26] are close to reality but rather complicated:

- the communication and energy consumption of the mobile devices are subject to medium access and (epidemic) routing protocols,
- the mobiles have varying tendencies to recharge depending on their energy levels and projected delays in arrival at the destinations,
- the mobiles are subject to a maximum number of devices that can be charged simultaneously by each charger,
- the chargers have limited, distance-dependent charging efficiency, and
- the chargers themselves are subject to varying energy reserves for charging the mobiles.

In this thesis, for tractable analysis and clearer examination, we make simplified abstractions about the system, as follows.

We consider two communication models, one where communication is possible at any location (cellular model) and one where the communication depends on the existence of co-located peers (ad hoc peer-to-peer model). For the first cellular model, we assume that a device with some energy can continuously transmit until its energy is depleted, irrespective of MAC/routing

protocols. The continuous transmission behavior represents a, corresponding, continuous data traffic demand of the device to continue communicating for as long as its energy allows it.[1] Hence, the amount of energy consumed can be expressed as distance traveled at constant speed. As long as the energy reserves are non-zero, the device is assumed to be continuously communicating. The only energy cost is assumed to be that of communication; the travel can continue, albeit without communication, once the energy is depleted. For the second ad hoc communication model, we assume a mobile device, which can also keep moving without energy, consumes energy only when forming a pair-wise connection with another peer in its neighborhood. In this case, a mobile may potentially travel long without encounters with others and thus without depletion. Both communication models are subject to congestion due to clustering and limited capacity.

Throughout the thesis, the charging-aware movements of mobiles are modeled based on the Random WayPoint (RWP) model [41], a well-known mobility model characterized by the notion of destinations. In the basic version of RWP, the mobile keeps moving straight between a series of waypoints (or, destinations) randomly generated in the space, yielding a zigzag trajectory over time. To embody recharging behavior, we assume the presence of a single fixed charging station that can attract depleted mobiles, diverting them temporarily from direct paths to the intended waypoints. The charger is able to restore the energy of any mobile at its location to an adequately high level immediately by using ultra-fast charging technologies [34, 58]. Once replenished, no recharge is needed again before arrival at the destination.

Note that the mobiles are assumed to behave like "reactive agents" [17, 40], i.e., triggered awareness of recharging only upon an energy drop to zero, with no precautionary charging or path planning in advance. Also, to reduce randomness and ease analysis, all the mobiles move at a uniform constant speed and never pause at any waypoint or the charger. Despite the risk of

[1]The energy may still drain fast continuously even for sporadic communication, since common wireless network interfaces can often incur high idle power consumption comparably to that in the active state [7, 25].

oversimplification in several aspects, the analytical results, as we will see, can well approximate extensions including random speeds, "proactive" recharging (Section 3.4), and multiple chargers (Section 4.5); besides, the effect of random pauses can be incorporated straightforwardly (Section 2.2).

The remainder of the thesis is organized as follows: First, in Section 1.2, we give a summary of the contributions made in the thesis. Then, in Chapter 2, we review the existing work and discuss their connections and differences to our work. In Chapter 3, we present an analytical mobility model in the presence of a charger in a 1-dimensional space, i.e., a road-like line segment. This is a simple but meaningful scenario, which accounts for movements on a "thoroughfare" path within an urban core. Each mobile follows the cellular model for communications and would recharge after depletion as long as it is possible to reach the charger before the intended waypoint (by detouring towards the opposite direction if needed). In Chapter 4, we extend the 1-dimensional charging-aware mobility of Chapter 3 to the more common 2-dimensional Euclidean spaces. We endow the charger with a range of attraction such that a depleted mobile would detour for recharging only if it passes through the vicinity of the charger and falls within its range. This attraction range can be regarded as an abstraction measuring the charger's interest/popularity plus the mobile's drive to detour for recharging. In Chapter 5, we conduct simulation studies to examine the practicalities of charging-aware mobility interacting with peer-to-peer ad hoc communications in a 2-dimensional Manhattan space (i.e. a grid of square cells imitating city blocks). The recharging behavior follows a discrete-time Manhattan version of the mobility model of Chapter 4; meanwhile, the processes of communication and energy consumption become subject to the availability of peers that have non-zero energy in the locality. Lastly, in Chapter 6, we conclude the thesis and outline worthwhile directions for the future work.

1.2 Thesis Contributions

A summary of the thesis contributions is as follows:

- For the 1-dimensional charging-aware mobility model, we derive *closed-form* probability density functions of the mobile location over a unit line segment, based on the recharging behavior. (See Theorem 3.4.1.1, 3.4.2.1, and Corollary 3.4.2.1.)

- For both the 1-dimensional and 2-dimensional cases, we describe the resulting density function with respect and as it relates to the corresponding RWP density. (See Section 3.4.1 and Theorem 4.4.3.1.)

- We examine the "distortion" compared to RWP behavior caused by the mobiles veering off their original paths to reach the charger, and find it different from "hotspot"-like concentration used in the literature. (See Sections 3.4.3 and 4.5.1.)

- We identify and explain the discontinuous nature of the mobile distributions as being caused by the effect of the boundary. (See Section 3.4.3.)

- We note subtleties, e.g., the interplay of how "energized" a system is (seen as energy present at the mobiles when they start their trips from waypoints) and higher congestion depending on whether the mobile is willing to detour or not from its path to a waypoint. (See Sections 3.5.3 and 5.4.)

- In the 1-dimensional case (cellular model), bounds of the probability that a mobile can (has energy) but cannot (due to congestion) communicate are given. (See Theorem 3.5.1.1 and Corollary 3.5.1.1.)

- In the 2-dimensional case, we identify, and explain a "dip" in the density around the charger, which is an unexpected new finding induced by detours in the 2-dimensional case. (See Section 4.5.2.)

- We use the distribution results for a single charger in 2-dimensional case to extricate the impact of the charger on the density, and subsequently, provide a method to approximate the density for multiple chargers. We also demonstrate some limitations of this technique. (See Section 4.5.3.)

- We compare the analytical 2-dimensional results with simulation results of mobility of nodes on a Manhattan street network with a single charger and notice similarities between them, suggesting the model is a good first step towards modeling a realistic system. (See Section 5.3.)

- Simulations of a Manhattan street network with multiple chargers, showcases the (dis)advantages of deploying multiple distributed chargers with short attraction ranges in comparison to a single charger with a relatively long attraction range. (See Section 5.5.)

Chapter 2

Literature Review

In this chapter we first categorize and review the rich collection of existing mobility models (Section 2.1), from basic to sophisticated ones, and recap the important results from formal analysis of random waypoint models (Section 2.2). Since the subject matter of this thesis falls within the general scope of charging-aware wireless networks, we also review the related work on energy-constrained networks (e.g. wireless sensor networks, mobile networks, etc) aided by *static* or *mobile* chargers (Section 2.3). Note that none of the scenarios considered in the literature fits exactly the one of our interest, i.e. human-carried (energy-hungry) mobile devices moving between random waypoints in the presence of static chargers that can attract and divert low-energy mobiles. Lastly, we briefly review the work on wireless capacity (Section 2.4), showing the different perspectives they have from our capacity-driven study.

2.1 Mobility Modeling

In this section we review the related work on *synthetic* mobility models for MANETs (Mobile Ad hoc NETworks), which can be classified into two types, namely *classic homogeneous i.i.d. models* and *heterogeneous non-i.i.d. models*. Note that there also exists extensive literature on *trace-based* mobility models that rely on empirical trajectories of mobile devices (with certain abstraction) to capture real-life movement patterns [3, 6, 66, 71]. The trace-based models, however, are commonly subject to dependence on specific scenarios, and thus remain challenged for valid generalization. Our goal is to synthesize simple

yet useful mobility models that permit tractable analysis and easy extensions to more sophisticated variants.

Additionally, we have omitted to review the "macroscopic" mobility models, e.g. [4, 8, 76], which concern the aggregate circulation of mobiles across the space and model the mobiles as flows in a product-form queuing network.[1] Our interest is in mobility modeling from the behavioral or "microscopic" level and analysis of the emergent distribution of mobile locations.

2.1.1 Classic Homogeneous I.I.D. Models

Classic mobility models, including *random walk* [23], *Random WayPoint* (RWP) [41], and *random direction* [67], assume i.i.d. parameters (e.g. in terms of the velocity, pause time, destination etc) over time and homogeneous movements across all mobiles in the network.

In the random walk model, the mobile determines at the beginning of each *epoch* (or *trip*) a random speed from $[v_{min}, v_{max}]$ ($v_{min}, v_{max} \in \mathbb{R}_{\geq 0}$) and a direction within $[0, 2\pi)$ (in the case of a 2-dimensional space). Then the mobile keeps moving at such a velocity until a random time interval (or travel distance) is achieved. If any space boundary is met, the path of the mobile would be reflected (like billiards) or wrapped around (if the space is toroidal), depending on the treatment of boundaries [49].

Like random walk, the RWP model is also epoch-based. The difference is that each time the mobile moves straight (at a random speed) towards a random *waypoint* in the space. Once the waypoint is reached, the mobile may *pause* there for a random interval before staring a new epoch. While the random walk model always yields a uniform distribution of the mobile location, it is observed that a mobile following RWP tends to visit the center of the area more often than regions near the boundaries due to the *border effect* [12] (Figure 2.1). On the other hand, the RWP model facilitates long-span trips (like Lévy flights [53]), which is considered an advantage over random walk for being more natural. It is normally far slower for a random walker to traverse

[1] The joint stationary probability distribution of a product-form queuing network can be computed easily as the product of marginal distributions.

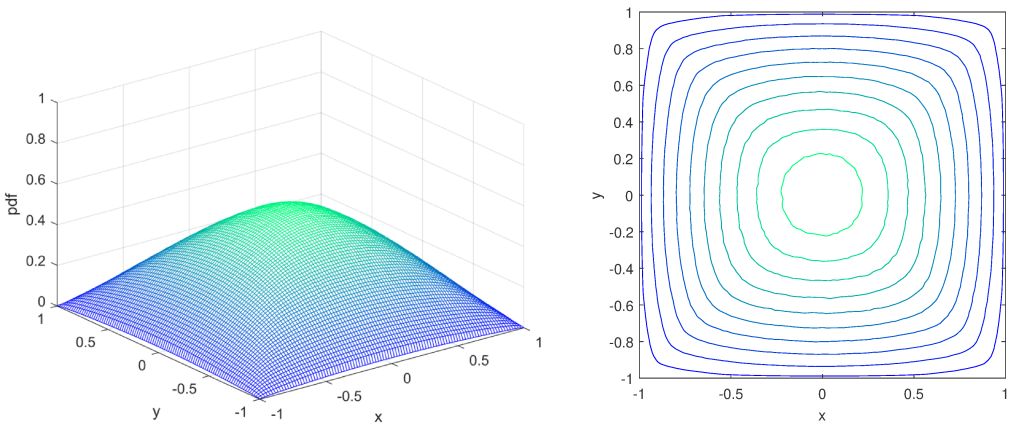

Figure 2.1: Border effect causing non-uniform density distribution for a mobile node following the RWP mobility model: (a) a mesh plot; (b) a contour plot.

distant regions of the space; the mobile can be stuck in a locality for long [16].

To overcome the imperfect uniformity of RWP, the random direction model lets the mobile update its velocity only when any space boundary is reached. A more common variant of random direction allows the mobile to pause and start the next epoch halfway before hitting the boundaries [67].

The above three mobility models are among the most used and studied in the literature owing to their simplicity and (quasi-)uniformity. Meanwhile, their unrealistic features, such as the instant changes of velocities, and the monotonous, homogeneous movement patterns, may invalidate the simulation results of networking protocols. To make up for the inadequacy, many more sophisticated models have emerged, mostly embodying paradigms of the classic ones as bases.

2.1.2 Heterogeneous Non-I.I.D. Models

Mobility models of this class aim to mimic possible complex movement behaviors of mobiles in practice by incorporating interdependence, heterogeneity, and spatial-temporal variation into the classic ones. Such models can be further categorized into three types with respect to the main feature, including *group mobility models* [22, 33, 69], *location-biased models* [35, 36, 38, 56, 62], and *social mobility models* [13, 14, 54, 57]. As we will see, our charging-aware

mobility basically falls into the category of location-biased models, with additional dependence on the energy states of mobiles; it also overlaps with social mobility if peer-to-peer communication is assumed for energy consumption (Chapter 5).

Group Mobility Models

The group mobility models are devised to depict the particular mobility where the mobiles travel in concert with each other to a common destination or pursuing a common target. Among the existing work, the Reference Point Group Mobility (RPGM) model stands as a major framework that generalizes the typical correlated movement patterns in searching or pursuing scenarios [33, 69]. Many other models, like the Column Mobility model and the Nomadic Community Mobility model [69], can be implemented through variation of RPGM.

In the RPGM model, the network would be divided into groups, each endowed with a logical center/anchor to determine general movement of the group. The location of each logical center is updated by imposing a random group motion vector $\overrightarrow{GM}$. Each mobile moves following a designated *reference point*, which is updated based on $\overrightarrow{GM}$. Once the next location of the reference point is computed, a random (bounded) motion vector $\overrightarrow{RM}$ is added as a small perturbation to yield the final location of the associated mobile. Different $\overrightarrow{GM}$'s can be included to create heterogeneous group movements within the same network.

Location-Biased Models

The location-biased models incorporate the likely bias of mobiles towards certain "hotspot" geographic areas to introduce non-uniform distribution in the space. For instance, as a heuristic extension to RWP, the Weighted WayPoint (WWP) model adds more weight to certain popular locations (e.g. classrooms, cafeterias) such that both the occurrence of destinations and pause time intervals therein are increased (Figure 2.2) [35]. Also, the weights of locations are allowed to vary over time for temporal diversity (e.g. lunch time

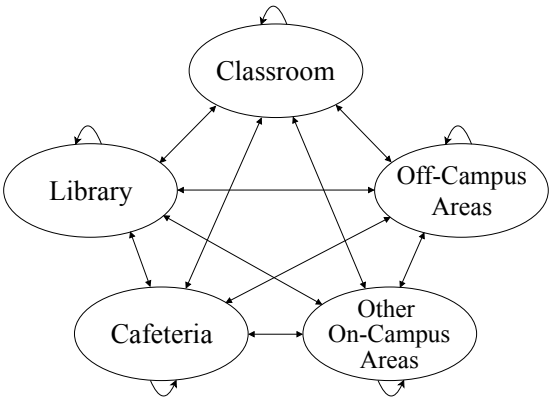

Figure 2.2: A schema of transition between highly weighted locations under the WWP model [35].

vs. non-business hours). The mobiles, however, still move independently and identically to each other, like the basic RWP model.

In [36], a sophisticated analytical variant of WWP, namely the Time-Variant Community (TVC) model, is proposed to extend the basic random direction model to capture the heterogeneity of mobility in both time and space. Motivated by the location preferences of humans as well as their time-varying and periodical behavior, a time-dependent Markov chain is constructed for each mobile, where each state corresponds to a delineated popular region in the space, or rather, a *community*. The mobiles would transfer between the communities and follow random direction mobility within each. A mobile is said to be in a *roaming* epoch when it moves freely in the whole space without limitation to any community; otherwise, it is in a *local* epoch. The incoming/outgoing probabilities of each community can be tuned to obtain the desired stationary mobile distribution. Based on this model, other metrics like the hitting/meeting time and average node degree can also be derived formally.

Another model following a similar idea of [35, 36] but based on random walks is the so-called Heterogeneous Random Walk (HRW) model, which captures the different speed zones in reality (e.g. downtown areas vs. highways) [62]. Specifically, the model assumes a unit square torus with several circular low-speed zones, in which the mobiles following random walks are allowed

speeds of smaller variances only. The stationary distribution of the mobile location is also approximated based on the theory of diffusion processes. Under this model, the mobiles are found to be more likely to cluster in low-speed zones.

A noteworthy location-biased model is the one named SMOOTH [56], which seeks to be simple and meanwhile realistic by capturing as many as seven features that are commonly observed in real-life movements. The seven features include: (1) inter-waypoint distances following Truncated Power Law (TPL) distributions;[2] (2) inter-contact times following TPL; (3) pause times following TPL; (4) non-uniform mobile distribution; (5) mobility with certain regularity; (6) inertia against exploration of new locations; (7) reinforced returning to familiar locations. Specifically, the chance of a mobile i exploring a new location is given by

$$\mathbb{P}_{explore}(i) = aD_i^{-b}$$

where D_i is the number of locations the mobile has visited so far, while a and b are empirical constants. To determine a new location, the mobile would follow a Lévy flight [53]. In the case that the mobile decides against exploration (in probability $1 - \mathbb{P}_{explore}(i)$), it would revisit one of the old locations, l, in probability $\mathbb{P}(l)$, which is in proportion to the number of times the mobile has visited l.

In [38], the classic RWP is generalized to a versatile analytical model, namely Markovian WayPoint (MWP), which targets hotspot modeling. The MWP model draws waypoints in the space following a Markov chain and allows the velocity to vary based on the end waypoints; besides, the mobiles are allowed to pause randomly not only upon arrival at but also halfway between (consecutive) waypoints. The MWP model can have its parameters tuned such that within the hotspot areas the mobiles would have their pause times elongated, would travel at lower speeds, or have more waypoints to visit. The main strength of this paper is the explicit expression (in the form of integrals)

[2] A TPL distribution is constructed by replacing the tail of a power-law distribution with an exponential distribution.

derived for the stationary mobile distribution in the presence of hotspots. Note that the work of [38] assumes that we have a basis for preferring certain locations rather than others. This type of preference is presented as input to their model to specify the hotspots. Instead, our interest is on identifying *how such hotspots emerge* in the presence of chargers. In effect, our analytical model provides a basis for producing more realistic inputs to Markovian, and similar, models (e.g. [36]).

Social Mobility Models

Although the group mobility and location-biased models described above have considerably extended the classic i.i.d. models (e.g. RWP) and can reflect various features in practical mobility, they turn out to be still deficient in capturing the *social interplay* between the movements of mobiles. For instance, supposing that the mobiles are socially attracted to each other, it might be more realistic to assume temporally stronger attraction from the popular locations when they are crowded than when they are not. To this end, the social mobility models like [13, 54, 55, 57] are proposed to embody this dimension.

In [57], the Community-based Mobility Model (CMM) partitions the space into square cells, each associated to multiple mobiles who have their current destinations located within the cell.[3] Each mobile i decides its next destination (upon arrival at the current one) by selecting a random point in the cell $S_{p,q}$ (with coordinates (p, q)) that has the maximum *social attractivity* defined as

$$SA_{p,q} = \frac{1}{w} \sum_{\substack{j=1, \\ j \in C_{S_{p,q}}}}^{n} m_{i,j},$$

where $C_{S_{p,q}}$ is the set of mobiles associated with (or destined for) cell $S_{p,q}$, $w = \left|C_{S_{p,q}}\right|$, and $m_{i,j} \in [0, 1]$ is a measure of the interaction between mobile i and j. This notion of social attractivity has enriched the concept of location popularity by relating to the temporal social relations among mobiles. Simulation results show that the CMM model can better approximate the real

[3]Unlike the TVC model, the term "community" in social mobility models refers to temporal social clusters formed by mobiles rather than fixed popular regions.

traces (e.g. [18]) than RWP in terms of the cumulative distributions of contact duration and inter-contact time.

Like [57], the SWIM (Small World In Motion) model from [54] considers the preference of humans towards nearer destinations as well as location popularity as in the likelihood of meeting others. Specifically, the whole space is partitioned into multiple square cells. For each mobile i, each cell C is assigned a weight $w_i(C)$ that corresponds to the probability that the mobile has a destination therein. Also, a special location h_i is randomly chosen for the mobile as its *home*. For mobile i, its cell weight is updated as

$$w_i(C) = \alpha \cdot distance(h_i, C) + (1 - \alpha) \cdot seen(C),$$

where $distance(h_i, C)$ is the distance from the home location h_i to the center of cell C, $seen(C)$ is the number of peers encountered by mobile i last time in C, and α is a coefficient balancing the two factors. The distribution of inter-contact time proves to follow TPL under this model.

The aforementioned model CMM, despite taking into account the social relations, suffers from the so-called *gregarious behavior* of mobiles; that is, the simulation may be stuck in a state where the mobiles all congregate in a single cell. To overcome this defect, the Home Cell Mobility Model (HCMM) in [13] strengthens the spatial attraction of CMM by defining for each mobile a *home cell* (similar to the home concept of SWIM). A mobile that is currently within its home cell simply follows the rules of CMM, except the social attractivity is now computed as $SA_{p,q} = \frac{1}{w} \sum_{j=1, j \in C'_{S_{p,q}}}^{n} m_{i,j}$, where $C'_{S_{p,q}}$ is the set of mobiles that share the same home cell $S_{p,q}$. If the mobile is not in its home cell, then it randomly chooses a destination within the current cell in probability p_e and returns to its home cell with $1 - p_e$.

2.2 Mobility Analysis

Despite the variety of synthetic mobility models, there has been far less derivation of analytical results (e.g. stationary mobile distribution) than their numerical studies, especially for RWP-based mobility. In this section we summarize a series of seminal results about the stationary mobile distribution of

RWP [10, 11, 38, 39, 47, 49]. At first we give a primer of *Palm calculus*, a statistical tool set that proves to be very useful for mobility analysis in the literature and our work.

2.2.1 Basics of Palm Calculus

Palm calculus is a collection of techniques that facilitates the computation of *time expectations* through *event expectations* (or *Palm expectations*) and vice versa. Specifically, for any *stationary* stochastic process $X(t)$, the *inversion formula* states that

$$\mathbb{E}[X(t)] = \lambda \mathbb{E}^{T_0}\left[\int_{T_0}^{T_1} X(\tau)\,\mathrm{d}\tau\right], \tag{2.1}$$

if $X(t)$ is continuous with $t \in \mathbb{R}_{\geq 0}$, or

$$\mathbb{E}[X(t)] = \lambda \mathbb{E}^{T_0}\left[\sum_{\tau=T_0}^{T_1-1} X(\tau)\right], \tag{2.2}$$

if $X(t)$ is discrete with $t \in \mathbb{Z}_{\geq 0}$ [48]. Here T_0 and T_1 ($T_0 \leq T_1$) are two consecutive time instants in the stationary regime when the event of interest occurs, and $\mathbb{E}^{T_0}(\cdot) = \mathbb{E}(\cdot|$ an event occurrence at $T_0)$ is an expectation operator conditioned on an occurrence of the event at time T_0. Besides, λ is the occurrence rate of this event. If the process is the (continuous) RWP mobility, for example, the event can be the mobile reaching a random waypoint, whereby λ is the arrival rate at waypoints, and $\mathbb{E}^{T_0}\left[\int_{T_0}^{T_1} X(\tau)\,\mathrm{d}\tau\right]$ is an integral measure evaluating the continuum of locations covered along the path between waypoints.

Leaving aside the rigorous proof, Equations (2.1)(2.2) can be derived intuitively. Take Equation (2.1) for instance, the time expectation on the left-hand side can be defined as[4]

$$\mathbb{E}[X(t)] = \lim_{T\to\infty} \frac{1}{T}\int_0^T X(\tau)\,\mathrm{d}\tau\,. \tag{2.3}$$

On the right-hand side, the intensity λ by definition can be formulated as

$$\lambda = \left[\mathbb{E}^{T_0}(T_1 - T_0)\right]^{-1} = \left[\lim_{K\to\infty} \frac{1}{K}\sum_{k=1}^{K}(T_k - T_{k-1})\right]^{-1}. \tag{2.4}$$

[4]This definition requires the process to be ergodic, which is however not necessary for proving the inversion formula [48]. The assumption of ergodicity is only to ease explanation of the intuition.

where T_k $(k = 0, 1, \ldots, K)$ is the time instant of an event occurrence in the stationary regime. Moreover, the remaining event expectation can be expanded into

$$\mathbb{E}^{T_0}\left[\int_{T_0}^{T_1} X(\tau)\,\mathrm{d}\tau\right] = \lim_{K\to\infty}\frac{1}{K}\sum_{k=1}^{K}\int_{T_{k-1}}^{T_k} X(\tau)\,\mathrm{d}\tau\,. \tag{2.5}$$

Combining Equations (2.4)(2.5) transforms the right-hand side of Equation (2.1) into

$$\begin{aligned}\lambda\mathbb{E}^{T_0}\left[\int_{T_0}^{T_1} X(\tau)\,\mathrm{d}\tau\right] &= \lim_{K\to\infty}\frac{\sum_{k=1}^{K}\int_{T_{k-1}}^{T_k} X(\tau)\,\mathrm{d}\tau}{\sum_{k=1}^{K}(T_k - T_{k-1})}\\ &= \lim_{T'\to\infty}\frac{\int_{T_0}^{T'} X(\tau)\,\mathrm{d}\tau}{T' - T_0}\end{aligned} \tag{2.6}$$

which, if assuming $T_0 = 0$ and $T' = T$, becomes identical to the time expectation of Equation (2.3). Equation (2.2) can be deduced similarly.

Note the subtle difference indicated above between the two expectation operators $\mathbb{E}^{T_0}(\cdot)$ and $\mathbb{E}(\cdot)$: unlike $\mathbb{E}(\cdot)$, $\mathbb{E}^{T_0}(\cdot)$ does *not* concern the *time spans* between event occurrences. This "time decoupling" property provides a unique way to compute time expectations of processes based on event expectations. For instance, if the objective is the (time-)expected location of a mobile that follows RWP, instead of averaging the mobile location over time, one can focus on pairs of random waypoints, estimate the path time in between (for λ^{-1}), and integrate the locations covered on the path (for $\mathbb{E}^{T_0}\left[\int_{T_0}^{T_1} X(\tau)\,\mathrm{d}\tau\right]$). Since the waypoints of RWP follow a uniformly random distribution in the space, this alternative approach turns out to be more tractable [47, 49]. Besides the inversion formula, Palm calculus also includes many other useful results, which nevertheless have little relevance to the thesis.

2.2.2 Analysis of Random Waypoint Mobility

The earliest work on analyzing the stationary mobile distribution for RWP mobility comes from [10, 11]. Assuming zero pause time at waypoints and non-zero speeds that are independent of waypoints, Bettstetter et al. prove that the stationary pdf $f_{X(t)}(x)$ of the mobile location $X(t)$ in a 1-dimensional

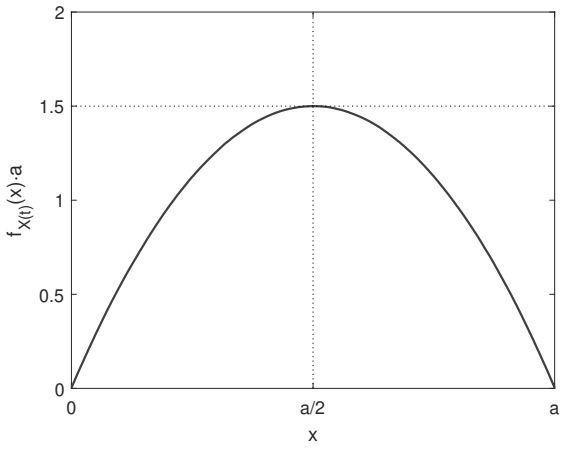

Figure 2.3: Stationary pdf $f_{X(t)}(x)$ of RWP mobility in the 1-dimensional space $[0, a]$ [11].

space $[0, a]$ ($a \in \mathbb{R}_+$) follows

$$f_{X(t)}(x) = -\frac{6}{a^3}x^2 + \frac{6}{a^2}x, \tag{2.7}$$

as shown in Figure 2.3. For the 2-dimensional case, they fail to derive an exact closed-form expression for the mobile distribution; instead, it is approximated in two manners. The first way is to pretend the movements projected onto the x and y axes are independent such that the 2-dimensional mobile distribution in the space $[0, 1]^2$ can be approximated by a product form of 1-dimensional results, i.e.

$$f_{X(t),Y(t)}(x, y) = f_{X(t)}(x)f_{Y(t)}(y) = 36xy(1 - x)(1 - y), \quad 0 \le x, y \le 1. \tag{2.8}$$

The second approximation is more accurate but at the expense of considerably greater complexity. We omit showing the formula for its non-trivial form.

They also consider the general mobility setting where a mobile can pause randomly at a waypoint at time t, in probability $p_p(t)$, or stay static perpetually from the very beginning, in probability p_s. The pausing probability can be given by $p_p(t) = \frac{\mathbb{E}(T_p)}{\mathbb{E}(T_p)+\mathbb{E}(T_m)}$, with $\mathbb{E}(T_p)$ being the expected pause time and $\mathbb{E}(T_m)$ the expected travel time between waypoints. In this case the stationary pdf $f_{\mathbf{X}(t)}(\mathbf{x})$ of the mobile location $\mathbf{X}(t)$ (assuming positive independent speeds) has the *additive* form

$$f_{\mathbf{X}(t)}(\mathbf{x}) = p_s f_{init}(\mathbf{x}) + (1 - p_s)p_p + (1 - p_s)(1 - p_p)f_m^0(\mathbf{x}), \tag{2.9}$$

where $f_{init}(\mathbf{x})$ is the initial mobile distribution and $f_m^0(\mathbf{x})$ is the component of movements without pauses nor static mobiles (e.g. Equation (2.7)). Note that the additivity of Equation (2.9) suggests that the mobile distribution under no pauses at waypoints can be extended easily to include the effect of pausing behavior; the pdf would appear more uniform and "flattened" with pauses added.

Using Palm calculus, Le Boudec for the first time finds the exact closed-form expressions of mobile distribution for regular 2-dimensional spaces (e.g. disks, squares) [47]. Specifically, for an arbitrary convex and bounded space, the stationary pdf $f_{\mathbf{X}(t)}(\mathbf{x})$, assuming positive independent speeds and no pausing, has a general integral form

$$f_{\mathbf{X}(t)}(\mathbf{x}) = \frac{1}{\alpha A^2} \int_0^{\pi} a_{\mathbf{x}}(\theta) a_{\mathbf{x}}(\theta + \pi) \left[a_{\mathbf{x}}(\theta) + a_{\mathbf{x}}(\theta + \pi) \right] \mathrm{d}\theta, \tag{2.10}$$

where A is the area of the space, α is the expected travel distance between waypoints, and $a_{\mathbf{x}}(\theta)$ is the distance from the mobile's location $\mathbf{x}$ to the space boundary at angle θ (Figure 2.4). Based on Equation (2.10), for example, one can derive the closed-form mobile distribution for the unit disk $\Omega = \{\mathbf{x} \in \mathbb{R}^2 \mid |\mathbf{x}| = \sqrt{x^2 + y^2} \leq 1\}$ as

$$f_{\mathbf{X}(t)}(\mathbf{x}) = \frac{45}{32\pi^2}(1 - |\mathbf{x}|^2) E(|\mathbf{x}|), \tag{2.11}$$

where $E(|\mathbf{x}|) = \int_0^{\frac{\pi}{2}} \sqrt{1 - |\mathbf{x}|^2 \sin^2(\theta)}\, \mathrm{d}\theta$ is the complete elliptic integral of the second kind (with modulus $|\mathbf{x}|$) [47]. The Palm calculus techniques are also used to implement fast simulation (or the so called "perfect simulation") for general mobility settings (e.g. RWP on graphs, spheres etc, with pauses) [47, 49].

Almost simultaneously, Hyytiä et al. derive via geometric deduction the same integral-form stationary mobile distribution as Equation (2.10) [39]. Another main strength of their work is the analysis of network performance based on the mobile distribution. For example, assuming an ad hoc network of m independent and identical mobiles that move in a unit disk and communicate following the boolean network model (i.e. any two mobiles within a radius

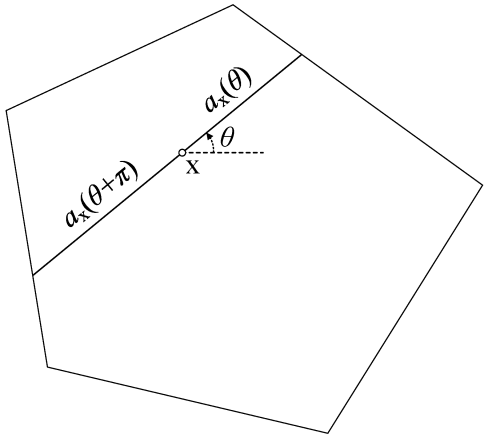

Figure 2.4: Illustration of the distances $a_{\mathbf{x}}(\theta)$ and $a_{\mathbf{x}}(\theta+\pi)$ [47].

R can connect to each other), the probability that a mobile at location $\mathbf{x}$ is connected to at least one peer can be given by

$$Q_m(R) = 2\pi \int_0^1 |\mathbf{x}| f_{\mathbf{X}(t)}(|\mathbf{x}|) \left\{1 - [1 - p(|\mathbf{x}|, R)]^{m-1}\right\} \mathrm{d}|\mathbf{x}|\,, \tag{2.12}$$

where

$$p(|\mathbf{x}|, R) = \int_{\mathbf{x}' \in \mathcal{B}_R(\mathbf{x})} f_{\mathbf{X}(t)}(|\mathbf{x}|)\, \mathrm{d}\mathbf{x}' \tag{2.13}$$

is the probability of a peer residing within the mobile's neighborhood $\mathcal{B}_R(\mathbf{x})$. The probability of the network forming a complete graph of connectivity is then approximated by $[Q_m(R)]^m$.

To model hotspots, Hyytiä et al. also extend RWP to a generic Markovian WayPoint (MWP) model [38, 39] to allow for pauses between waypoints, waypoint-dependent speeds, and non-uniform waypoints. Concerning the distances $a_{\mathbf{x}}(\theta)$ and $a_{\mathbf{x}}(\theta+\pi)$ of Equation (2.10), suppose the source waypoint located at $\mathbf{w}_0 = \mathbf{x} + l_0(\cos\theta, \sin\theta)$ follows an *a priori* known pdf $f(\mathbf{w}_0)$, where l_0 is the distance from $\mathbf{w}_0$ to the mobile's location $\mathbf{x}$, and the transition from $\mathbf{w}_0$ to a destination waypoint at $\mathbf{w}_1 = \mathbf{x} - l_1(\cos\theta, \sin\theta)$ follows a given pdf $g(\mathbf{w}_0, \mathbf{w}_1)$. Then, leaving aside pauses and dependent speeds, the stationary pdf of the mobile location is formulated as

$$f_{\mathbf{X}(t)}(\mathbf{x}) = \frac{1}{\alpha} \int_0^{2\pi} \int_0^{a_{\mathbf{x}}(\theta+\pi)} \int_0^{a_{\mathbf{x}}(\theta)} f(\mathbf{w}_0) g(\mathbf{w}_0, \mathbf{w}_1)(l_0 + l_1)\, \mathrm{d}l_0\, \mathrm{d}l_1\, \mathrm{d}\theta\,. \tag{2.14}$$

2.3 Charging-Aware Wireless Networks

In the thesis we assume the charger has a relatively short effective charging range and make no differentiation between wired and wireless charging. This is justified by the fact that most wireless charging technologies in practice are still subject to unsatisfactory efficiency over long distance; meanwhile, the space settings for our models are targeted on mapping to large areas in the real world (e.g. the size of a city). Here we briefly summarize the prevailing wireless charging technologies (as below), considering their frequent appearance in existing work.

One of the most common charging techniques is *inductive coupling* based on electromagnetic induction. Due to its simplicity, inductive charging has been standardized (i.e. Qi® [65]) and commercialized to augment various products (e.g. cellphones, electric toothbrushes) since early on. Because of severe power decay, however, inductive charging is viable only in *short-range* scenarios that allow a few centimeters at most. Another charging technology, *magnetic resonant coupling*, stems from the discovery that coils resonating at identical frequencies can achieve efficient power transfer even over meters (e.g. 40% around 2 meters) [46]. Despite relatively high complexity of circuits, the efficiency of resonant charging and its capacity for concurrent charging of multiple devices make it promising for applications in daily *mid-range* scenarios [73]. Lastly, the *Radio-Frequency (RF) waves* emitted from antennas can be used to charge batteries, if the waves are harvested for energy rather than demodulated as signals. While *long-range* charging (e.g. over hundreds of meters) is feasible by radio, the power transfer still suffers from path loss, which suits this technology only to ultra-low-power devices (e.g. RF identifications) [28, 63]. Such attenuation can be remedied by directional radiation using beamforming [24], but its application is subject to safety concerns and the requirements of tracking and line-of-sight paths.

2.3.1 Static Chargers

As opposed to the case of mobile chargers, the work assuming mobile rechargeable nodes and static chargers [20, 21, 32, 37, 42, 51, 68] are certainly more related to our scope, which, as mentioned, is about depicting and analyzing the usual charging-aware movement behavior of urban mobile users. Despite the relevance, however, the existing work is still markedly different from ours in two aspects:

(1) The mobile nodes in literature mostly have no notion of natural destinations, neither would they change course because of the attraction from chargers taking effect. Instead, it is assumed the mobiles have their own agendas of travel that are oblivious to the charging needs (e.g. [51]). Or even, there is no explicit modeling of trajectories but only presumed distribution (usually uniform) of the mobile locations, with the mobiles modeled as a (homogeneous) point process (e.g. [37]).

(2) Previously the chargers can often provide wide coverage of the network area, being able to charge a node regardless of its location (by assuming RF-based charging). Hence detours are unnecessary for the mobiles in this case. Further, a mobile may sometimes be able to harvest energy from multiple chargers simultaneously for a higher power gain (e.g. [32, 68]). This, again, is different from our setting, as we assume the chargers are normally scattered, each with a relatively short charging range only to serve mobiles in its very locality.

We recap the existing work as follows. In [37], Huang et al. investigate mobile recharging in a hybrid cellular architecture, where the chargers, namely Power Beacons (PBs), are assumed to exist to provide adequate coverage for recharging purposes comparable to that of Base Stations (BSs) providing communication coverage. Each PB can either "spread out" its radio waves isotropically for the mobiles to harvest collectively, or charge a single mobile located nearby via beamforming. For the analytical model, a stochastic-geometry approach is followed: the PBs and BSs are both modeled as independent homoge-

neous Poisson processes, while the mobile nodes assume a *uniform* distribution in the Voronoi cells with BSs as the generator points.

The objective of [37] is to understand the possible ways to balance four key parameters of the network, including the densities of PBs and BSs and the charging/transmission power of PBs and the mobiles respectively, so that the interference at BSs is below a given level and each mobile would almost surely (for large energy storage) or highly likely (for small energy storage) sustain its transmission power with supply from the PBs. The energy dynamics of mobiles are not modeled in this paper, neither does it consider the concrete mobility or clustering effect around the PBs.

Unlike the approach of [37], Madhja et al. [51] endow the mobile nodes of an ad hoc network with the random walk mobility (see Section 2.1 for the description of random walks). A single wireless charger of finite energy is situated in the center of a rectangular space, with a circular charging area $C_{R(t)}$. In each time slot t, any mobile that falls within the radius $R(t)$ of the charger receives an amount of energy (by magnetic resonant coupling) depending on the distance to the charger, the mobile's energy sufficiency, and the path time within (Figure 2.5). Their goal is to adapt the charging range $R(t) \in [R_{\min}, R_{\max}]$ of the charger at discrete levels, such that (1) the total number of mobiles charged before the charger dies or (2) the time until the last mobile dies is maximized. After proving the NP-hardness of both problems, they present three simple heuristics that exploit the knowledge about energy and locations of the mobiles to different extents:

(1) *Least Distant Agent.* This scheme lets the charger flip the radius $R(t)$ like a fair coin between a minimum $R'_{\min}$ and the maximum $R_{\max}$, where $R'_{\min}$ (if $R'_{\min} \geq R_{\min}$) is supposedly the minimum range required to cover the mobile closest to the charger.

(2) *Maintain Working Agents.* Based on the energy and location information of the mobiles, the charger would set $R(t)$ as small as possible such that at least a number of μ mobiles have energy in each slot t.

(3) *Maximize Charges over Energy Ratio.* The charger would simply follow

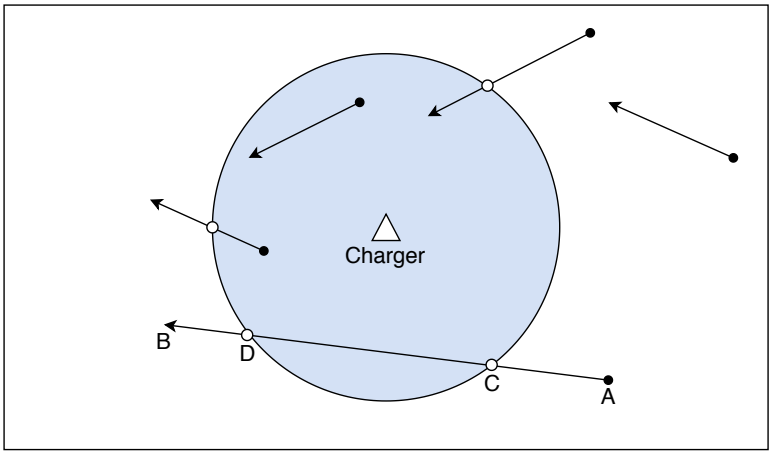

Figure 2.5: Five possible cases of mobiles traversing the charging area $C_{R(t)}$ of a centered charger [51]. As an example, the power transfer along the path A→B occurs only for the segment C→D.

$R(t) = \text{argmax}_{R_j} \frac{\nu_j^{\lambda}(t)}{\varepsilon_j(t)}$, where $\nu_j^{\lambda}(t)$ is the number of mobiles charged in slot t raised to a power of $\lambda \geq 1$ and $\varepsilon_j(t)$ is the energy transferred.

Still, the charger in this paper has no effect on trajectories of the mobiles, and the adaptive charging range is beyond the scope of our work. The chargers in our work always assume a constant minimal range for charging.

In [32], He et al. investigate the deployment of wireless rechargeable sensor networks composed of RFID readers and tags, where the readers can not only retrieve sensory data from the tags but also charge the tags through radio waves. Their main goal is to place a minimum number of readers to cover the whole network area such that the tags have enough energy overall to sustain operation for sensing; formally, the average power (over time) received by a tag from the readers should be higher than the average power for consumption. Two forms of this optimization problem are considered, including *point provisioning*, which concerns energy supply for static tags, and *path provisioning*, which aims to charge mobile tags (that are attached to pedestrians, for example) by exploiting their mobility. Inspired by solutions to coverage problems in traditional sensor networks, they propose to deploy the readers on vertices of a triangular lattice that span the area. For the two energy provisioning problems, they derive different upper bounds for optimizing the side lengths

of triangles in the lattice. For path provisioning, the mobile tags move indifferently to the locations of readers and their stationary distribution is assumed to be known a priori.

A study akin to [32] is conducted in [20], where, given a limited number of chargers, Chiu et al. seek optimal partial coverage of the network area to minimize the chances of end devices being depleted. Assuming chargers can be deployed on vertices of a virtual square lattice (only), they devise a heuristic two-phase algorithm that tends to place the chargers at "hotspots" in terms of passage of depleted devices. Unlike [32] and [20], Dai et al. assume the chargers have predetermined locations [21], and their objective is to adjust the charging power such that the total charging utility (in proportion to the charging power received) of the devices is maximized, *while* no point in the area is exposed to electromagnetic radiation at excessive/hazardous levels. This problem is formulated into a linear program, which is further simplified and addressed by a series of distributed approximation algorithms. A similar problem to [21] is also studied in [60], with extra hardware constraints (e.g. on nodes' capacity for recharging) taken into account. No mobility is considered in [21, 60], since the devices are assumed to be static (throughout the execution process at least).

Additionally, for completeness, we review the notion of detours to static charging stations of Electric Vehicles (EVs). The work on EVs is largely interested in the aggregate impact on the electricity grid rather than on individual vehicles or any communications thereof. Bayram et al. [9] model the power draw from the grid and the ways to schedule recharging of EVs but are not concerned about the paths followed by the vehicles. Closer to the notion of impact on the mobility of individual vehicles, albeit in terms of queuing delays at charging stations, is the work by Bae et al. [5]. They adopt a fluid-flow approximation of the aggregate EV traffic and additionally assume that the charging stations, when they cannot fulfill the instantaneous demand, result in queuing of EVs. This is different from the case of the mobile devices, where the necessary charging current/power is small and the device footprint is minor compared to the needs of an EV, and hence queuing of devices is uncommon.

An interesting direction has been introduced by the work of Wang at al. [72] which address the problem of charger location planning, in an optimization setting but with various possible objectives, but again without looking at the characterization of how individual mobile paths are influenced by the charger placement.

There also exist studies on charging-aware path planning of EVs or UAVs (Unmanned Aerial Vehicles) [1, 19, 59, 70], which bear notable similarity to our work. For instance, to achieve persistent timely surveillance of a 2-dimensional grid space, Scherer and Rinner [70] coordinate the flight of a network of UAVs, prescribing them cyclic paths that tend to pass the least recently sensed cells before returning to a base station for replenishment. On the other hand, assuming charging stations along roads that are prone to congestion, Alizadeh et al. [1] seek optimal paths and charging decisions of EVs (in large numbers) that can minimize the overall travel time and charging cost. While both [1, 70] acknowledge the factor of recharging needs in mobility, the distinction is that the vehicles, which cannot move without energy, are certain to revisit a charging station before long. In contrast, a mobile node in our case is exempt from such strict constraints on energy reserves and reliance upon chargers. Overall, our focus of interest in the thesis is the formal analysis of a *descriptive* mobility model to understand the geographic mobile distribution subject to random recharging behavior—as opposed to *prescriptive* path planning driven directly and solely by optimization.

2.3.2 Mobile Chargers

There exists extensive literature on mobile chargers, in particular in the context of wireless sensor networks [2, 44, 50, 61, 75]. This type of mobile charger research is generally not concerned with the wireless channel capacity but, rather, with path planning of the chargers. It also includes an implicit assumption that the energy required to move the mobile charger is inconsequential to the ability of chargers to charge the nodes. Hence, this model fits the general setting of vehicles (or even unmanned aerial vehicles) moving around with chargers, approaching and recharging static wireless sensor nodes, but it

does not capture the case of mobile nodes seeking a static charger, which is the scope of the thesis.

In [75], for instance, the authors consider the scenario of a multi-functional vehicle that can collect data from the sensor nodes as a sink while moving around and meanwhile provide wireless charging services (based on magnetic resonance). The vehicle must return to a (fixed) home service station periodically for data uploading and self-replenishment. Their main goal is to jointly optimize the traveling path and charging schedule of this vehicle such that the whole sensor network operates perpetually with no node depleted and the total energy consumption, including the power for locomotion and wireless charging, is minimized. Further, the (multi-hop) data flow from the sensor nodes to the vehicle is optimized once the optimal traveling path is determined.

In [50], Madhja et al. address the coordination between multiple mobile chargers (with finite energy) to maximize the network lifespan. Unlike [75], which assumes global network information is available for centralized planning, they seek distributed protocols that use no or only local knowledge. The proposed schemes all operate in two phases, i.e. a coordination and a charging phase. In the coordination phase, the chargers would exchange state information about their energy levels and positions between neighboring pairs and based on this decide partition of the network area. Chargers with sufficient energy are supposed to be responsible for covering larger areas. When each charger knows the real-time energy and positions of sensor nodes in its area, its charging path can be improved by prioritizing sub-areas that contain more low-energy sensors. When no local knowledge is available about the nodes, the chargers would traverse the entirety of its area and conduct charging "blindly".

The scenarios described in [50, 75], and many other literature papers (e.g. [61]), are "niche" setups; that is, despite reaching near a static node, the charger cannot or should not physically connect to it, and hence has to resort to wireless energy transfer. The much more common case of pedestrian users in an urban setting trying to find an outlet to plug their mobile devices (or, recently, a wireless recharging table), is not captured.

A new paradigm generalizing the concept of mobile chargers is peer-to-peer

charging or *energy sharing*, [15, 52, 74]. For example, Bulut and Szymanski in [15] examine the possibility that mobile nodes forming "social" groups can charge each other. While interesting and plausible as a future direction, it assumes that mobility is already accounted for in the social network groupings, and charger locations are not modeled, as any node is a potential charger.

2.4 Wireless Capacity

Following the canonical work of Gupta and Kumar [31] and Grossglauser and Tse [30], Ko et al. investigate the *asymptotic* throughput of an energy-constrained MANET of m mobiles supplied by n energy-sufficient Wireless Charging Vehicles (WCVs) [44]. They assume a space of unit area and an underlying *i.i.d.* mobility model such that both the mobiles and WCVs follow a uniform distribution. The packet forwarding is scheduled in two phases [30]: each source node forwards a packet to a relay node (if no destination node nearby) only in an even time slot, and each destination receives from a relay (or a source if nearby) only in an odd slot. The reception of a packet is always successful if the transmitter is the only one within a radius R of the receiver. The charging area around a WCV is modeled as a set of concentric rings serving different levels of charging efficiency; a random subset of mobiles would be chosen for recharging if there are too many around the WCV. Given this setting, they prove that the network throughput scales as $\Theta\left(\min\left(1, \frac{n}{m}\right) \cdot \mathsf{c}^{\min\left(1, \frac{n}{m}\right)}\right)$, with $0 < \mathsf{c} < 1$ being a constant.

On the other hand, as mentioned in subsection 2.3.1, Huang et al. [37] study the feasible deployments of a cellular network under two constraints, including an *outage constraint* for an acceptable SINR (Signal-to-Interference-plus-Noise Ratio) at BSs and a *power-outage constraint* for acceptable power received by mobiles from the PBs. To satisfy the outage constraint, they prove a necessary condition for mobiles with large energy storage, i.e.

$$z_m q \lambda_p \lambda_b^{\frac{\alpha}{2}} \geq \mathsf{c}_1 ,$$

where q and λ_p are the charging power and density of PBs respectively, λ_b is the density of BSs, z_m is the array gain of PBs for power transfer, α is the

path loss exponent, and c_1 is a constant depending on the mobiles' (fixed) duty cycle ω. In the case of mobiles with small energy storage, the necessary condition for satisfying both the outage and power-outage constraints is given by

$$z_m q \lambda_p^{\frac{\beta}{2}} \lambda_b^{\frac{\alpha}{2}} \geq \mathsf{c}_2 \quad \text{and} \quad z_m q \lambda_b^{\frac{\alpha}{2}} \geq \mathsf{c}_3 \,,$$

where β is the path loss exponent for power transfer and c_2 and c_3 are two constants related to the network deployment.

There exists other similar work on the capacity/throughput performance of rechargeable wireless networks, e.g. [43, 45, 68]. These studies, in general, either seek to derive a throughput scaling law like [31, 44] or concern network-wide configuration of transmission power and node densities like [37]. Apart from the differences in settings, our focus of interest, i.e. the *location-dependent* congestion resultant from the clustering effect of charging-aware mobility interacting with capacity constraints, still remains open to exploration.

Chapter 3

Charging-Aware Mobility in 1-D Space

3.1 Introduction

In this chapter we study the interaction between charging-aware mobility and wireless capacity on a line segment. Each mobile is assumed to communicate continuously until its energy is exhausted. A mobile with no energy to communicate is still allowed to move, as we assume human carriers that use independent energy sources for locomotion. Upon exhaustion, the mobile would turn towards the charger for recharging (possibly via a detour backwards) if the charger location is not beyond the intended waypoint.

The remainder of this chapter is structured as follows: In Section 3.2 we provide the simplified system model and give examples of the concept of detours we model. Section 3.4 includes the key analytical results regarding the stationary distribution of the mobiles subject to detours (subsection 3.3) and the distribution subject to availability (or depletion) of energy (subsection 3.4.2), as well as a comparison (subsection 3.4.3) of analytical results versus simulation results, confirming the accuracy of the developed formulas. It also investigates the approximations for random energy budgets (or speeds) and detours started out of sync with depletion (subsection 3.4.4). The capacity-driven study of mobility versus capacity is unfolded in Section 3.5 where bounds are derived and explored (subsection 3.5.1) and the relative impact of detours (versus no detours) is examined (subsection 3.5.3). Section 3.6 concludes this

chapter.

3.2 Assumptions

Without loss of generality, we investigate the trajectory of a mobile node in a 1-dimensional space $\mathcal{S} = [0, 1]$, in the presence of a stationary charger located at $c \in \mathcal{S}$. Similarly to the random waypoint model, a mobile that has arrived at a waypoint W_{k-1}, will move to the next, uniformly randomly selected, waypoint located at $W_k \in \mathcal{S}$ ($k \in \mathbb{Z}_+$). We assume the mobile, whose energy is consumed only for communications, departs from each waypoint with an initial amount of energy that translates to an ability to continuously transmit while traveling up to a distance d, at a constant speed, v. In the following, d is also assumed to be constant to ease the analysis. However, as explained in subsection 3.4.4, a constant d well approximates the cases where this travel distance is chosen randomly from selected distributions with mean d.

In the case of energy depletion before reaching W_k, say at position W'_k, the mobile would be attracted and detour from W'_k to the charger at c for replenishment, *only if* c resides in the opposite direction of the travel to W_k. Upon arriving at the charger, the mobile is assumed to be restored to its full capacity or a sufficient energy level such that it will not require any further recharging before continuing its travel to reach W_k, i.e., a maximum of a single recharge event from the origin waypoint to the destination waypoint.

Note that the mobile moves *myopically* in the sense that it will not recharge or detour for the sake of recharging until the actual energy depletion occurs. We examine a relaxed version of this behavior in subsection 3.4.4, allowing also for detours to occur before (or after) energy depletion.

Typical trajectories of the mobile are shown in Figure 3.1. In Figure 3.1(a), the waypoint W_k is reached before the energy is depleted (which would have happened at W'_k). In Figure 3.1(b), the energy is depleted at W'_k but the charger is "further" away than the destination W_k; hence the mobile reaches its destination with its energy depleted—the path from W'_k to W_k being without any energy to allow communications. In Figure 3.1(c) the mobile's energy is

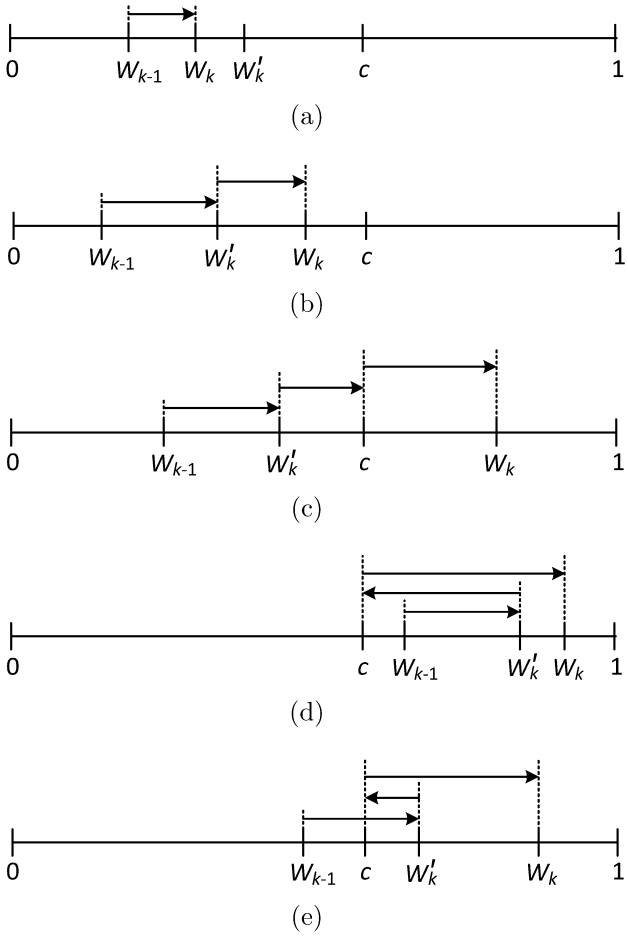

Figure 3.1: Typical trajectories over $\mathcal{S}$ assuming $W_{k-1} < W_k$. The mobile takes a detour to the charger at c only in (d)(e).

depleted at W'_k, and it proceeds to the charger at location c and subsequently to the destination, W_k—the path from W'_k to c traversed without any energy for communications. In those three cases (Figures 3.1(a)–3.1(c)) the mobile did not change its travel direction, i.e., no *detour* occurred. In Figures 3.1(d) and 3.1(e), the mobile will have to detour to get to the charger because its energy was depleted and the charger is in a direction opposite to the mobile's original travel direction—during the travel from W'_k to c the mobile has no energy to allow it to communicate.

Given this basic 1-dimensional charging-aware mobility, we first seek to derive the stationary distribution of the mobile's location $X(t)$ over time $t \in \mathbb{R}$.

3.3 Stationary Expectation of Mobile Location

We follow the well-established approach of applying Palm calculus to mobility models [47]. The stationary expectation of the mobile's location can be expressed as

$$\mathbb{E}\left[X(t)\right] = \lambda \mathbb{E}^{T_0}\left(\int_{T_0}^{T_1} X(\tau)\,\mathrm{d}\tau\right) = \lambda \int_0^1 \int_0^1 \int_{T_0}^{T_1} X(\tau)\,\mathrm{d}\tau\,\mathrm{d}w_{T_0}\,\mathrm{d}w_{T_1} \tag{3.1}$$

where $T_0 \in \mathbb{R}$ is an arbitrary time instant in the stationary regime, $T_1 > T_0$ is the time when the mobile first reaches a waypoint W_{T_1} after T_0, and $\mathbb{E}^{T_0}(\cdot) = \mathbb{E}(\cdot|\xi_{T_0})$ denotes the expectation conditioned on the event ξ_{T_0} that the mobile arrives at a waypoint W_{T_0} at time T_0. For brevity, it is assumed $T_0 = 0$, and $W_{T_0} = W_0$, $W_{T_1} = W_1$ hereafter. Also, $\lambda^{-1} = \frac{\alpha}{v}$ is the expected travel time between waypoints, with α being the expected travel distance, which includes the segments traveled for detours when the mobile needs to reach a charger.

Depending on the waypoint locations W_0, W_1, and the setting of charger location c, Equation (3.1) should be evaluated in two cases depending whether the mobile takes a detour for charging.

3.3.1 Case I: Direct Path

The mobile travels directly to its next waypoint, W_1, without a detour to the charger (Figures 3.1(a)-3.1(c)), if:

1. the mobile has enough energy to cover the distance from waypoint W_0 to W_1, i.e. $|W_0 - W_1| \leq d$, *or*

2. the mobile's energy is exhausted but it does not change its travel direction, because the charger is in the direction of travel to waypoint W_1 (as shown in Figures 3.1(b) and 3.1(c)), i.e.

$$W' = \begin{cases} W_0 + d \leq c, & \text{if } W_0 < W_1 \\ W_0 - d \geq c, & \text{if } W_0 > W_1 \end{cases} \tag{3.2}$$

Table 3.1: Intervals of Integration for Case I.

$w_0 \le w_1$	c	$\mathcal{W}_0$	$\mathcal{W}_1$
Yes	$[0, d)$	$[0, 1-d]$	$[w_0, w_0+d]$
		$(1-d, 1]$	$[w_0, 1]$
	$[d, 1]$	$[0, 1-d]$	$[w_0, w_0+d]$
		$(1-d, 1]$	$[w_0, 1]$
		$[0, c-d]$	$(w_0+d, 1]$
No	$[0, 1-d]$	$[d, 1]$	$[w_0-d, w_0)$
		$[0, d)$	$[0, w_0)$
		$[c+d, 1]$	$[0, w_0-d)$
	$(1-d, 1]$	$[d, 1]$	$[w_0-d, w_0)$
		$[0, d)$	$[0, w_0)$

Table 3.2: Intervals of Integration for Case II.

$w_0 \le w_1$	c	$\mathcal{U}_0$	$\mathcal{U}_1$
Yes	$[0, d)$	$[0, 1-d)$	$(w_0+d, 1]$
	$[d, 1]$	$(c-d, 1-d)$	$(w_0+d, 1]$
No	$[0, 1-d]$	$(d, c+d)$	$[0, w_0-d)$
	$(1-d, 1]$	$(d, 1]$	$[0, w_0-d)$

Hence, the expectation of location in the case the mobile follows a direct path is given by[1]

$$\begin{aligned}\lambda\mathbb{E}^0_{\mathtt{I}}\left(\int_0^{T_1} X(\tau)\,\mathrm{d}\tau\right) &= \lambda\mathbb{E}^0\left(\int_0^{T_1}\left[W_0 + \frac{\tau}{T_1}(W_1 - W_0)\right]\mathrm{d}\tau\right)\\ &= \lambda\mathbb{E}^0\left(T_1\int_0^1 [(1-\rho)W_0 + \rho W_1]\,\mathrm{d}\rho\right)\\ &= \frac{\lambda}{\nu}\int_{\mathcal{W}_0}\int_{\mathcal{W}_1} |w_0 - w_1| \int_0^1 [(1-\rho)w_0 + \rho w_1]\,\mathrm{d}\rho\,\mathrm{d}w_1\,\mathrm{d}w_0\end{aligned} \tag{3.3}$$

where the intervals of integration, $\mathcal{W}_0$ and $\mathcal{W}_1$, depend on the relative values of w_0 and w_1 and also the value of c, as enumerated in Table 3.1.

[1]The subscript $\mathtt{I}$ in $\mathbb{E}^0_{\mathtt{I}}(\cdot)$ denotes that this expectation corresponds to Case I, where the mobile follows a direct path to its destinations.

3.3.2 Case II: Path with Detour

As opposed to Case I, the mobile would take a detour to the charger before reaching waypoint W_1, if $|W_0 - W_1| > d$ *and* the point of energy depletion occurrence, W', resides between W_1 and the charger location c (Figures 3.1(d)(e)). In this case, the trajectory can be partitioned into three components: 1) the travel from waypoint W_0 to W', 2) the travel from W' to the charger location c, and 3) the part from c to waypoint W_1. Thus the expectation can be formulated accordingly as

$$\begin{aligned}\lambda \mathbb{E}^0_{\mathtt{II}}\left(\int_0^{T_1} X(\tau)\,\mathrm{d}\tau\right) &= \lambda \mathbb{E}^0\left(\int_0^{T'} X(\tau)\,\mathrm{d}\tau + \int_{T'}^{T_c} X(\tau)\,\mathrm{d}\tau + \int_{T_c}^{T_1} X(\tau)\,\mathrm{d}\tau\right) \\ &= \frac{\lambda}{\nu}\int_{\mathcal{U}_0}\int_{\mathcal{U}_1} \psi(w_0, w_1)\,\mathrm{d}w_1\,\mathrm{d}w_0\end{aligned} \tag{3.4}$$

where T' and T_c denote the time instants when the mobile reaches W' and c respectively, and

$$\begin{aligned}\psi(w_0, w_1) = d\int_0^1 [(1-\varrho_1)w_0 + \varrho_1 w']\,\mathrm{d}\varrho_1 \\ + |w' - c|\int_0^1 [(1-\varrho_2)w' + \varrho_2 c]\,\mathrm{d}\varrho_2 \\ + |c - w_1|\int_0^1 [(1-\varrho_3)c + \varrho_3 w_1]\,\mathrm{d}\varrho_3\end{aligned}$$

with w' following Equation (3.2). The intervals of integration $\mathcal{U}_0$ and $\mathcal{U}_1$ are detailed as in Table 3.2.

3.4 Stationary Distribution of Mobile Location

3.4.1 Overall Stationary Mobile Distribution

Now we present the main results of this chapter as a series of formal statements, whose proofs can be found in the Appendices. Firstly, we have the following theorem:

Theorem 3.4.1.1. *The stationary pdf, $f_{X(t)}(x)$, of the mobile location $X(t)$ is*

Table 3.3: Sub-Domains of PDF, $f_{X(t)}(x)$.

d	c	$\mathcal{X}_1$	$\mathcal{X}_2$	$\mathcal{X}_3$
$[0, \frac{1}{2}]$	$[0, d)$	$[0, c)$	$[c, d)$	$[d, 1]$
	$[d, 1-d]$	$[0, c)$	$\emptyset$	$[c, 1]$
	$(1-d, 1]$	$[0, 1-d]$	$(1-d, c]$	$(c, 1]$
$(\frac{1}{2}, 1]$	$[0, 1-d]$	$[0, c)$	$[c, d)$	$[d, 1]$
	$(1-d, d)$	$[0, 1-d]$	$(1-d, d)$	$[d, 1]$
	$[d, 1]$	$[0, 1-d]$	$(1-d, c]$	$(c, 1]$

Table 3.4: Intervals of Integration, $\mathcal{V}_0$, $\mathcal{V}_1$, and $\mathcal{V}_1'$.

$w_0 \le w_1$	c	$\mathcal{V}_0$	$\mathcal{V}_1$	$\mathcal{V}_1'$
Yes	$[d, 1]$	$[0, c-d)$	$(w_0+d, c]$	$(c, 1]$
No	$[0, 1-d]$	$(c+d, 1]$	$[c, w_0-d)$	$[0, c)$

a piecewise quadratic function:

$$\alpha f_{X(t)}(x) = \begin{cases} 1-(1-x)^2, & \text{if } x \in \mathcal{X}_1 \\ 1-(1-x)^2 - x^2 + (1-d)^2, & \text{if } x \in \mathcal{X}_2 \\ 1-x^2, & \text{if } x \in \mathcal{X}_3 \end{cases} \tag{3.5}$$

where the sub-domains $\mathcal{X}_1$, $\mathcal{X}_2$, and $\mathcal{X}_3$ depend on the travel distance before energy depletion, d, and the charger location, c, as in Table 3.3.

Proof. See Appendix A. □

Note that the integration needed to compute the value of coefficient $\alpha^{-1} = \frac{\lambda}{\nu}$ follows the same intervals of w_0 and w_1 as in Table 3.1 and 3.2. Thus the calculation of α^{-1} is straightforward. Alternatively, given the pdf expressions derived in Theorem 3.4.1.1, we can calculate the area of $[0,1] \times [0, \alpha f_{X(t)}(x)]$, which is equal to α. Following the second method, we have for $d \le \frac{1}{2}$ that

$$\alpha = \begin{cases} \alpha_1(c,d), & \text{if } c \in [0, d) \\ c^2 - c + \frac{2}{3}, & \text{if } c \in [d, 1-d] \\ \alpha_2(c,d), & \text{if } c \in (1-d, 1] \end{cases} \tag{3.6}$$

where

$$\alpha_1(c,d) = \frac{4}{3}d^3 - 3d^2 + 2d + \frac{c^3}{3} - (1-d)^2 c + \frac{2}{3}(1-d)^3$$

$$\alpha_2(c,d) = c^2 - c + \frac{2}{3} - \frac{c^3}{3} + (1-d)^2 c - \frac{2}{3}(1-d)^3$$

while for $d > \frac{1}{2}$ there is

$$\alpha = \begin{cases} \alpha_1(c,d), & \text{if } c \in [0, 1-d] \\ \frac{4}{3}d^3 - 3d^2 + 2d, & \text{if } c \in (1-d, d) \\ \alpha_2(c,d), & \text{if } c \in [d, 1] \end{cases} \tag{3.7}$$

Note that Theorem 3.4.1.1 provides an extension, to account for detours, of the stationary distribution results known for the 1-dimensional RWP model (Equation (2.7) and Figure 2.3 in Section 2.2). The derived closed-form stationary pdf of the mobile location, which extends the results of RWP to model charging-aware mobility, is one of the main contributions of the thesis.

3.4.2 Stationary Distribution under Energy Depletion

Next, we wish to express the stationary distribution for the location of a node given that it has incurred energy depletion or not. This is needed to separate a node that has energy and hence contributes to the traffic load and one that does not. We introduce the state $U(t) \in \{0, 1\}$ of the mobile, to encode whether it has incurred energy depletion ($U(t) = 1$) or not ($U(t) = 0$). For the former case, we need to filter out the movements while energy is depleted:

1. *Direct path.* The mobile would be exhausted only while moving from W' to W_1 or c, assuming $|W_0 - W_1| > d$. Instead of Equation (3.3), the expectation of location of concern now is

$$\begin{aligned} &\lambda \mathbb{E}_{\mathrm{I}}^{0} \left(\int_{T'}^{T_1} X(\tau)\, \mathrm{d}\tau + \int_{T'}^{T_c} X(\tau)\, \mathrm{d}\tau \right) \\ &\quad = \frac{\lambda}{\nu} \Bigg(\int_{\mathcal{V}_0} \int_{\mathcal{V}_1} |w' - w_1| \int_0^1 [(1-\varrho)w' + \varrho w_1]\, \mathrm{d}\varrho\, \mathrm{d}w_1\, \mathrm{d}w_0 \\ &\qquad + \int_{\mathcal{V}_0} \int_{\mathcal{V}_1'} \tilde{\psi}(w_0, w_1)\, \mathrm{d}w_1\, \mathrm{d}w_0 \Bigg) \end{aligned} \tag{3.8}$$

   where $\tilde{\psi}(w_0, w_1)$ is defined (below) by Equation (3.10), and the intervals of integration, $\mathcal{V}_0$, $\mathcal{V}_1$, and $\mathcal{V}_1'$, are set as in Table 3.4. The three intervals would all be $\emptyset$, if $w_0 \leq w_1$ and $c \in [0, d)$, or $w_0 > w_1$ and $c \in (1-d, 1]$.

2. *Path with detour.* The energy depletion spans the detour segment of travel of the mobile from W' to c for recharging. The expectation in

Equation (3.4) is thus reduced to

$$\lambda \mathbb{E}^0_{\text{II}} \left(\int_{T'}^{T_c} X(\tau)\, \mathrm{d}\tau \right) = \frac{\lambda}{\nu} \int_{\mathcal{U}_0} \int_{\mathcal{U}_1} \tilde{\psi}(w_0, w_1)\, \mathrm{d}w_1\, \mathrm{d}w_0 \tag{3.9}$$

where

$$\tilde{\psi}(w_0, w_1) = |w' - c| \int_0^1 [(1 - \varrho_2)w' + \varrho_2 c]\, \mathrm{d}\varrho_2 \,. \tag{3.10}$$

The intervals of integration $\mathcal{U}_0$ and $\mathcal{U}_1$ still follow Table 3.2.

By deducing the expectations of Equations (3.8)(3.9), we obtain the second theorem, which, together with Corollary 3.4.2.1 (as below), adds to our main contributions of the thesis:

Theorem 3.4.2.1. *The joint stationary pdf, $f_{X(t),U(t)=1}(x)$, of the mobile location $X(t)$* given that its energy is depleted*, is a piecewise quadratic function:*

$$\alpha f_{X(t),U(t)=1}(x) = \begin{cases} \frac{x^2}{2}, & \text{if } x \in \mathcal{X}'_1 \\ g_2(x,d), & \text{if } x \in \mathcal{X}'_2 \\ g_3(x,d), & \text{if } x \in \mathcal{X}'_3 \\ \frac{(1-x)^2}{2}, & \text{if } x \in \mathcal{X}'_4 \end{cases} \tag{3.11}$$

where

$$g_2(x,d) = c_{11}\frac{x^2}{2} + c_{12}\frac{(1-d)^2}{2} + c_{13}(1-x)(x-d) + c_{14}(1-d-x)x$$
$$g_3(x,d) = c_{21}\frac{(1-x)^2}{2} + c_{22}\frac{(1-d)^2}{2} + c_{23}(1-x)(x-d) + c_{24}(1-d-x)x$$

and the sub-domains, $\mathcal{X}'_1$, $\mathcal{X}'_2$, $\mathcal{X}'_3$, and $\mathcal{X}'_4$, depend on the values of d and c, as in Table 3.5.

Proof. See Appendix B. □

Corollary 3.4.2.1. *The joint stationary pdf, $f_{X(t),U(t)=0}(x)$, of the mobile location $X(t)$* given that the mobile has energy *is given by*

$$f_{X(t),U(t)=0}(x) = f_{X(t)}(x) - f_{X(t),U(t)=1}(x). \tag{3.12}$$

Table 3.5: Sub-Domains and Coefficients of Sub-Functions of PDF, $f_{X(t),U(t)=1}(x)$.

d	c	$\mathcal{X}'_1$	$\mathcal{X}'_2$	$\mathcal{X}'_3$	$\mathcal{X}'_4$	c_{11}	c_{12}	c_{13}	c_{14}	c_{21}	c_{22}	c_{23}	c_{24}
$[0, \frac{1}{2}]$	$[0, d)$	$[0, c)$	$[c, d)$	$[d, 1-d]$	$(1-d, 1]$	0	1	0	1	1	0	0	1
	$[d, 1-d]$	$[0, d)$	$[d, c)$	$[c, 1-d]$	$(1-d, 1]$	1	0	1	0	1	0	0	1
	$(1-d, 1]$	$[0, d)$	$[d, 1-d]$	$(1-d, c]$	$(c, 1]$	1	0	1	0	0	1	1	0
$(\frac{1}{2}, 1]$	$[0, 1-d]$	$[0, c)$	$[c, 1-d]$	$(1-d, d)$	$[d, 1]$	0	1	0	1	0	1	0	0
	$(1-d, d)$	$[0, 1-d]$	$(1-d, c)$	$[c, d)$	$[d, 1]$	0	1	0	0	0	1	0	0
	$[d, 1]$	$[0, 1-d]$	$(1-d, d)$	$[d, c]$	$(c, 1]$	0	1	0	0	0	1	1	0

3.4.3 Numerical Results

To verify the derived stationary mobile distributions, we simulate the 1-dimensional charging-aware mobility (Section 3.2) on the line segment $[0, 1]$, which is partitioned into 10^3 equisized subintervals ("sites"). The mobile is initially placed at random uniformly on this line segment and then moves to another random waypoint by "hopping" over the subintervals at a step size 10^{-3}. Each hop consumes one unit of energy (if the mobile has any). Upon depletion of energy, the mobile would turn towards the charger for recharging, although the subinterval of the destination may be reached first, which triggers the trip to

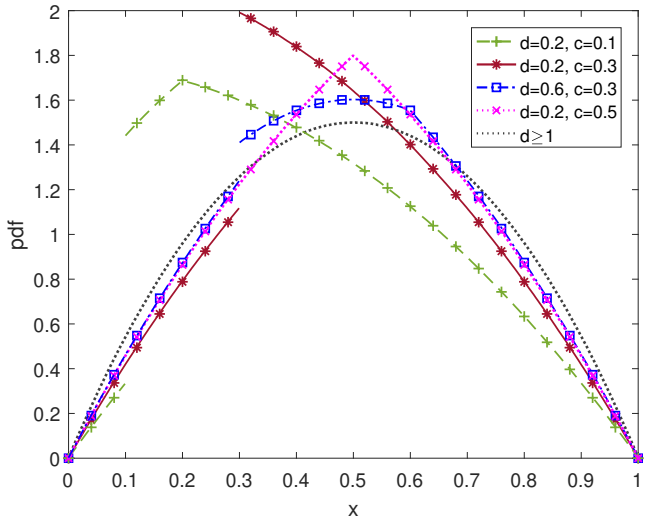

Figure 3.2: Analytical results as per Theorem 3.4.1.1 versus simulation results for $c = 0.1, 0.3, 0.5$, and $d = 0.2$, 0.6, and $d \geq 1$ (RWP). The agreement between analytical and simulation results is exact.

a new uniformly generated waypoint. The path to the destination waypoint is subject to the detour options as exemplified in Figure 3.1. The mobile's probability density at a certain location is approximated by the count of visits to the enclosing subinterval, normalized by the total count of visits/hops across the line and the step size 10^{-3}. Figure 3.2 provides a comparison of the simulation versus analytical results of the probability density function (pdf) of the mobile location. The charger locations, c, used are 0.1, 0.3, and 0.5, and the energy budget, d, is 0.2, 0.6, and $d \geq 1$. Note that the case $d \geq 1$ is essentially the original RWP, as it obviates any recharging and, hence, any need for detours.

It can be seen that the analysis indeed provides an accurate characterization of the mobile distribution. By comparison to the RWP behavior ($d \geq 1$), the charger creates a hot spot in its locality to which the mobile would gravitate for recharging. The attraction to the charger appears to have less effect on the mobile distribution in a highly-energized system (i.e. $d > \frac{1}{2}$) than in an under-energized one (i.e. $d \leq \frac{1}{2}$), which is unsurprising.

Specifically, two patterns of the mobile distribution shown in Fig. 3.2 are worth mentioning:

1. The distribution always exhibits a discontinuity at the charger location, except when the charger resides at the very middle (i.e. $c = 0.5$). This common discontinuity appears to result from the *boundary effect*. Indeed, as Appendix C confirms, removal of the boundaries causes the discontinuity to disappear. For example, assume $d = 0.2$ and $c = 0.3$. Then, since the charger "sees" more space to its right, the mobile returns to the charger more often when moving to the right than it does when moving to the left, which results in an unbalanced probability mass on the two sides.

2. The charger location, if deployed relatively close to the boundary, i.e. $c \in [0, d)$ ($c \in (1-d, 1]$ resp.), is *not* the highest density "hotspot" even in an under-energized system; instead, the hotspot appears to be at d ($1-d$ resp.). As shown in Fig. 3.2, for ($d = 0.2, c = 0.1$), the hotspot

is around location $x = 0.2$ $(= d)$ instead of the charger at $x = 0.1$ $(= c)$. The increase of probability from location c to d is another reflection of the boundary effect on charging-aware movements. Unlike the case $(d = 0.2, c = 0.3)$, assuming a mobile that travels from the left edge, the mobile cannot be arbitrarily close to the charger when it starts to detour for recharging, because of the limitation of d. As a result, and similarly to the case of RWP $(d \geq 1)$, the probability increases towards the middle within region $[c, d)$ (or, symmetrically, $(1 - d, c]$).

Figure 3.3 displays the comparison of simulation results versus the analytical results (Corollary 3.4.2.1) for the stationary pdf of the mobile location given that it has energy (i.e. $U(t) = 0$), with $c = 0.1, 0.3, 0.5$, and $d = 0.2$, 0.6. Besides the agreement of simulation with the analysis, the aforementioned two patterns, i.e., the discontinuity and the "hotspot deviation", are still present. The discovery of such novel patterns of the distorted mobile distribution, which result from the mobile's recharging behavior and the boundary effect, is one of the main contributions of the thesis. When comparing Figure 3.2 and 3.3, it is evident that, apart from a scaling inflicted by conditioning on the mobile having energy, the mobile is very likely to have energy (i.e. unlikely to have its energy depleted) if located near either boundary (within $[0, d)$ or $(1-d, 1]$), unless the charger is also nearby and close to the boundary (which can distort the mobile distribution). This comes from the fact that the mobile moving inwards would never incur energy depletion within distance d of either boundary.

3.4.4 The Role of the Budget Parameter d

The presented charging-aware mobility model assumes that the mobile always incurs energy depletion after traveling a constant distance d from its originating waypoint (provided the next waypoint is more than d away). However, in d we conflate three, technically independent, parameters: (i) the *energy budget* upon departing from a waypoint, (ii) the travel *distance* from a waypoint to the point of energy depletion, and (iii) the *duration* of travel starting from a

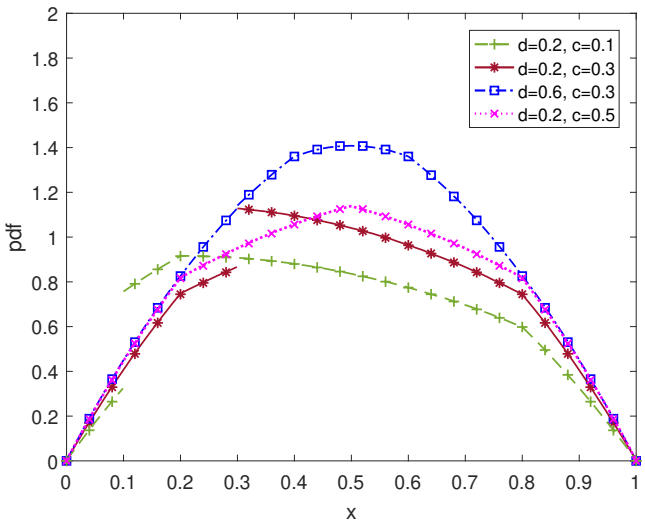

Figure 3.3: Analytical results as per Corollary 3.4.2.1 for nodes with energy, versus simulation results for $c = 0.1, 0.3, 0.5$, and $d = 0.2$, 0.6. The agreement between analytical and simulation results is exact.

waypoint and up to energy depletion. The three parameters are reduced to a single one because, (a), the device is assumed to be continuously communicating as long as it has energy, and, (b), the users are assumed to have a constant speed when moving. Given the uncertainties around (a) and (b), one could be called to see d as an average of a random distribution rather than as a constant. Let us assume that the time that the detour is taken is a random variable D subject to $\mathbb{E}(D) = d$. We first examine distributions of D against the approximating simplification of a constant d.

As shown in Figure 3.4(a), the mobile has similar distributions of location under an exponentially distributed D. The noticeable difference around location $1 - d = 0.8$ comes from the fact that the mobile now may incur energy depletion before reaching $1 - d$ when moving from the right boundary. With regard to the left side, however, the mobile would be first drawn back to the charger at $c = 0.1$ and thus less likely to encounter it at location $d = 0.2$ with its energy depleted. When D follows a truncated normal distribution as $D \sim \mathcal{N}(0.2, \sigma^2; 0, \infty)$ with $\sigma = 0.1$, similarity of the mobile distributions remains. As the variance σ^2 increases, however, the mobile shows less attraction to the charger because of the growing possibility of D having large values, like

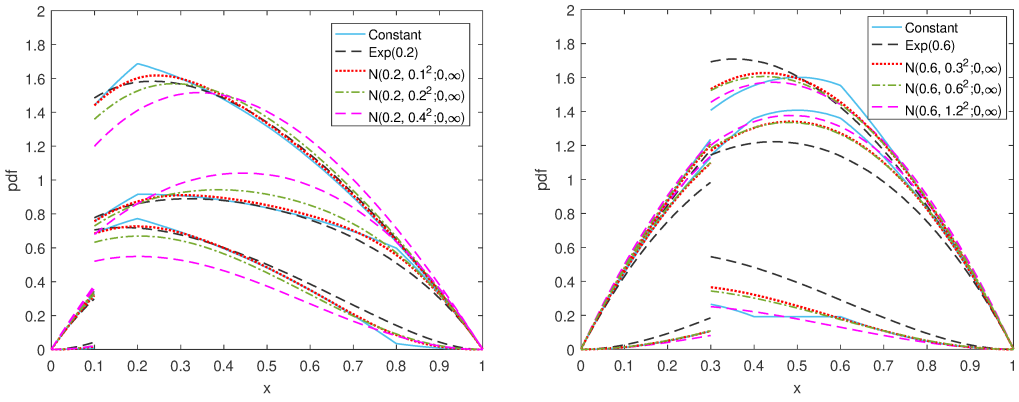

(a) (b)

Figure 3.4: Simulation results of the pdf under a random D following exponential or truncated normal distributions: (a) $d = 0.2$, $c = 0.1$; (b) $d = 0.6$, $c = 0.3$. The additional lines (in correspondence to Figures 3.2 and 3.3) nearest to the bottom correspond to the results for the mobiles with depleted energy.

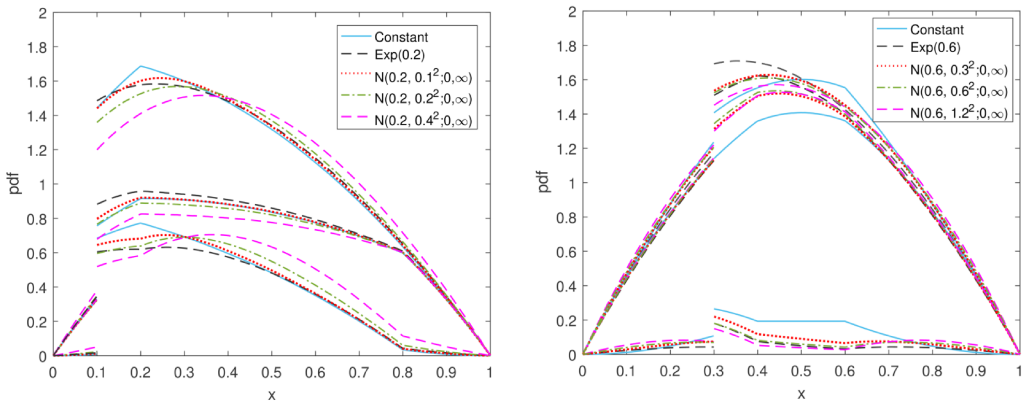

(a) (b)

Figure 3.5: Simulation results of the pdf under the variant model MD* with a random D^* following exponential or truncated normal distributions: (a) $d = 0.2$, $c = 0.1$; (b) $d = 0.6$, $c = 0.3$.

in a highly-energized system.

When $d = 0.6$ and $c = 0.3$, as in Figure 3.4(b), the mobile distributions under a constant d can approximate those under a truncated normal D fairly well, but less so if $D \sim \text{Exp}(0.6)$. Presumably, under the exponential distribution the mobile can be far less energized with smaller D and thus more attracted to the charger at $c = 0.3$. On the other hand, when $D \sim \mathcal{N}(0.6, \sigma^2; 0, \infty)$, the mobile would become more energized overall as σ increases, despite the minor

increase of probability that D attains a small value (e.g. $D \leq 0.1$). Generally, for a closer approximation to systems involving a random D, one can consider the weighted sum of mobile distributions from several systems energized with different constant values of d.

In addition to the random energy budget D, we investigate an extended model that allows advanced or delayed detours for recharging. That is, the mobile, which is still bound to exhaust its energy after traveling a constant distance d, can start a detour upon reaching a distance D^*, with D^* drawn from a random distribution and $\mathbb{E}(D^*) = d$. In this scenario, it is possible the mobile acts proactively and initiates the detour long enough before energy depletion such that no outage occurs throughout the path to the charger/destination. On the other hand, the mobile may sometimes decide "sluggishly" (e.g. long after energy depletion) to detour for charging, which can be costly in terms of both travel distance and outage time if the destination is not reached first.

Mobile distributions under this variant model (denoted $\mathsf{MD}^\star$) are shown in Figure 3.5. Firstly, it can be seen that the new results are generally still well characterized by the original model (denoted MD) for the given distributions of D^*. Secondly, as shown in Figure 3.5(a), when $D^* \sim \text{Exp}(0.2)$ or $D^* \sim \mathcal{N}(0.2, \sigma^2; 0, \infty)$ with $\sigma = 0.1$, the mobile under model $\mathsf{MD}^\star$ is more likely to have energy especially between 0.1 ($= c$) and 0.2 ($= d$) than under model MD, because of the potentially proactive charging behavior. In the case that $D^* \sim \mathcal{N}(0.2, \sigma^2; 0, \infty)$ with σ equal to 0.2 or 0.4, however, the mobile may have deviated far beyond the point of energy depletion and even reached the destination before deciding to take a detour. As a result, the attraction to the charger would drop while the outage time along the detour or direct path (to the destination) tends to increase. As for Figure 3.5(b), owing to the relatively high energy budget ($d = 0.6$), there is a greater chance that the mobile still has energy when it arrives at the charger/destination.

3.5 Interaction with Wireless Capacity

3.5.1 Bounds

Armed with the results from the previous section, we can now consider the case of a system with a number of independent, but statistically identical, users/devices. Their stationary distribution with respect to location under the assumption that they have energy (Corollary 3.4.2.1) allows them to compete for the wireless capacity at that location/site. If the number of mobiles, perceived as traffic demand, is larger than the wireless capacity at that location, not all mobiles will be able to transmit successfully. Hence, areas where mobiles congregate, as in around chargers, are areas of wireless medium congestion. In this section we study the interplay between charging-aware mobility and wireless congestion.

We first clarify, the terminology of certain states of a mobile. A mobile is said to be *operational* if it has energy (i.e., its energy is not depleted). A mobile is *blocked* if it is operational but fails to communicate due to exceeding capacity (discussed below); a *communicating* mobile is one that is operational and not blocked.

The distributions of location derived previously provide the basis for further performance analyses of (1-dimensional) networks composed of charging-aware mobiles. With Equation (3.12) the stationary probability that any mobile falls into a region $\mathcal{R} \subseteq \mathcal{S}$ and is not depleted of energy can be given by

$$p(\mathcal{R}) = \mathbb{P}\left(X(t) \in \mathcal{R}, U(t) = 0\right) = \int_{\mathcal{R}} f_{X(t),U(t)=0}(x)\,\mathrm{d}x\,. \tag{3.13}$$

Given a network of m i.i.d. mobiles with $[X_i(t)]_{1\leq i\leq m}$ and $[U_i(t)]_{1\leq i\leq m}$, for instance, one can learn about the spatial clustering of operational mobiles in region $\mathcal{R}$ through the counting variable

$$N(\mathcal{R}) = \sum_{i=1}^{m} \mathbb{1}\left(X_i(t) \in \mathcal{R} \wedge U_i(t) = 0\right) \tag{3.14}$$

whose (binomial) distribution is then

$$\mathbb{P}(N(\mathcal{R}) = n) = \binom{m}{n} p^n(\mathcal{R})\left[1 - p(\mathcal{R})\right]^{m-n}\,.$$

More importantly, suppose the whole segment $\mathcal{S}$ is partitioned into a number of s disjoint intervals $\left[\mathcal{I}_j\right]_{1\le j\le s}$, each of length $\Delta = s^{-1}$, and the number of mobiles per interval that can communicate concurrently is limited by a *capacity* $\omega \in \mathbb{Z}_+$. Note that we assume fair medium access such that the contending mobiles in any interval are equally likely to be blocked upon exceeding capacity; besides, each mobile would keep consuming energy (if any) at a constant rate, despite being blocked. Then, as part of our main contributions, we can assess the conditions of mobile communications as follows:

Theorem 3.5.1.1. *Given a network of m i.i.d. charging-aware mobiles and a capacity constraint ω, the probability, $\mathbb{P}\left(C(t)=0, X(t)\in\mathcal{R}, U(t)=0\right)$, that each mobile is blocked ($C(t)=0$) in any region $\mathcal{R}=\cup_{j\in\mathcal{J}(\mathcal{R})}\mathcal{I}_j\subseteq\mathcal{S}$, where $\mathcal{J}(\mathcal{R})\subseteq\{1,2,...,s\}$, is lower-bounded as*

$$\mathbb{P}\left(C(t)=0, X(t)\in\mathcal{R}, U(t)=0\right) \ge \sum_{j\in\mathcal{J}(\mathcal{R})} \max\left(p(\mathcal{I}_j)-\frac{\omega}{m},\ 0\right) \tag{3.15}$$

where $C(t)$ denotes the communication state of each mobile.

Proof. Assume that the line segment $\mathcal{S}=[0,1]$ is partitioned into a number of s disjoint unit-sized intervals $\left[\mathcal{I}_j\right]_{1\le j\le s}$ (i.e. $\mathcal{S}=\cup_{j=1}^{s}\mathcal{I}_j$, $\cap_{j=1}^{s}\mathcal{I}_j=\emptyset$, and $\left|\mathcal{I}_j\right|=\delta$, $\forall j$). Also, for notational convenience, we define a special "interval" $\mathcal{I}_0$ and the counting variable

$$N(\mathcal{I}_0)=\sum_{i=1}^{m}\mathbb{1}\left(X_i(t)\in\mathcal{S}\wedge U_i(t)=1\right)$$

that accounts for the number of exhausted (depleted energy) mobiles over the entire segment. Then, the counting variables $\left[N(\mathcal{I}_j)\right]_{0\le j\le s}$, where each $N(\mathcal{I}_j)$ ($j\ge 1$) is defined as in Equation (3.14), would follow a multinomial distribution, i.e.

$$\begin{aligned}
&\mathbb{P}\big(\mathbf{n}=[n_j]_{1\le j\le s}\big)\\
&\quad=\mathbb{P}\left(N(\mathcal{I}_0)=n_0, N(\mathcal{I}_1)=n_1, ..., N(\mathcal{I}_s)=n_s\right)\\
&\quad=\begin{cases}\frac{m!}{\prod_{j=0}^{s}n_j!}\prod_{j=0}^{s}p^{n_j}(\mathcal{I}_j), & \text{if } \sum_{j=0}^{s}n_j=m\\ 0, & \text{otherwise}\end{cases}
\end{aligned} \tag{3.16}$$

where $p(\mathcal{I}_j)$ is defined as in Equation (3.13).

Furthermore, we delineate a region $\mathcal{R} = \cup_{j\in\mathcal{J}(\mathcal{R})}\mathcal{I}_j \subseteq \mathcal{S}$, where $\mathcal{J}(\mathcal{R}) \subseteq \{1, 2, ..., s\}$. Given the capacity (per interval) ω, the probability, $\mathbb{P}(C(t) = 0, X(t) \in \mathcal{R}, U(t) = 0)$, that each mobile falls into $\mathcal{R}$ with energy but remains blocked $(C(t) = 0)$ can be lower-bounded as

$$\begin{aligned}
&\mathbb{P}(C(t) = 0, X(t) \in \mathcal{R}, U(t) = 0) \\
&\quad = \frac{1}{m}\sum_{\forall \mathbf{n}} \mathbb{P}(\mathbf{n}) \sum_{j\in\mathcal{J}(\mathcal{R})} \max\left(n_j - \omega,\ 0\right) \\
&\quad \geq \sum_{j\in\mathcal{J}(\mathcal{R})} \max\left(\frac{1}{m}\sum_{\forall \mathbf{n}} \mathbb{P}(\mathbf{n})\, n_j - \frac{\omega}{m},\ 0\right) \\
&\quad = \sum_{j\in\mathcal{J}(\mathcal{R})} \max\left(p(\mathcal{I}_j) - \frac{\omega}{m},\ 0\right)
\end{aligned} \tag{3.17}$$

which proves Theorem 3.5.1.1. □

Remark 1. Theorem 3.5.1.1 (as well as Corollary 3.5.1.1) appears generalizable to higher-dimensional spaces tessellated with countable equisized tiles, considering that the division $\left[\mathcal{I}_j\right]_{1\leq j\leq s}$ and the probability $p(\mathcal{I}_j)$ (Equation 3.13) can be defined in higher dimensions.

Corollary 3.5.1.1. *The probability, $\mathbb{P}(C(t) = 1, X(t) \in \mathcal{R})$, that each mobile communicates ($C(t) = 1$) in any region $\mathcal{R} = \cup_{j\in\mathcal{J}(\mathcal{R})}\mathcal{I}_j \subseteq \mathcal{S}$ is upper-bounded as*

$$\mathbb{P}(C(t) = 1, X(t) \in \mathcal{R}) \leq p(\mathcal{R}) - \sum_{j\in\mathcal{J}(\mathcal{R})} \max\left(p(\mathcal{I}_j) - \frac{\omega}{m},\ 0\right). \tag{3.18}$$

Proof. This follows from Theorem 3.5.1.1 and the fact that the probability of a mobile falling into any region $\mathcal{R}$ without energy depletion equals $p(\mathcal{R})$. □

3.5.2 Tightness of Bounds

Now we can assess the tightness of the bounds of Equations (3.15)(3.18) against simulation results. From Corollary 3.4.2.1 the stationary mobile distribution, $f_{X(t),U(t)=0}(x)$, assuming $d \leq \frac{1}{2}$ and $c \in [d, 1-d]$, can be given by

$$\alpha f_{X(t),U(t)=0}(x) = \begin{cases} 2x - \frac{3x^2}{2}, & \text{if } x \in [0, d) \\ d + (1-d)x - \frac{x^2}{2}, & \text{if } x \in [d, c) \\ \frac{1}{2} + dx - \frac{x^2}{2}, & \text{if } x \in [c, 1-d] \\ \frac{1}{2} + x - \frac{3x^2}{2}, & \text{if } x \in (1-d, 1] \end{cases} \tag{3.19}$$

As a general case, suppose $\mathcal{R} = \mathcal{S}$. Then, by plugging Equation (3.19) into Equation (3.15), we can calculate the lower bound $\sum_{j \in \mathcal{J}(\mathcal{S})} \max\left(p(\mathcal{I}_j) - \frac{\omega}{m},\ 0\right)$, as long as the values of m, ω, d, c, and s are given. For example, for $m = 8000$, $\omega = 4$, $d = 0.2$, $c = 0.3$ (thus $\alpha = c^2 - c + \frac{2}{3} = 0.4567$), and $s = 10^3$, we have $\mathbb{P}\left(C(t) = 0, X(t) \in \mathcal{R}, U(t) = 0\right) \geq 29\%$, which is quite close to 31.27%, the corresponding result from the simulation.

Figure 3.6 shows the probabilities that each mobile is blocked or communicating versus different settings of ω, with $m = 8000$, $d = 0.2$, and different positions of the charger $c = 0.1, 0.3, 0.5$. Specifically, Figure 3.6(a), depicts the lower bound versus the simulation results for the probability of blocking. The shaded areas indicate the difference between the two lines. It can be seen that the lower bound of Equation (3.15) becomes less tight as the capacity ω increases. Figure 3.6(b) depicts the upper bound on the probability of successful communication versus the simulation results. It is evident that the simulation results diverge further from the upper bound (Equation (3.18)) as the capacity increases. These patterns demonstrate the fact that the bounds derived apply best to heavily loaded systems, where at any time a good portion of mobiles tend to be blocked due to the constraint of a low capacity.[2] Hence, the bound provides a better prediction if we focus $\mathcal{R}$ to the popular regions where the operational mobiles tend to cluster (e.g. $\mathcal{R} = [0.3, 0.5]$ when $c = 0.3$).

3.5.3 Effects and Tradeoffs of Detours

Finally we explore the effects and tradeoffs related to the detours the mobiles would take to recharge. For this we consider the (MD) model used so far where, once the energy is depleted, the mobile will move towards the charger possibly causing the mobile to move further away from its destination. As an alternative, we also consider the model, called M, where a mobile will not detour to recharge. In this model, a mobile will only be able to recharge if the charger is on the path towards the destination. In both cases, mobiles are given an energy budget of d when they arrive at a waypoint and start towards

[2]Equivalently, the system load and thus the bound accuracy would increase with the total number of mobiles m.

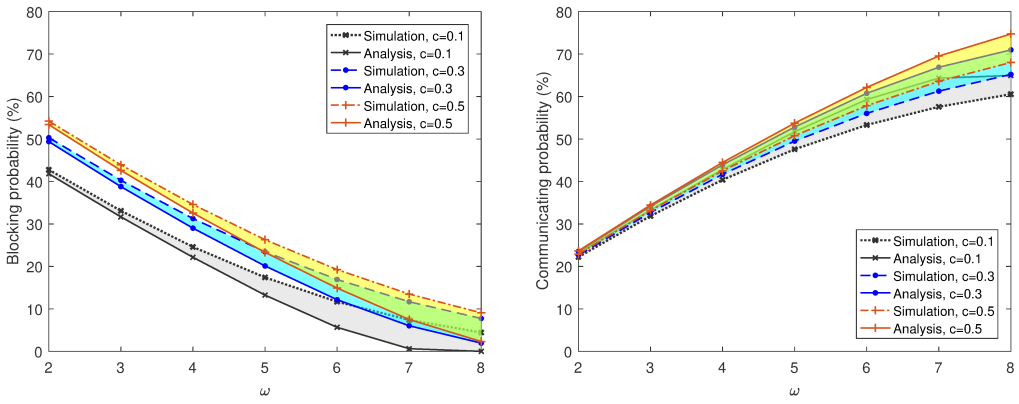

(a) (b)

Figure 3.6: Simulation vs. analytical results for a mobile being (a) blocked or (b) communicating, for various capacities (per interval), ω, with $m = 8000$, $d = 0.2$, and $c = 0.1, 0.3, 0.5$, respectively.

a new one. As one of our main contributions, we will investigate the interplay of the energy budget d and the extent of congestion depending on whether detours are considered or not.

We also note that in Figure 3.6, the performance of mobiles appears to be affected by the charger location; a centered charger would maximize the communication activity of mobiles. This is primarily because the expected travel distance to the charger decreases as the charger location moves inwards, which lets the network of mobiles as a whole gain more energy. Thus in the following experiment we plot results for different charger locations to study and compare the two mobility models, MD and M.

Under the mobility model MD, each mobile appears more likely to be blocked (because of exceeding capacity instead of energy depletion) or communicating successfully in a highly-energized system ($d = 0.6$) than in an under-energized one ($d = 0.2$), regardless of the charger location and capacity, as shown in Figure 3.7. When the capacity is low ($\omega = 2$), the mobiles, especially those under-energized, tend to be blocked more if the charger is placed at the innermost location. This is because the mobiles can visit the charger more easily when it is centered; hence, it results in more operational mobiles in the entire segment. Meanwhile, the chances of successful communication remain steady because of saturation of the capacity. Under a high capacity ($\omega = 8$),

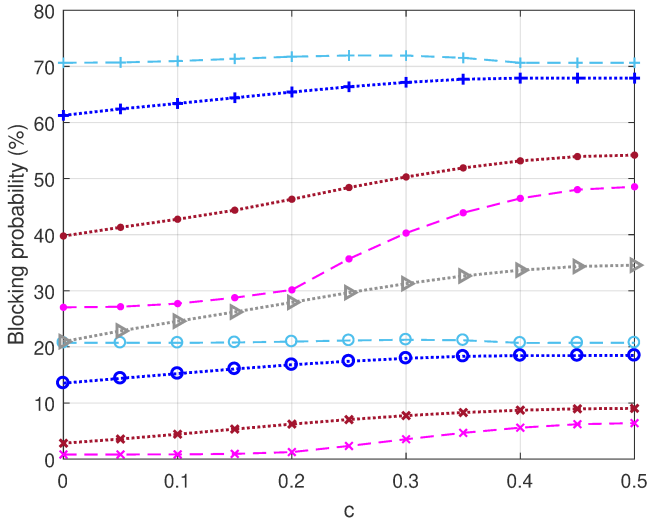

(a)

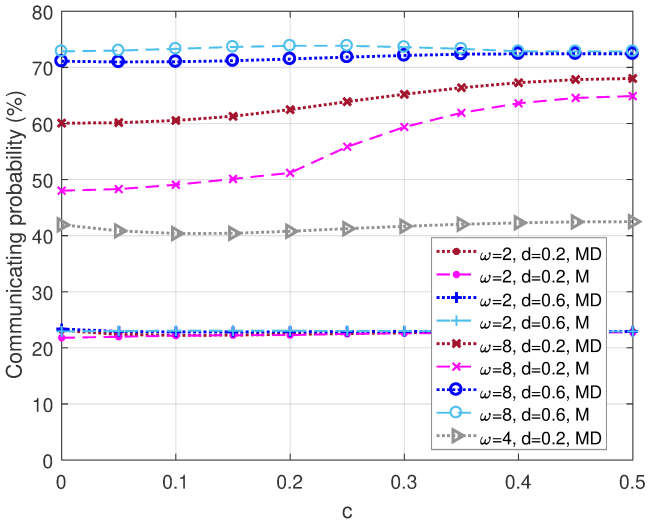

(b)

Figure 3.7: Simulation results for a mobile being (a) blocked or (b) communicating, assuming $d = 0.2$ and 0.6, and $\omega = 2$, 4, and 8, with c being the location of the charger.

when the charger location is placed inwards, under-energized mobiles have their communication improved, to a greater extent than the highly-energized ones (which see only minor improvements). Under-energized mobiles need to detour to recharge at the charger more often, and thus the more central the charger is, the more improvement is seen in terms of communication. Under mobility model MD, the performance of under-energized mobiles shows a higher sensitivity to the charger location than that of highly-energized ones.

A noteworthy pattern regarding the MD model is that the mobiles are not guaranteed to be more likely to communicate when the charger is placed inwards, although their energy keeps increasing (Figure 3.8). As shown in Figure 3.7(b), when $\omega = 4$ and $d = 0.2$, the communicating probability of a mobile under MD descends somewhat to its lowest around 0.1 before increasing again. This type of behavior has been seen when capacity $\omega < 8$ and is more prominent when the mobiles are under-energized. We make the following inferences about the reasons. When the charger is located at the boundary, the mobiles would rarely visit the charger without taking potentially long detours. As the charger location is placed further inwards, the mobiles can, on average, be more likely to recharge; meanwhile, however, the distortion of mobile distribution starts to emerge, which overshadows any energy gains. Specifically, when the charger is placed (not very far) away from the left boundary, mobiles that travel from the right would mostly not visit locations beyond but congregate in the locality before the charger (Figure 3.3). As a result, the exceeding capacity worsens. As the charger location moves further towards the center (from around $x = 0.15$), the mobiles can travel shorter to recharge and their distribution becomes less distorted by the charger; then, more mobiles, with energy, are able to communicate. Also, the effect of the distorted mobile distribution on communication intensifies more at medium capacities. When the capacity is high (e.g. $\omega = 8$), the communication of operational mobiles would still be accommodated even if there is heavy clustering. At a low capacity (e.g. $\omega = 2$), the performance of communication would remain inferior, being impacted little by the charger location.

When we consider the mobility model, M, where mobiles are not allowed to detour towards the charger, the above pattern shown in model MD does not occur for any charger location and capacity. The probabilities of blocking (because of exceeding capacity instead of energy depletion) and successful communication of the under-energized mobiles are lower than for the MD model. This is because fewer mobiles would have energy without the compensation from detours for recharging. However, highly-energized mobiles under model M are more likely to be blocked or communicate successfully than under model

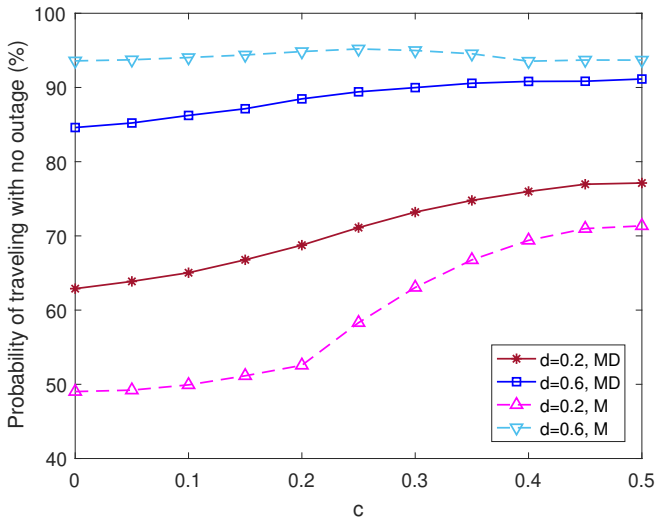

Figure 3.8: Probabilities of traveling while having energy, under the MD and the M models, for arbitrary capacity, versus location of the charger (c). The two top lines are for over-energized systems ($d = 0.6$) while the two bottom lines are for under-energized systems ($d = 0.2$).

MD. The longer paths of the MD model (which allows detours) have a reducing effect on the overall energy. This can be seen in Figure 3.8 where the fraction of time a mobile travels while having energy is plotted for different placements of the charger. Generally, under-energized mobiles are more prone to energy shortage, which can be ameliorated by the detours for recharging. The highly-energized ones, however, have their energy conditions and performance impaired because of the redundant traveling. Note that the energy gains from detours are always at the expense of (possibly large) delays in the arrival times at waypoints. As shown in Figure 3.9, it would take long for the mobiles that follow mobility MD to reach the waypoints, especially if the mobiles are under-energized and the charger is deployed far away from the center.

We note an interesting tradeoff between the MD and M models. If the system has low energy, then a model (MD) where mobiles detour towards the charger is preferred; if the system is highly energized then no detour works best. If it is not known whether there is high or low energy, movements with detours suggest the middle ground. However, detours will obviously cause significant delays towards reaching a waypoint.

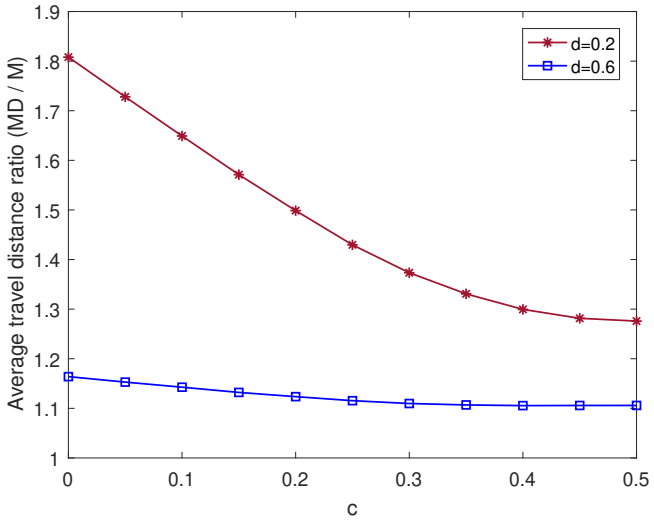

Figure 3.9: Average ratio of travel distance (between waypoints) under model MD over that under M, with $d = 0.2$ and 0.6, vs. charger location (c).

3.6 Chapter Summary

This chapter proposes an analytical model of user mobility in the presence of recharging opportunities for a 1-dimensional system. We verify the analysis with simulation and analyze the effect of the boundaries on the location of mobiles. We find that the boundaries create discontinuities in the location of mobiles at the charger location and, if the charger is very near to the boundary (i.e. within d, the energy budget, of the boundary), the highest concentration is not at the charger location. We add capacity limitations to our model and derive an upper bound for the probability that a mobile can communicate and a lower bound for the probability that a mobile has energy but is blocked due to a lack of capacity. We find that these bounds are tighter when capacity is more constrained. Finally we analyze the tradeoffs of systems where mobiles take detours versus systems where no detours are made for different placement of chargers. Unsurprisingly, placing the charger in the center has slightly better performance. We find that if there is not much energy in the system, a model with detours is beneficial as long as delays to arrive at the intended destinations can be tolerated. If the energy of the system is not known, a heuristic that promotes detours may improve performance. In high energy systems no detour is preferable.

Chapter 4

Charging-Aware Mobility in 2-D Space

4.1 Introduction

In this chapter we study the 2-dimensional charging-aware mobility in a unit disk in the Euclidean plane. In addition to the energy budget d of the mobile, we introduce a parameter d' to account for the charger's attraction range; a depleted mobile falling within a radius d' of the charger would be diverted for recharging. Based on this model, we analyze the overall stationary mobile distribution across the area, examine the energy-wise mobile distribution through simulation, and provide the approximate results for multiple chargers.

The rest of the chapter is organized as follows: In Section 4.2, we first describe assumptions of the 2-dimensional mobility model and illustrate the trajectory involving a detour to the charger. In Section 4.3, we formulate the case-wise stationary expectation of the mobile location (depending on whether the mobile takes a detour or not), in preparation for the analysis of Section 4.4. In Section 4.4, we analyze the overall stationary mobile distribution under the assumed mobility model, making remarks on its implications and generalizations. In Section 4.5, we demonstrate the analytical results by simulation (subsection 4.5.1) and obtain the numerical results of mobile distribution subject to energy availability (subsection 4.5.2); besides, we consider the extension to multiple chargers and propose a solution of approximation based on individual chargers (subsection 4.5.3). We summarize the chapter in Section 4.6.

4.2 Assumptions

We assume the space is a *unit disk* $\Omega = \{z \in \mathbb{R}^2 \mid |z| \leq 1\}$ in the 2-dimensional Euclidean plane. A static charger is deployed at a location $c = (a, b) \in \Omega$. Like the RWP model, the mobile starts its movement from a random source waypoint at $W_0 = (U_0, V_0) \in \Omega$, and moves, at a constant speed v, towards a random destination at $W_1 = (U_1, V_1) \in \Omega$; upon arrival at W_1, the mobile *immediately* (with no pause) turns towards another randomly selected location in the area as the destination of a new *trip*, and so on. From each waypoint, the mobile, which keeps consuming its energy (if any) for communication only, departs with an energy budget that permits continuous communication up to a *constant* travel distance $d \geq 0$. In the case that the mobile has traveled d (from the source) but still not reached the destination, it could deviate from the straight path and detour to the charger for replenishment *as soon as* it ever falls into the "attraction" range of the charger, i.e. within a radius $d' > 0$ of c (Figure 3.1). The *detour point* is denoted by $W_q = (U_q, V_q) = W_0 + Q(\cos\Theta_0, \sin\Theta_0)$, where $Q = |W_0 - W_q|$ is the distance between W_0 and W_q and $\Theta_0 = \angle(W_1 - W_0)$ is the angle of the destination W_1 with respect to the source W_0.

Note that the mobile is assumed to behave like a "reactive agent", in the sense that it would *not* initiate a detour to the charger *until* passing the *depletion point* at $W_d = (U_d, V_d) = W_0 + d(\cos\Theta_0, \sin\Theta_0)$ (thus $Q \geq d$). Also, the mobile would recharge sufficiently such that it need not detour again before arriving at the destination. Given this charging-aware mobility model, our primary goal is to derive the time stationary pdf (probability density function) $f_{Z(t)}(z)$ of the mobile location $Z(t)$ over time t.

4.3 Stationary Expectation of Mobile Location

Next we redefine W_0 and W_1 as waypoints in the stationary regime. Following the Palm inversion formula [47], we can calculate the (time) stationary

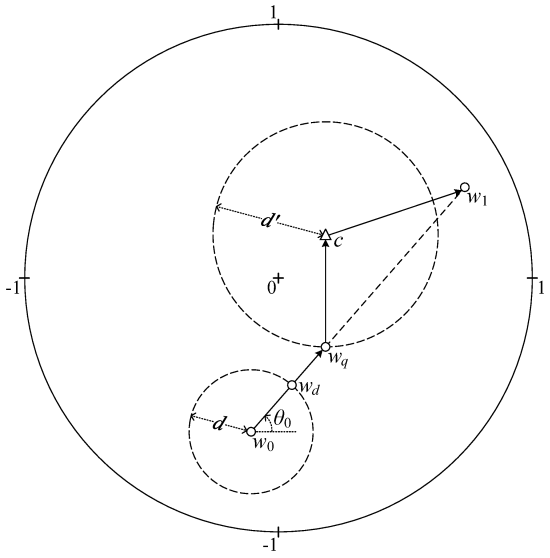

Figure 4.1: A trip of the mobile involving a detour to the charger. The detour starts from w_q (after the depletion point w_d), which is at a distance of d' to the charger.

expectation of the mobile location as

$$\mathbb{E}\left[Z(t)\right] = \lambda \mathbb{E}^0 \left[\int_0^{T_1} Z(\tau)\,\mathrm{d}\tau\right] = \frac{\lambda}{\pi^2} \iint_{\Omega^2} \int_0^{T_1} Z(\tau)\,\mathrm{d}\tau\,\mathrm{d}w_0\,\mathrm{d}w_1 \tag{4.1}$$

where $\mathbb{E}^0(\cdot) = \mathbb{E}(\cdot|\xi_0)$ is the conditional expectation given the event ξ_0 that the mobile departs from a source w_0 at time $T_0 = 0$, and T_1 is the time instant when the mobile arrives at a destination w_1. Also, $\lambda^{-1} = \frac{\alpha}{v}$ is the expected trip time (including detours, if any) between any source-destination pair, with α being the expected trip distance. Note that $\pi^{-2} = f(w_0)f(w_1)$, since the waypoints follow a uniform distribution over the unit disk.

4.3.1 Case I: Direct Path

The mobile would move straight to the destination without detouring to the charger, if *either* of the following two conditions is satisfied:

1) The distance between the source w_0 and the destination w_1 is less than or equal to d, so that the mobile can reach the destination before its energy is depleted, i.e.

$$|w_0 - w_1| = \sqrt{(u_0 - u_1)^2 + (v_0 - v_1)^2} \leq d. \tag{4.2}$$

2) When the destination cannot be reached within d from the source (i.e. $|w_0 - w_1| > d$), the charger is located too distantly to attract and divert the mobile after depletion. Formally, this means the minimum distance from the charger c to the path from the depletion point w_d to w_1 is larger than d', i.e.

$$\min_{z \in \mathcal{P}(w_d, w_1)} |z - c| > d' \tag{4.3}$$

where $\mathcal{P}(w_d, w_1) = \{z = (1 - \varrho)w_d + \varrho w_1 \mid \varrho \in [0, 1)\}$.[1]

Accordingly, the expectation of Equation (4.1) assuming that the mobile only takes direct paths can be expanded as

$$\begin{aligned}
\lambda \mathbb{E}_{\mathrm{I}}^0 \left[\int_0^{T_1} Z(\tau) \, \mathrm{d}\tau \right] &= \lambda \mathbb{E}^0 \left[\int_0^{T_1} w_0 + \frac{w_1 - w_0}{T_1} \tau \, \mathrm{d}\tau \right] \\
&= \lambda \mathbb{E}^0 \left[T_1 \int_0^1 (1 - \rho_0) w_0 + \rho w_1 \, \mathrm{d}\rho_0 \right] \\
&= \frac{1}{\pi^2 \alpha} \iint_{\mathcal{W}_{\mathrm{I}}} |w_0 - w_1| \int_0^1 (1 - \rho_0) w_0 + \rho_0 w_1 \, \mathrm{d}\rho_0 \, \mathrm{d}w_0 \, \mathrm{d}w_1
\end{aligned} \tag{4.4}$$

where $\mathcal{W}_{\mathrm{I}} \subset \mathbb{R}^4$ is the admissible domain of double integration over w_0 and w_1, i.e.

$$\mathcal{W}_{\mathrm{I}} = \begin{cases} \mathcal{W}_0 \cup \mathcal{W}_1 \cup \mathcal{W}_2 \cup \mathcal{W}_3, & \text{if } d \le d' \\ \mathcal{W}_0 \cup \mathcal{W}_1 \cup \mathcal{W}_2 \cup \mathcal{W}_4, & \text{if } d > d' \end{cases} \tag{4.5}$$

with

$$\begin{cases}
\mathcal{W}_0 = \{(w_0, w_1) \mid w_0 \in \Omega \setminus \overline{\mathcal{D}}(c, d' + d), w_1 \in \mathcal{L}(w_0, c, d')\} \\
\mathcal{W}_1 = \{(w_0, w_1) \mid w_0 \in \overline{\mathcal{D}}(c, d' + d) \setminus \overline{\mathcal{D}}(c, \sqrt{d'^2 + d^2}) \cap \Omega, \\
\qquad\qquad w_1 \in \mathcal{L}(w_0, c, d') \cup \overline{\mathcal{D}}(w_0, d) \cap \Omega\} \\
\mathcal{W}_2 = \{(w_0, w_1) \mid w_0 \in \overline{\mathcal{D}}(c, \sqrt{d'^2 + d^2}) \setminus \overline{\mathcal{D}}(c, |d' - d|) \cap \Omega, \\
\qquad\qquad w_1 \in \mathcal{F}(w_0, \theta_3, \theta_4) \cup \overline{\mathcal{D}}(w_0, d) \cap \Omega\} \\
\mathcal{W}_3 = \{(w_0, w_1) \mid w_0 \in \overline{\mathcal{D}}(c, |d' - d|) \cap \Omega, w_1 \in \overline{\mathcal{D}}(w_0, d) \cap \Omega\} \\
\mathcal{W}_4 = \{(w_0, w_1) \mid w_0 \in \overline{\mathcal{D}}(c, |d' - d|) \cap \Omega, w_1 \in \Omega\}
\end{cases} \tag{4.6}$$

and

$$\mathcal{L}(w_0, c, d') = \Omega \setminus \overline{\mathcal{F}}(w_0, \theta_1, \theta_2) \cup \overline{\mathcal{F}}(w_0, \theta_1, \theta_2, d_0) \setminus \mathcal{D}(c, d'). \tag{4.7}$$

Relevant basic domains are defined as follows.

[1] Hence the detour point (if any) can be defined as $w_q = \operatorname{argmin}_{\varrho \in [0,1)} \mathcal{P}(w_d, w_1)$ subject to $|c - w_q| \le d'$.

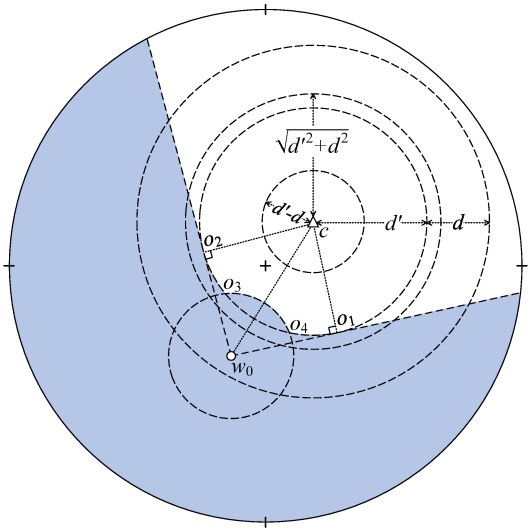

Figure 4.2: Illustration of the admissible domain of integration over w_1 given $w_0 \in \overline{\mathcal{D}}(c, d' + d) \setminus \overline{\mathcal{D}}(c, \sqrt{d'^2 + d^2}) \cap \Omega$, such that the mobile would follow a direct path throughout the trip. The shaded area corresponds to $w_1 \in \mathcal{L}(w_0, c, d') \cup \overline{\mathcal{D}}(w_0, d) \cap \Omega$.

- $\overline{\mathcal{D}}(c, d' + d)) = \{z \mid |z - c| \leq d' + d\}$: the closed disk centered at the charger c with radius $d' + d$. Similar definitions apply to $\overline{\mathcal{D}}(c, \sqrt{d'^2 + d^2})$, $\overline{\mathcal{D}}(w_0, d)$, $\overline{\mathcal{D}}(c, |d' - d|)$, and $\mathcal{D}(c, d') = \{z \mid |z - c| < d'\}$ (which is an open disk).

- $\overline{\mathcal{F}}(w_0, \theta_1, \theta_2) = \{z \mid \angle(z - w_0) \in [\theta_1, \theta_2]\}$: the sector confined by two rays (originating from the source w_0) angled towards $\theta_1 = \angle(o_1 - w_0)$ and $\theta_2 = \angle(o_2 - w_0)$ respectively, where o_1 and o_2 (Figure 4.2) are the two intersections between circles $C(c, d') = \{z \mid |z - c| = d'\}$ and $C(w_0, d_0)$, with $d_0 = \sqrt{|c - w_0|^2 - d'^2}$. The definition of $\overline{\mathcal{F}}(w_0, \theta_1, \theta_2, d_0)$ follows that of $\overline{\mathcal{F}}(w_0, \theta_1, \theta_2)$, except the sector is now enclosed with an arc, i.e. $|z - w_0| \leq d_0$, $\forall z$. For $\mathcal{F}(w_0, \theta_3, \theta_4)$, we have $\angle(z - w_0) \in (\theta_3, \theta_4)$ with $\theta_3 = \angle(o_3 - w_0)$ and $\theta_4 = \angle(o_4 - w_0)$, where o_3 and o_4 are the intersections between circles $C(c, d')$ and $C(w_0, d)$.

4.3.2 Case II: Path with Detour

As opposed to the case of direct paths, the mobile would detour to the charger if (1) the energy budget cannot cover the distance to the destination (i.e.

$|w_1 - w_0| > d$) *and* (2) the mobile will fall within a radius of d' of the charger after depletion occurs (i.e. $\min_{z\in\mathcal{P}(w_d,w_1)} |z - c| \leq d'$). The corresponding expectation of the mobile location in this case is given by

$$\begin{aligned}\lambda\mathbb{E}^0_{\mathtt{II}}\left[\int_0^{T_1} Z(\tau)\,\mathrm{d}\tau\right] &= \lambda\mathbb{E}^0\left[\int_0^{T_q} Z(\tau)\,\mathrm{d}\tau + \int_{T_q}^{T_c} Z(\tau)\,\mathrm{d}\tau + \int_{T_c}^{T_1} Z(\tau)\,\mathrm{d}\tau\right] \\ &= \frac{1}{\pi^2\alpha}\iint_{\mathcal{W}_{\mathtt{II}}} \psi(w_0, w_1)\,\mathrm{d}w_0\,\mathrm{d}w_1\end{aligned} \tag{4.8}$$

where T_q and T_c are the time instants the mobile arrives at the detour point w_q and the charger c respectively. The integrand function $\psi(w_0, w_1)$ consists of three components, i.e.

$$\begin{aligned}\psi(w_0, w_1) = |w_0 - w_q| &\int_0^1 (1-\rho_1)w_0 + \rho_1 w_q\,\mathrm{d}\rho_1 \\ + |w_q - c| &\int_0^1 (1-\rho_2)w_q + \rho_2 c\,\mathrm{d}\rho_2 \\ + |c - w_1| &\int_0^1 (1-\rho_3)c + \rho_3 w_1\,\mathrm{d}\rho_3\end{aligned} \tag{4.9}$$

which correspond to the three legs involved along the path, including $w_0 \to w_q$, $w_q \to c$, and $c \to w_1$ (Figure 4.1). As a complement to $\mathcal{W}_{\mathtt{I}}$, the admissible domain of integration, $\mathcal{W}_{\mathtt{II}}$, is defined as

$$\mathcal{W}_{\mathtt{II}} = \begin{cases}\mathcal{W}_5 \cup \mathcal{W}_6 \cup \mathcal{W}_7 \cup \mathcal{W}_8, & \text{if } d \leq d' \\ \mathcal{W}_5 \cup \mathcal{W}_6 \cup \mathcal{W}_7, & \text{if } d > d'\end{cases} \tag{4.10}$$

where

$$\begin{cases}\mathcal{W}_5 = \{(w_0, w_1) \mid w_0 \in \Omega \setminus \overline{\mathcal{D}}(c, d'+d), w_1 \in \Omega \setminus \mathcal{L}(w_0, c, d')\} \\ \mathcal{W}_6 = \{(w_0, w_1) \mid w_0 \in \overline{\mathcal{D}}(c, d'+d) \setminus \overline{\mathcal{D}}(c, \sqrt{d'^2 + d^2}) \cap \Omega, \\ \qquad\qquad w_1 \in \Omega \setminus \mathcal{L}(w_0, c, d') \setminus \overline{\mathcal{D}}(w_0, d)\} \\ \mathcal{W}_7 = \{(w_0, w_1) \mid w_0 \in \overline{\mathcal{D}}(c, \sqrt{d'^2 + d^2}) \setminus \overline{\mathcal{D}}(c, |d'-d|) \cap \Omega, \\ \qquad\qquad w_1 \in \Omega \setminus \mathcal{F}(w_0, \theta_3, \theta_4) \setminus \overline{\mathcal{D}}(w_0, d)\} \\ \mathcal{W}_8 = \{(w_0, w_1) \mid w_0 \in \overline{\mathcal{D}}(c, |d'-d|) \cap \Omega, w_1 \in \Omega \setminus \overline{\mathcal{D}}(w_0, d)\}\end{cases} \tag{4.11}$$

4.4 Stationary Distribution of Mobile Location

The stationary distribution of the mobile location, $f_{Z(t)}(z)$, can be induced from the stationary expectations of Equations (4.4)(4.8). In subsections 4.4.1 and

4.4.2, we first make substitutions for variables of the integrals with respect to the mobile's location z, and then in subsection 4.4.3, we formulate the mobile distribution in Theorem 4.4.3.1 based on the transformed integrals.

4.4.1 Direct Path

Firstly, for the case that the mobile takes a direct path only, we can change the variables ρ_0, w_0, and w_1 as follows:

$$\begin{cases} \rho_0 = \dfrac{l_0}{l_0 + l_1} \\ w_0 = z - l_0(\cos\theta_0, \sin\theta_0) \\ w_1 = z + l_1(\cos\theta_0, \sin\theta_0) \end{cases} \tag{4.12}$$

where $z = (x, y) = r(\cos\vartheta, \sin\vartheta)$, and l_0 (l_1 resp.) is the distance from z to the source w_0 (destination w_1 resp.). The Jacobian (determinant) of such change of variables is computed to be $J(x, y, l_0, l_1, \theta_0) = 1$. Suppose $d' + d \le 1 - |c|$ such that $\overline{\mathcal{D}}(c, d' + d) \subseteq \Omega$. Then, leaving aside the scalar $(\pi^2\alpha)^{-1}$ (to be covered in subsection 4.4.3), Equation (4.4) can be expanded as

$$\begin{aligned} &\iint_{\mathcal{W}_1} |w_0 - w_1| \int_0^1 (1-\rho_0)w_0 + \rho_0 w_1 \,\mathrm{d}\rho_0 \,\mathrm{d}w_0 \,\mathrm{d}w_1 \\ &\quad = \int_{\mathcal{Z}_0} z \cdot f_0(z)\,\mathrm{d}z + \int_{\mathcal{Z}_1} z \cdot f_1(z)\,\mathrm{d}z + \int_{\mathcal{Z}_2} z \cdot f_2(z)\,\mathrm{d}z \\ &\qquad + \int_{\mathcal{Z}_3} z \cdot f_3(z)\,\mathrm{d}z + \int_{\mathcal{Z}_4} z \cdot f_4(z)\,\mathrm{d}z \end{aligned} \tag{4.13}$$

where the domains of integration, $\mathcal{Z}_2$, $\mathcal{Z}_3$, and $\mathcal{Z}_4$, and the pdf's, $f_3(z)$ and $f_4(z)$, are defined depending on the value of d relative to d'. Specifically, we have

$$\mathcal{Z}_0 = \Omega \setminus \overline{\mathcal{D}}(c, d' + d) \tag{4.14}$$

$$\mathcal{Z}_1 = \overline{\mathcal{D}}(c, d' + d) \setminus \overline{\mathcal{D}}(c, \sqrt{d'^2 + d^2}) \tag{4.15}$$

$$\mathcal{Z}_2 = \begin{cases} \overline{\mathcal{D}}(c, \sqrt{d'^2 + d^2}) \setminus \overline{\mathcal{D}}(c, d'), & \text{if } d \le 2d' \\ \overline{\mathcal{D}}(c, \sqrt{d'^2 + d^2}) \setminus \overline{\mathcal{D}}(c, d - d'), & \text{if } d > 2d' \end{cases} \tag{4.16}$$

$$\mathcal{Z}_3 = \begin{cases} \overline{\mathcal{D}}(c, d') \setminus \overline{\mathcal{D}}(c, |d' - d|), & \text{if } d \le 2d' \\ \overline{\mathcal{D}}(c, d - d') \setminus \overline{\mathcal{D}}(c, d'), & \text{if } d > 2d' \end{cases} \tag{4.17}$$

$$\mathcal{Z}_4 = \begin{cases} \overline{\mathcal{D}}(c, |d' - d|), & \text{if } d \le 2d' \\ \overline{\mathcal{D}}(c, d'), & \text{if } d > 2d' \end{cases} \tag{4.18}$$

and

$$f_0(z) = \int_{\theta_5-\theta_6}^{\theta_5+\theta_6} \phi_0 \,\mathrm{d}\theta_0' + \int_{\theta_5+\theta_6}^{\theta_5-\theta_6+\pi} \phi_1 \,\mathrm{d}\theta_0' + \int_{\theta_5-\theta_6+\pi}^{\theta_5+\theta_6+\pi} \phi_2 \,\mathrm{d}\theta_0' + \int_{\theta_5+\theta_6+\pi}^{\theta_5-\theta_6+2\pi} \phi_1 \,\mathrm{d}\theta_0' \tag{4.19}$$

$$f_1(z) = \int_{\theta_5-\theta_6}^{\theta_5+\theta_6} \phi_0 \,\mathrm{d}\theta_0' + \int_{\theta_5+\theta_6}^{\theta_5-\theta_6+\pi} \phi_1 \,\mathrm{d}\theta_0' + \int_{\theta_5-\theta_6+\pi}^{\theta_5-\theta_7+\pi} \phi_2 \,\mathrm{d}\theta_0' + \int_{\theta_5-\theta_7+\pi}^{\theta_5+\theta_7+\pi} \phi_3 + \phi_4 \,\mathrm{d}\theta_0' + \int_{\theta_5+\theta_7+\pi}^{\theta_5+\theta_6+\pi} \phi_2 \,\mathrm{d}\theta_0' + \int_{\theta_5+\theta_6+\pi}^{\theta_5-\theta_6+2\pi} \phi_1 \,\mathrm{d}\theta_0' \tag{4.20}$$

$$f_2(z) = \int_{\theta_5-\theta_6}^{\theta_5+\theta_6} \phi_0 \,\mathrm{d}\theta_0' + \int_{\theta_5+\theta_6}^{\theta_5-\theta_6+\pi} \phi_1 \,\mathrm{d}\theta_0' + \int_{\theta_5-\theta_6+\pi}^{\theta_5-\theta_7+\pi} \phi_0 + \phi_4 + \phi_5 \,\mathrm{d}\theta_0' + \int_{\theta_5-\theta_7+\pi}^{\theta_5+\theta_7+\pi} \phi_3 + \phi_4 \,\mathrm{d}\theta_0' + \int_{\theta_5+\theta_7+\pi}^{\theta_5+\theta_6+\pi} \phi_0 + \phi_4 + \phi_5 \,\mathrm{d}\theta_0' + \int_{\theta_5+\theta_6+\pi}^{\theta_5-\theta_6+2\pi} \phi_1 \,\mathrm{d}\theta_0' \tag{4.21}$$

$$f_3(z) = \begin{cases} f_{3a}(z), & \text{if } d \le 2d' \\ f_{3b}(z), & \text{if } d > 2d' \end{cases} \tag{4.22}$$

$$f_4(z) = \begin{cases} f_{4a}(z), & \text{if } d \le d' \\ f_{4b}(z), & \text{if } d > d' \end{cases} \tag{4.23}$$

$$f_{3a}(z) = \int_{\theta_5+\theta_7-\pi}^{\theta_5-\theta_7+\pi} \phi_0 + \phi_6 \,\mathrm{d}\theta_0' + \int_{\theta_5-\theta_7+\pi}^{\theta_5+\theta_7+\pi} \phi_7 \,\mathrm{d}\theta_0' \tag{4.24}$$

$$f_{3b}(z) = \int_{\theta_5-\theta_6}^{\theta_5+\theta_6} \phi_0 \,\mathrm{d}\theta_0' + \int_{\theta_5+\theta_6}^{\theta_5-\theta_6+\pi} \phi_1 \,\mathrm{d}\theta_0' + \int_{\theta_5-\theta_6+\pi}^{\theta_5+\theta_6+\pi} \phi_0 + \phi_4 + \phi_5 \,\mathrm{d}\theta_0' + \int_{\theta_5+\theta_6+\pi}^{\theta_5-\theta_6+2\pi} \phi_1 \,\mathrm{d}\theta_0' \tag{4.25}$$

$$f_{4a}(z) = \int_0^{2\pi} \phi_7 \,\mathrm{d}\theta_0' \tag{4.26}$$

$$f_{4b}(z) = \int_0^{2\pi} \phi_0 + \phi_6 \,\mathrm{d}\theta_0' \tag{4.27}$$

where

$$\begin{cases} \theta_0' = \theta_0 + \pi \\ \theta_5 = \operatorname{atan2}(b-y, a-x) \\ \theta_6 = \arcsin\left(\dfrac{d'}{|z-c|}\right) \\ \theta_7 = \arccos\left(\dfrac{d^2 + |z-c|^2 - d'^2}{2d|z-c|}\right) \end{cases} \tag{4.28}$$

and

$$\begin{cases} \phi_0 = \int_0^{l_4+d} \int_0^{l_2} l_0 + l_1 \, \mathrm{d}l_1 \, \mathrm{d}l_0 \\ \phi_1 = \int_0^{l_3} \int_0^{l_2} l_0 + l_1 \, \mathrm{d}l_1 \, \mathrm{d}l_0 \\ \phi_2 = \int_0^{l_3} \int_0^{-l_5} l_0 + l_1 \, \mathrm{d}l_1 \, \mathrm{d}l_0 \\ \phi_3 = \int_0^{l_5+d} \int_0^{d-l_0} l_0 + l_1 \, \mathrm{d}l_1 \, \mathrm{d}l_0 \end{cases} \qquad \begin{cases} \phi_4 = \int_{l_5+d}^{l_3} \int_0^{-l_5} l_0 + l_1 \, \mathrm{d}l_1 \, \mathrm{d}l_0 \\ \phi_5 = \int_{l_4+d}^{l_5+d} \int_0^{d-l_0} l_0 + l_1 \, \mathrm{d}l_1 \, \mathrm{d}l_0 \\ \phi_6 = \int_{l_4+d}^{d} \int_0^{d-l_0} l_0 + l_1 \, \mathrm{d}l_1 \, \mathrm{d}l_0 \\ \phi_7 = \int_0^{d} \int_0^{d-l_0} l_0 + l_1 \, \mathrm{d}l_1 \, \mathrm{d}l_0 \end{cases} \tag{4.29}$$

with

$$\begin{cases} l_2 = \sqrt{1 - r^2 \sin^2(\theta_0' - \vartheta)} + r \cos\big(\theta_0' - \vartheta\big) \\ l_3 = \sqrt{1 - r^2 \sin^2(\theta_0' - \vartheta)} - r \cos\big(\theta_0' - \vartheta\big) \\ l_4 = |z - c| \cos\big(\theta_0' - \theta_5\big) - \sqrt{d'^2 - |z - c|^2 \sin^2(\theta_0' - \theta_5)} \\ l_5 = |z - c| \cos\big(\theta_0' - \theta_5\big) + \sqrt{d'^2 - |z - c|^2 \sin^2(\theta_0' - \theta_5)} \end{cases} \tag{4.30}$$

The variables defined in Equation (4.28)(4.30) are illustrated in Figure 4.3(a).

4.4.2 Path with Detour

In this case, the expected mobile location is evaluated in a piecewise manner, corresponding to the three legs of a trip that includes a detour to the charger. Again, assume $d' + d \leq 1 - |c|$. For the first leg from the source w_0 to the detour point w_q, suppose w_0 and w_1 are such that $w_d \in \Omega \setminus \overline{\mathcal{D}}(c, d')$ and thus $w_q \neq w_d$; the variables can then be changed as

$$\begin{cases} \rho_1 = \dfrac{l_0}{l_0 - l_5} \\ w_0 = z - l_0(\cos\theta_0, \sin\theta_0) \\ w_1 = z + l_1(\cos\theta_0, \sin\theta_0) \end{cases} \tag{4.31}$$

of which the Jacobian is $J(x, y, l_0, l_1, \theta_0) = \frac{l_0+l_1}{l_0-l_5} = \frac{l_0+l_1}{|w_0-w_q|}$. When $w_d \in \overline{\mathcal{D}}(c, d')$ and $w_q = w_d$, we have $\rho_1 = \frac{l_0}{d}$ and the Jacobian equal to $\frac{l_0+l_1}{d} = \frac{l_0+l_1}{|w_0-w_q|}$. Hence, generally, the expected mobile location (ignoring $(\pi^2\alpha)^{-1}$ for now) for the first

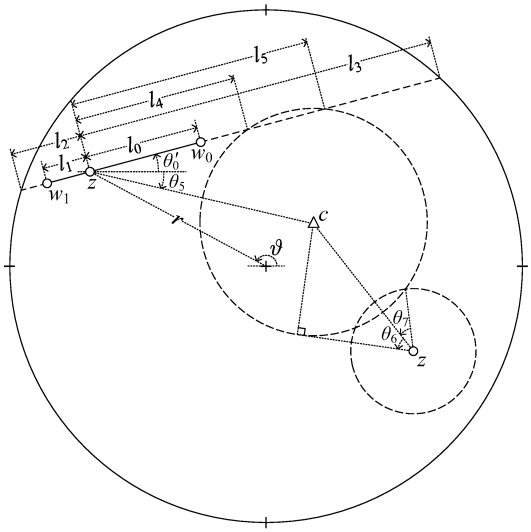

(a)

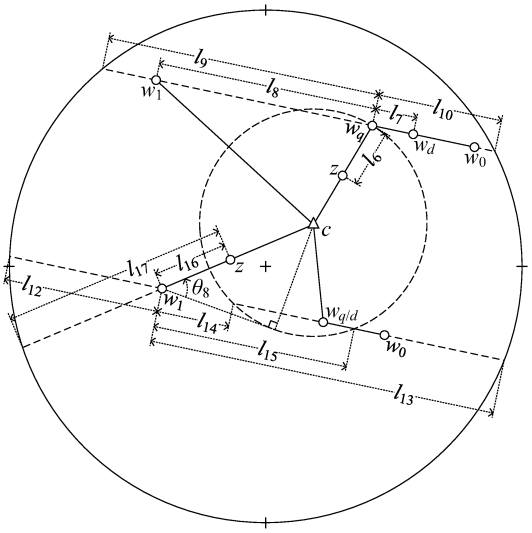

(b)

Figure 4.3: Illustration of angles and distances defined in the case of (a) direct paths and (b) paths with detours.

component of $\psi(w_0, w_1)$ is

$$\begin{aligned}
&\iint_{\mathcal{W}_{\mathrm{II}}} |w_0 - w_q| \int_0^1 (1-\rho_1)w_0 + \rho_1 w_q \,\mathrm{d}\rho_1 \,\mathrm{d}w_0 \,\mathrm{d}w_1 \\
&\quad = \int_{\mathcal{Z}_0} z \cdot f_5(z) \,\mathrm{d}z + \int_{\mathcal{Z}_1} z \cdot f_6(z) \,\mathrm{d}z + \int_{\mathcal{Z}_2} z \cdot f_7(z) \,\mathrm{d}z \\
&\qquad + \int_{\mathcal{Z}_3} z \cdot f_8(z) \,\mathrm{d}z + \int_{\mathcal{Z}_4} z \cdot f_9(z) \,\mathrm{d}z
\end{aligned} \tag{4.32}$$

where the domains $\mathcal{Z}_0$ to $\mathcal{Z}_4$ are defined as in Equations (4.15) to (4.18), while the pdf's are given by

$$f_5(z) = \int_{\theta_5-\theta_6+\pi}^{\theta_5+\theta_6+\pi} \phi_8 \, \mathrm{d}\theta_0' \tag{4.33}$$

$$f_6(z) = \int_{\theta_5-\theta_6+\pi}^{\theta_5-\theta_7+\pi} \phi_8 \, \mathrm{d}\theta_0' + \int_{\theta_5-\theta_7+\pi}^{\theta_5+\theta_7+\pi} \phi_9 + \phi_{10} \, \mathrm{d}\theta_0' + \int_{\theta_5+\theta_7+\pi}^{\theta_5+\theta_6+\pi} \phi_8 \, \mathrm{d}\theta_0' \tag{4.34}$$

$$\begin{aligned} f_7(z) = &\int_{\theta_5-\theta_6+\pi}^{\theta_5-\theta_7+\pi} \phi_{10} + \phi_{11} \, \mathrm{d}\theta_0' + \int_{\theta_5-\theta_7+\pi}^{\theta_5+\theta_7+\pi} \phi_9 + \phi_{10} \, \mathrm{d}\theta_0' \\ &+ \int_{\theta_5+\theta_7+\pi}^{\theta_5+\theta_6+\pi} \phi_{10} + \phi_{11} \, \mathrm{d}\theta_0' \end{aligned} \tag{4.35}$$

$$f_8(z) = \begin{cases} f_{8a}(z), & \text{if } d \le 2d' \\ f_{8b}(z), & \text{if } d > 2d' \end{cases} \tag{4.36}$$

$$f_9(z) = \begin{cases} f_{9a}(z), & \text{if } d \le d' \\ f_{9b}(z), & \text{if } d > d' \end{cases} \tag{4.37}$$

$$f_{8a}(z) = \int_{\theta_5+\theta_7-\pi}^{\theta_5-\theta_7+\pi} \phi_{12} \, \mathrm{d}\theta_0' + \int_{\theta_5-\theta_7+\pi}^{\theta_5+\theta_7+\pi} \phi_{13} \, \mathrm{d}\theta_0' \tag{4.38}$$

$$f_{8b}(z) = \int_{\theta_5-\theta_6+\pi}^{\theta_5+\theta_6+\pi} \phi_{10} + \phi_{11} \, \mathrm{d}\theta_0' \tag{4.39}$$

$$f_{9a}(z) = \int_0^{2\pi} \phi_{13} \, \mathrm{d}\theta_0' \tag{4.40}$$

$$f_{9b}(z) = \int_0^{2\pi} \phi_{12} \, \mathrm{d}\theta_0' \tag{4.41}$$

with

$$\begin{cases} \phi_8 = \displaystyle\int_0^{l_3} \int_{-l_5}^{l_2} l_0 + l_1 \, \mathrm{d}l_1 \, \mathrm{d}l_0 \\ \phi_9 = \displaystyle\int_0^{l_5+d} \int_{d-l_0}^{l_2} l_0 + l_1 \, \mathrm{d}l_1 \, \mathrm{d}l_0 \\ \phi_{10} = \displaystyle\int_{l_5+d}^{l_3} \int_{-l_5}^{l_2} l_0 + l_1 \, \mathrm{d}l_1 \, \mathrm{d}l_0 \end{cases} \qquad \begin{cases} \phi_{11} = \displaystyle\int_{l_4+d}^{l_5+d} \int_{d-l_0}^{l_2} l_0 + l_1 \, \mathrm{d}l_1 \, \mathrm{d}l_0 \\ \phi_{12} = \displaystyle\int_{l_4+d}^{d} \int_{d-l_0}^{l_2} l_0 + l_1 \, \mathrm{d}l_1 \, \mathrm{d}l_0 \\ \phi_{13} = \displaystyle\int_0^{d} \int_{d-l_0}^{l_2} l_0 + l_1 \, \mathrm{d}l_1 \, \mathrm{d}l_0 \end{cases} \tag{4.42}$$

For the path from the detour point w_q to the charger c, define l_7 as the distance from the depletion point w_d to w_q, l_6 as the distance from w_q to the current location z, and l_8 as the distance from w_q to the destination w_1 (Figure

4.3(b)). For $z \in \overline{\mathcal{D}}(c, d') \setminus \{c\}$, the substitutions of variables can be given by

$$\begin{cases} \rho_2 = \dfrac{l_6}{l_6 + |z-c|} \\ w_0 = z - l_6(\cos\theta_5, \sin\theta_5) + (l_7 + d)(\cos\theta_0', \sin\theta_0') \\ w_1 = z - l_6(\cos\theta_5, \sin\theta_5) - l_8(\cos\theta_0', \sin\theta_0') \end{cases} \tag{4.43}$$

whose Jacobian is $J(x, y, l_7, l_8, \theta_0') = -\cos(\theta_0' - \theta_5)\frac{l_7+l_8+d}{|z-c|}$ with $l_6 = d' - |z-c|$, when $w_d \in \Omega \setminus \overline{\mathcal{D}}(c, d')$ (i.e. $w_q \neq w_d$). When $w_d \in \overline{\mathcal{D}}(c, d')$ (i.e. $w_q = w_d$), we have $J(x, y, l_6, l_8, \theta_0') = \frac{l_8+d}{|z-c|}$ with $l_7 = 0$. The corresponding expected mobile location is then

$$\iiint_{\mathcal{W}_{\mathrm{II}}} |w_q - c| \int_0^1 (1-\rho_2)w_q + \rho_2 c \ \mathrm{d}\rho_2 \, \mathrm{d}w_0 \, \mathrm{d}w_1 = \int_{\overline{\mathcal{D}}(c,d')\setminus\{c\}} z \cdot f_{10}(z) \, \mathrm{d}z \tag{4.44}$$

where

$$\begin{aligned} f_{10}(z) = &\int_{\theta_5+\frac{\pi}{2}}^{\theta_5+\frac{3\pi}{2}} \int_0^{\hat{l}_{10}-d} \int_0^{\hat{l}_9} -\cos(\theta_0' - \theta_5)\frac{l_7 + l_8 + d}{1-\hat{\rho}_2} \, \mathrm{d}l_8 \, \mathrm{d}l_7 \, \mathrm{d}\theta_0' \\ &+ \int_0^{d'-|z-c|} \int_0^{2\pi} \int_0^{l_9} \frac{l_8 + d}{1-\rho_2} \, \mathrm{d}l_8 \, \mathrm{d}\theta_0' \, \mathrm{d}l_6 \end{aligned} \tag{4.45}$$

with

$$\begin{cases} l_9 = \sqrt{1 - r_q^2 \sin^2(\theta_0' - \vartheta_q)} + r_q \cos(\theta_0' - \vartheta_q) \\ l_{10} = \sqrt{1 - r_q^2 \sin^2(\theta_0' - \vartheta_q)} - r_q \cos(\theta_0' - \vartheta_q) \end{cases} \tag{4.46}$$

Here r_q and ϑ_q denote polar coordinates of the detour point w_q, i.e. $w_q = (u_q, v_q) = r_q(\cos\vartheta_q, \sin\vartheta_q)$; their definitions based on l_6 are given by

$$\begin{cases} r_q = \sqrt{l_6^2 + r^2 - 2rl_6\cos(\vartheta - \theta_5)} \\ \vartheta_q = \operatorname{atan2}(y - l_6\sin\theta_5, x - l_6\cos\theta_5) \end{cases} \tag{4.47}$$

Note that $\hat{l}_9$ and $\hat{l}_{10}$ are simply l_9 and l_{10} (following Equation (4.46)) specific to $w_q \neq w_d$ or $|w_q - c| = d'$. In this case, $l_6 = d' - |z-c|$ for r_q and ϑ_q in Equation (4.47). Correspondingly, $\hat{\rho}_2 = \frac{d'-|z-c|}{d'}$. For $z \in \{c\}$, we define the pdf as $\lim_{z\to c} f_{10}(z) = +\infty$.

Lastly, for the path from the charger to the destination w_1, suppose l_{16} is the distance from the current location z to w_1 (Figure 4.3(b)). Again, we have for $z \in \Omega \setminus \{c\}$ that

$$\begin{cases} \rho_3 = \dfrac{|z-c|}{l_{16} + |z-c|} \\ w_0 = z - l_{16}(\cos\theta_5, \sin\theta_5) + (l_7 + l_8 + d)(\cos\theta_0', \sin\theta_0') \\ w_1 = z - l_{16}(\cos\theta_5, \sin\theta_5) \end{cases} \tag{4.48}$$

When $w_d \in \Omega \backslash \overline{\mathcal{D}}(c, d')$, the Jacobian $J(x, y, l_{16}, l_7, \theta_0') = -\frac{l_7+l_8+d}{|z-c|}$, where $l_8 = l_{15}$ (Equation (4.52)). When $w_d \in \overline{\mathcal{D}}(c, d')$, there is $J(x, y, l_{16}, l_8, \theta_0') = -\frac{l_8+d}{|z-c|}$ (with $l_7 = 0$). The expected mobile location can then be expanded as

$$\begin{aligned} &\iint_{\mathcal{W}_{\mathrm{II}}} |c - w_1| \int_0^1 (1-\rho_3)c + \rho_3 w_1 \,\mathrm{d}\rho_3 \,\mathrm{d}w_0 \,\mathrm{d}w_1 \\ &\quad = \int_{\Omega \backslash \overline{\mathcal{D}}(c,d')} z \cdot f_{11}(z) \,\mathrm{d}z + \int_{\overline{\mathcal{D}}(c,d') \backslash \{c\}} z \cdot f_{12}(z) \,\mathrm{d}z \end{aligned} \tag{4.49}$$

where

$$f_{11}(z) = \int_0^{l_{17}} \int_{\theta_5-\theta_8}^{\theta_5+\theta_8} \left(\int_0^{\hat{l}_{10}-d} \frac{l_7 + l_{15} + d}{\rho_3} \,\mathrm{d}l_7 + \int_{l_{14}}^{l_{15}} \frac{l_8 + d}{\rho_3} \,\mathrm{d}l_8 \right) \mathrm{d}\theta_0' \,\mathrm{d}l_{16} \tag{4.50}$$

$$\begin{aligned} f_{12}(z) = &\int_0^{d'-|z-c|} \int_0^{2\pi} \left(\int_0^{\hat{l}_{10}-d} \frac{l_7 + l_{15} + d}{\rho_3} \,\mathrm{d}l_7 + \int_0^{l_{15}} \frac{l_8 + d}{\rho_3} \,\mathrm{d}l_8 \right) \mathrm{d}\theta_0' \,\mathrm{d}l_{16} \\ &+ \int_{d'-|z-c|}^{l_{17}} \int_{\theta_5-\theta_8}^{\theta_5+\theta_8} \left(\int_0^{\hat{l}_{10}-d} \frac{l_7 + l_{15} + d}{\rho_3} \,\mathrm{d}l_7 + \int_{l_{14}}^{l_{15}} \frac{l_8 + d}{\rho_3} \,\mathrm{d}l_8 \right) \mathrm{d}\theta_0' \,\mathrm{d}l_{16} \end{aligned} \tag{4.51}$$

with

$$\begin{cases} \theta_8 = \arcsin\left(\dfrac{d'}{l_{16} + |z-c|} \right) \\ l_{14} = (l_{16} + |z-c|)\cos(\theta_0' - \theta_5) - \sqrt{d'^2 - (l_{16} + |z-c|)^2 \sin^2(\theta_0' - \theta_5)} \\ l_{15} = (l_{16} + |z-c|)\cos(\theta_0' - \theta_5) + \sqrt{d'^2 - (l_{16} + |z-c|)^2 \sin^2(\theta_0' - \theta_5)} \\ l_{17} = r\cos(\vartheta - \theta_5) + \sqrt{1 - r^2 \sin^2(\vartheta - \theta_5)} \end{cases} \tag{4.52}$$

Also, the pdf for $z \in \{c\}$ is defined as $\lim_{z \to c} f_{12}(z) = +\infty$.

4.4.3 Integration

After the preparation in subsections 4.4.1 and 4.4.2, now we prove Theorem 4.4.3.1, giving the main result of this chapter, which is also a main contribution of the thesis.

Theorem 4.4.3.1. *Suppose a charging-aware mobile with an energy budget $d \geq 0$, a charger located at $c \in \Omega$ with an attraction range $d' > 0$, and*

$d' + d \leq 1 - |c|$. *The stationary pdf* $f_{Z(t)}(z)$ *of the mobile location* $Z(t)$ *over the unit disk* $\Omega = \{z \in \mathbb{R}^2 \mid |z| \leq 1\}$ *is a piecewise function:*

$$\pi^2 \alpha \cdot f_{Z(t)}(z) = f_{\mathrm{RWP}}(z) + \begin{cases} g_0(z) - h_0(z), & \text{if } z \in \Omega \setminus \overline{\mathcal{D}}(c, d') \\ g_1(z) - h_1(z), & \text{if } z \in \overline{\mathcal{D}}(c, d') \setminus \{c\} \\ +\infty, & \text{if } z \in \{c\} \end{cases} \tag{4.53}$$

where the functions $f_{RWP}(z)$, $h_0(z)$, $h_1(z)$, $g_0(z)$, *and* $g_1(z)$ *follow the definitions of Equations (4.62)(4.63) and (4.65)–(4.67).*

Proof. We can combine the derived pdf's of the mobile location, i.e. $f_0(z)$ to $f_{12}(z)$, based on the associated domains of integration over z, i.e. $\mathcal{Z}_0$ to $\mathcal{Z}_4$. The combination of Equations (4.13)(4.32) and further evaluation of the inner integrals over l_0 and l_1 yield

$$\begin{aligned} &\iint_{\mathcal{W}_{\mathrm{I}}} |w_0 - w_1| \int_0^1 (1-\rho_0) w_0 + \rho_0 w_1 \,\mathrm{d}\rho_0 \,\mathrm{d}w_0 \,\mathrm{d}w_1 \\ &\quad + \iint_{\mathcal{W}_{\mathrm{II}}} |w_0 - w_q| \int_0^1 (1-\rho_1) w_0 + \rho_1 w_q \,\mathrm{d}\rho_1 \,\mathrm{d}w_0 \,\mathrm{d}w_1 \\ &= \int_{\mathcal{Z}_0} z \cdot \tilde{f}_0(z) \,\mathrm{d}z + \int_{\mathcal{Z}_1} z \cdot \tilde{f}_1(z) \,\mathrm{d}z + \int_{\mathcal{Z}_2} z \cdot \tilde{f}_2(z) \,\mathrm{d}z \\ &\quad + \int_{\mathcal{Z}_3} z \cdot \tilde{f}_3(z) \,\mathrm{d}z + \int_{\mathcal{Z}_4} z \cdot \tilde{f}_4(z) \,\mathrm{d}z \end{aligned} \tag{4.54}$$

where

$$\tilde{f}_0(z) = f_0(z) + f_5(z) = f_{\mathrm{RWP}}(z) - h_0(z) \tag{4.55}$$

$$\tilde{f}_1(z) = f_1(z) + f_6(z) = f_{\mathrm{RWP}}(z) - h_0(z) \tag{4.56}$$

$$\tilde{f}_2(z) = f_2(z) + f_7(z) = f_{\mathrm{RWP}}(z) - h_0(z) \tag{4.57}$$

$$\tilde{f}_3(z) = \begin{cases} \tilde{f}_{3a}(z), & \text{if } d \leq 2d' \\ \tilde{f}_{3b}(z), & \text{if } d > 2d' \end{cases} \tag{4.58}$$

$$\tilde{f}_{3a}(z) = f_{3a}(z) + f_{8a}(z) = f_{\mathrm{RWP}}(z) - h_1(z) \tag{4.59}$$

$$\tilde{f}_{3b}(z) = f_{3b}(z) + f_{8b}(z) = f_{\mathrm{RWP}}(z) - h_0(z) \tag{4.60}$$

$$\tilde{f}_4(z) = f_{4a/b}(z) + f_{9a/b}(z) = f_{\mathrm{RWP}}(z) - h_1(z) \tag{4.61}$$

with

$$\begin{cases} f_{\mathrm{RWP}}(z) = \displaystyle\int_0^{2\pi} \frac{1}{2} l_2 l_3 (l_2 + l_3)\, \mathrm{d}\theta_0' \\ h_0(z) = \displaystyle\int_{\theta_5-\theta_6}^{\theta_5+\theta_6} \frac{\varphi_0}{2}\, \mathrm{d}\theta_0' \\ h_1(z) = \displaystyle\int_0^{2\pi} \frac{\varphi_1}{2}\, \mathrm{d}\theta_0' \end{cases} \tag{4.62}$$

and

$$\begin{cases} \varphi_0 = l_2(l_3 - l_4 - d)(l_2 + l_3 + l_4 + d) \\ \varphi_1 = l_2(l_3 - d)(l_2 + l_3 + d) \end{cases} \tag{4.63}$$

The term $f_{\mathrm{RWP}}(z)$ accounts for the mobile distribution assuming random waypoint mobility (with no detour) [47].

Equations (4.62)(4.63) show that the pdf's $f_0(z)$ to $f_{9b}(z)$ can be unified into succinct forms. Intuitively, this simplification comes from the causality that the probability density of a location being visited, provided the mobile has not taken a detour (if any) to the charger, does *not* depend on whether the detour will occur afterwards.

In addition, by equating l_6 with l_{16}, Equations (4.45)(4.51) can be combined as

$$\begin{aligned} &\iint_{\mathcal{W}_{\mathrm{II}}} |w_q - c| \int_0^1 (1-\rho_2) w_q + \rho_2 c \;\mathrm{d}\rho_2\, \mathrm{d}w_0\, \mathrm{d}w_1 \\ &\qquad + \iint_{\mathcal{W}_{\mathrm{II}}} |c - w_1| \int_0^1 (1-\rho_3) c + \rho_3 w_1\, \mathrm{d}\rho_3\, \mathrm{d}w_0\, \mathrm{d}w_1 \\ &\quad = \int_{\Omega \setminus \overline{\mathcal{D}}(c,d')} z \cdot g_0(z)\, \mathrm{d}z + \int_{\overline{\mathcal{D}}(c,d') \setminus \{c\}} z \cdot g_1(z)\, \mathrm{d}z \end{aligned} \tag{4.64}$$

where

$$g_0(z) = f_{11}(z) = \int_0^{l_{17}} \left(1 + \frac{l_{16}}{|z-c|}\right) \cdot \frac{\gamma_0}{2}\, \mathrm{d}l_{16} \tag{4.65}$$

$$\begin{aligned} g_1(z) &= f_{10}(z) + f_{12}(z) \\ &= \int_0^{d'-|z-c|} \left(1 + \frac{l_{16}}{|z-c|}\right) \cdot \frac{\gamma_1}{2}\, \mathrm{d}l_{16} + \int_{d'-|z-c|}^{l_{17}} \left(1 + \frac{l_{16}}{|z-c|}\right) \cdot \frac{\gamma_0}{2}\, \mathrm{d}l_{16} \\ &\quad + \int_{\theta_5+\frac{\pi}{2}}^{\theta_5+\frac{3\pi}{2}} \frac{d'}{|z-c|} \cdot \frac{\varphi_2}{2}\, \mathrm{d}\theta_0' \end{aligned} \tag{4.66}$$

with

$$\begin{cases} \gamma_0 = \displaystyle\int_{\theta_5-\theta_8}^{\theta_5+\theta_8} (l_{13}-l_{14}-d)(l_{13}+l_{14}+d)\,\mathrm{d}\theta_0' \\ \gamma_1 = \displaystyle\int_0^{2\pi} l_{12}(l_{12}+2d)+(l_{13}-d)(l_{13}+d)\,\mathrm{d}\theta_0' \\ \varphi_2 = -\cos\big(\theta_0'-\theta_5\big)\cdot \hat{l}_{12}(\hat{l}_{13}-d)(\hat{l}_{12}+\hat{l}_{13}+d) \end{cases} \tag{4.67}$$

and

$$\begin{cases} l_{12} = \sqrt{1-r_1^2\sin^2(\theta_0'-\vartheta_1)} + r_1\cos\big(\theta_0'-\vartheta_1\big) \\ l_{13} = \sqrt{1-r_1^2\sin^2(\theta_0'-\vartheta_1)} - r_1\cos\big(\theta_0'-\vartheta_1\big) \end{cases} \tag{4.68}$$

Here r_1 and ϑ_1 are polar coordinates of the destination w_1, i.e.

$$\begin{cases} r_1 = \sqrt{l_{16}^2+r^2-2rl_{16}\cos(\vartheta-\theta_5)} \\ \vartheta_1 = \operatorname{atan2}(y-l_{16}\sin\theta_5, x-l_{16}\cos\theta_5) \end{cases} \tag{4.69}$$

Like $\hat{l}_9$ and $\hat{l}_{10}$, $\hat{l}_{12}$ and $\hat{l}_{13}$ are l_{12} and l_{13} in the specific case of $|w_1-c|=d'$ (thus $l_{16}=d'-|z-c|$ for r_1 and ϑ_1).

It is not difficult to derive that

$$f_{\mathrm{RWP}}(z) = 4(1-r^2)E(r) \tag{4.70}$$

where $E(r)=\int_0^{\frac{\pi}{2}}\sqrt{1-r^2\sin^2(\theta)}\,\mathrm{d}\theta$ is the complete elliptic integral of the second kind (with modulus r). Numerical computation of such integrals has been facilitated by extensive studies on the subject [64]. Nonetheless, while there is

$$h_1(z) = 4(1-r^2)E(r) - 2d^2E(r) - \pi d, \tag{4.71}$$

the function $h_0(z)$ defies a closed-form expression. The difficulty remains for $g_0(z)$ and $g_1(z)$, which can be expanded but only partially to complex forms. On account of this, the pdf's are left in the form of integrals. □

Remark 1. For the computation of coefficient $(\pi^2\alpha)^{-1}$, one can refer to the definition of α, i.e. the expected travel distance (including detours), or formally,

$$\begin{aligned} \alpha = \frac{1}{\pi^2}\Bigg(& \iint_{\mathcal{W}_{\mathrm{I}}} |w_0-w_1|\,\mathrm{d}w_0\,\mathrm{d}w_1 \\ & + \iint_{\mathcal{W}_{\mathrm{II}}} |w_0-w_q|+|w_q-c|+|c-w_1|\,\mathrm{d}w_0\,\mathrm{d}w_1 \Bigg) \end{aligned} \tag{4.72}$$

Equivalently, the value of α can be obtained by integrating the function of $\pi^2\alpha \cdot f_{Z(t)}(z)$ from the right-hand side of Equation (4.53) over the area Ω, i.e., $\alpha = \pi^{-2}\int_\Omega \pi^2\alpha \cdot f_{Z(t)}(z)\,\mathrm{d}z$, since $\int_\Omega f_{Z(t)}(z)\,\mathrm{d}z = 1$. Nonetheless, we resist the temptation to give a more explicit expression of α, considering the lack of a closed form for $f_{Z(t)}(z)$. Moreover, the value of α need not be computed if the interest is in the ratio of densities between different locations.

Remark 2. The condition $d' + d \leq 1 - |c|$ has been imposed for a simpler analysis. Its relaxation (such that, e.g., $d' \leq 1 - |c|$ or $d' > 1 - |c|$) would require non-trivial but straightforward adaptation of the pdf's from $f_0(z)$ to $f_{12}(z)$, so as to account for changes (e.g. more segmentation) of the domains of integrals.

Remark 3. The derivation of Theorem 4.4.3.1 can be generalized to other convex and bounded areas, with redefinition of segment lengths like l_2, l_3, l_{12}, l_{13}, and l_{17}, which intersect with and thus depend on the boundary. Also, the coefficient $\pi^2\alpha$ should be replaced with $A^2\alpha$, where A is the area size.

Remark 4. The obtained pdf $f_{Z(t)}(z)$ counts all movements of the mobile, regardless of whether its energy is depleted or not. For the distribution of the mobile only in a certain state, e.g. having energy, we can filter out in integration any path from the depletion point w_d (if any) to the destination w_1 or to the charger c. Such refinements are left for future work. Here we only show the numerical results of energy-wise mobile distribution from simulation (subsection 4.5.2).

4.5 Numerical Results

4.5.1 Mobile Distribution

In this subsection we summarize the simulation results of mobile distribution and compare to the corresponding analytical results as per Theorem 4.4.3.1. Specifically, we simulate the charging-aware mobility (Section 4.2) within a unit disk centered at (0, 0). The square $[-1, 1] \times [-1, 1]$ enclosing the unit disk is split by a grid into 10^4 (square) cells, each of area $\Delta^2 = 0.02^2$. While

the mobile moves in the disk (at a constant speed), the distance traveled in each cell is counted over time. The probability of a cell being visited is then approximated by the travel distance accumulated in the cell normalized by the total distance covered during the simulation. The density is the result of the division of the probability mass by the cell area Δ^2.

Figure 4.4 shows the results for energy budget $d = 0.2$, attraction range $d' = 0.2$, and charger location at $c = (-0.6, 0)$. Note that the corresponding analytical results are an exact match and thus are omitted. As easily noticed in Figure 4.4(a), the density of mobile visits spikes over cells in the vicinity of the charger, which demonstrates the attraction effect; that is, the depleted mobile would detour (straight) to the charger for recharging anytime it falls within the attraction range, and the closer a cell is located to the charger, the more likely it would be traveled by detours. Leaving aside the salient spike, the mobile distribution appears to follow the shape of a dome, with a hotspot (of much less magnitude) at the center/origin of the disk area and density vanishing towards the boundary. Such non-uniform distribution is unrelated to the charger but has been found to come from RWP under the *boundary effect* [11]. Specifically, to reach a random destination a mobile following RWP in a bounded area often needs to traverse the center region, which would then receive more visits than regions near the boundary. Besides, we note an intriguing observation that the density tends to *dip* slightly around a distance of d' to the charger from any direction. This feature will be explained in subsection 4.5.2.

As further illustrated in Figure 4.4(b), the contours of density centered at the origin, instead of being all symmetric like under RWP, are now subject to distortion due to the presence of the charger. It can be seen that certain contours become concave around the charger's attraction range ($d' = 0.2$), implying the dips aforementioned. Figure 4.4(b) also shows the symmetry of mobile distribution between the two half-disk areas with respect to the x-axis, or more generally, the line passing through the origin and the charger location c. This results from the circular symmetry of the disk area. On the other hand, the distribution appears to be asymmetric near the charger with respect to $x = a = -0.6$, as evidenced by the eccentric contours surrounding

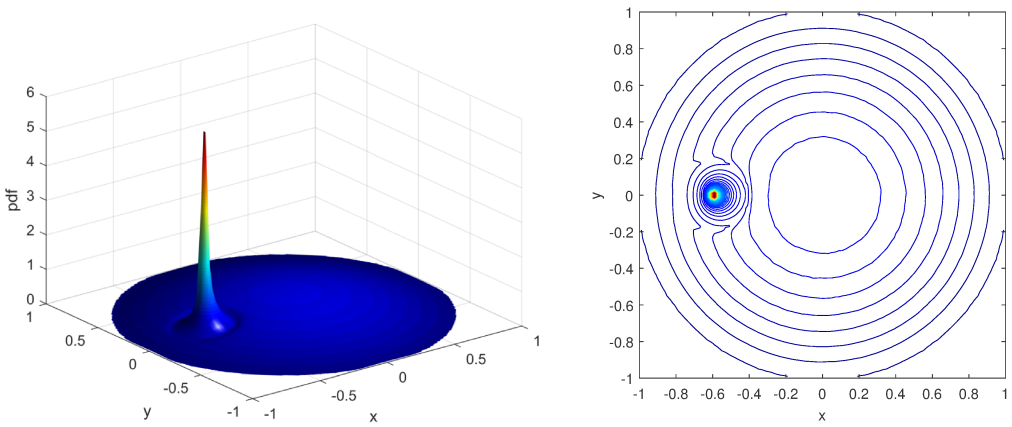

(a) (b)

Figure 4.4: Simulation results of mobile distribution for $d = 0.2$, $d' = 0.2$, $c = (-0.6, 0)$: (a) a 3-dimensional surface plot; (b) a contour plot.

the charger.

For a clearer demonstration, we plot the cross sections of mobile distribution on the xz-plane in Figure 4.5, with $d = 0.1, 0.2$, $d' = 0.1, 0.2$, $a = \pm 0.6, \pm 0.3, 0$, and $b = 0$. Firstly, the analysis of Theorem 4.4.3.1 has its validity confirmed. Secondly, as indicated, asymmetric distribution is present around each charger except for the one located in the very middle, i.e. $a = 0$. For each pair of cells that are at the same distance to the charger (on opposite sides), the density tends to be higher on the side facing the center than the other side, towards the boundary. Such patterns are attributed to the boundary effect, especially on paths involving detours for recharging. As exemplified in Figure 4.6, where $d = d' = 0.2$ and $c = (-0.6, 0)$, suppose the area is divided by $x = -0.6$ into two circular segments (west and east). Given a pair of random waypoints A and D in the two regions respectively, the mobile may travel from A towards D, following the path $\mathsf{A}{\to}\mathsf{B}{\to}c{\to}\mathsf{D}$. Because of smaller room in the west region, the waypoint D is more likely than A to be located within a radius d' of the charger. Consequently, the segment $c{\to}\mathsf{D}$ can have a length shorter than d', causing less coverage and density to the west of the charger within its attraction range. In the case of movement in the reverse direction from D to A, the path $\mathsf{D}{\to}\mathsf{E}{\to}c{\to}\mathsf{A}$ would unbalance the density even more by "transferring" the depletion point E and segment $\mathsf{E}{\to}c$ across regions.

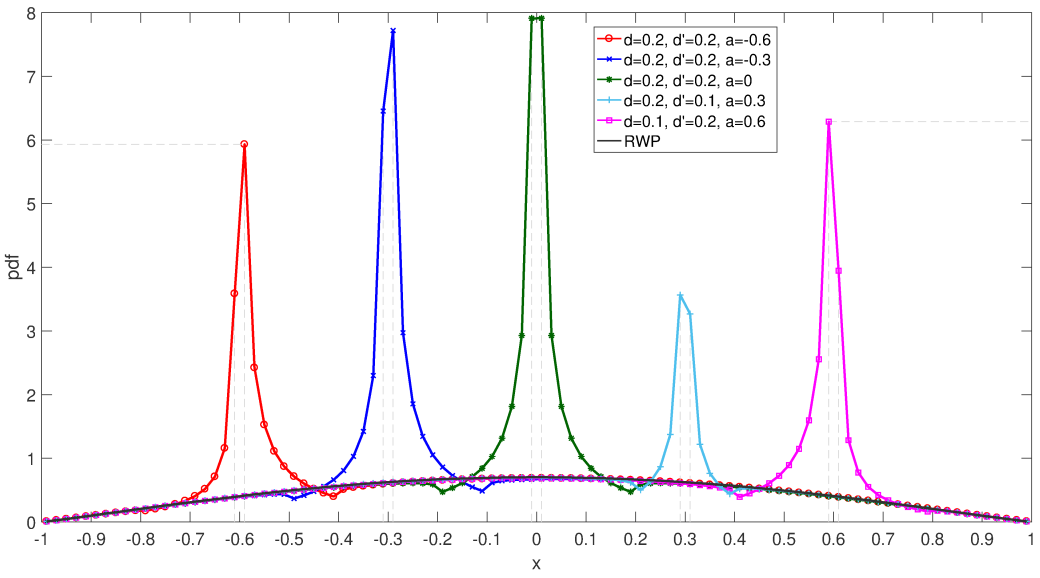

Figure 4.5: Cross-sectional plots (in the xz-plane) of simulation (lines) versus analytical (markers) results as per Theorem 4.4.3.1, for $d = 0.2, 0.3$, $d' = 0.1, 0.2$, $a = \pm 0.6, \pm 0.3, 0$, $b = 0$, and RWP.

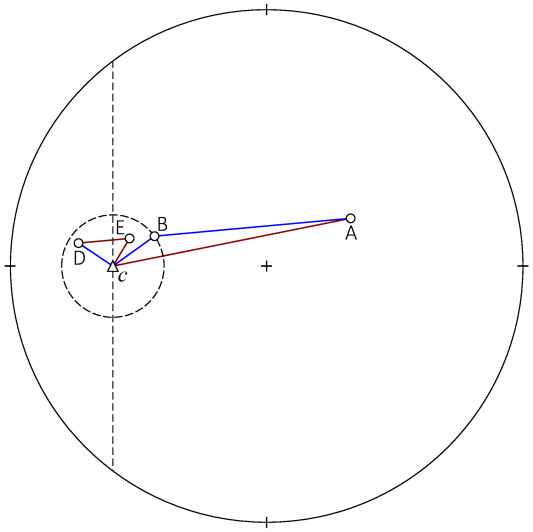

Figure 4.6: Examples of paths causing asymmetry of distribution around the charger, assuming $d = d' = 0.2$ and $c = (-0.6, 0)$.

The west region only contains part of the segment $\mathsf{D}\rightarrow\mathsf{E}$, which does not pass through the charger.

Figure 4.5 also shows that the spike at the charger tends to increase as the charger location moves inwards to the center, provided both of the values of d and d' remain unchanged (at 0.2). This pattern, again, is due to the boundary

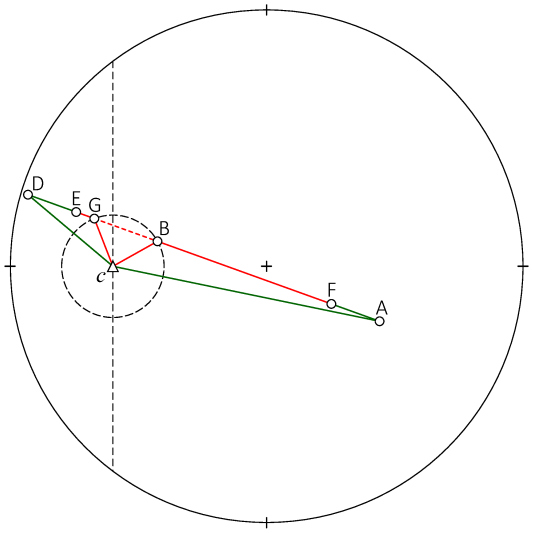

Figure 4.7: Examples of paths causing differences in distribution between the energy states, assuming $d = d' = 0.2$ and $c = (-0.6, 0)$.

effect on RWP, which results in the mobile visiting the center regions and thus detouring to the charger therein more often than when near the boundary. Furthermore, when the attraction range d' decreases, e.g. from 0.2 to 0.1 (with $d = 0.2$ and $|a| = 0.3$), the spike diminishes and the mobile distribution tends towards that of RWP. This degenerate case of charging-aware mobility is increasingly likely as the mobile (1) is missing the attraction range of the charger after depletion and (2) is passing beyond the range when depletion occurs. When the energy budget d decreases from 0.2 to 0.1 (with $d' = 0.2$ and $|a| = 0.6$), the spike is observed to rise, according with the fact that a mobile of lower energy reserves would be less likely to reach its destination within d or slip by the charger with no detour. Lastly, it appears that the density values, excluding those of cells within a radius d' of each charger, are barely distinguishable between the charging-aware mobility and RWP. This suggests a "quasi-local distortion" effect of the charger; that is, cells outside the charger's attraction range would bear slim to unnoticeable reduction of density. Like the case of 1-dimensional mobility, the findings of the distortion effects of the charger, including asymmetrically spiked density at the charger, dipped density surrounding the charger (to be explained in subsection 4.5.2), and the quasi-locality of distortion, are some of the main contributions of the

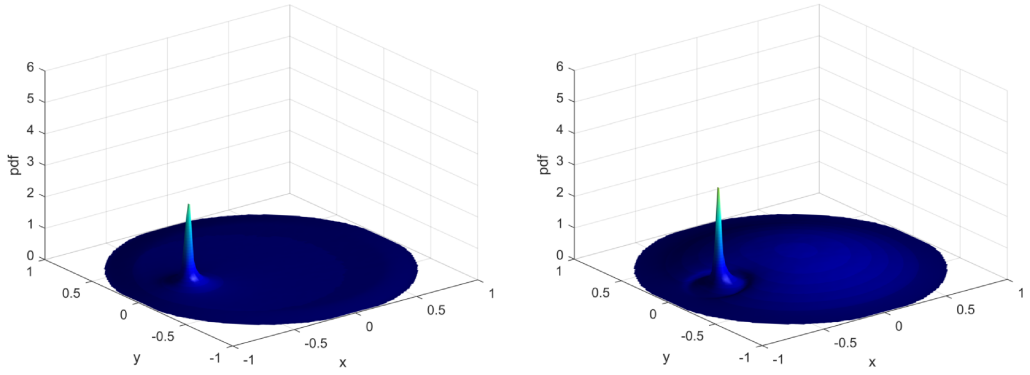

(a) (b)

Figure 4.8: Simulation results of mobile distribution for $d = 0.2$, $d' = 0.2$, $c = (-0.6, 0)$, given that the mobile (a) has energy and (b) is depleted respectively.

thesis.

4.5.2 Energy-Wise Mobile Distribution

Next, we display in Figure 4.8 the simulation results of mobile distribution dependent on the energy state (i.e. having energy or not) of the mobile, assuming $d = d' = 0.2$ and $c = (-0.6, 0)$. The comparison between Figures 4.8 and Figure 4.4(a) shows that the distribution of a depleted mobile retains the shape featuring dips around the charger, plus a dome over the area; meanwhile, an operational mobile (i.e. having energy) assumes density that would decrease monotonically over distance from the charger in any direction, for the given settings. These patterns are further illustrated in Figure 4.9, which plots the cross sections of energy-wise mobile distribution from simulation for $d = 0.1, 0.2$, $d' = 0.1, 0.2$, $a = \pm 0.6, \pm 0.3, 0$, and $b = 0$ (corresponding to Figure 4.5). Like in Figure 4.5, the spike in density would be the highest when the charger is located at the center, regardless of the energy state. On the other hand, despite similar magnitude of values, the distribution of an operational mobile appears to be more symmetric in general about the charger location than a depleted mobile.

The differences in mobile distribution between the two energy states can be explained by the examples of Figure 4.7. Suppose $d = d' = 0.2$ and $c = (-0.6, 0)$ and the mobile moves from a random waypoint A to another D. After traveling

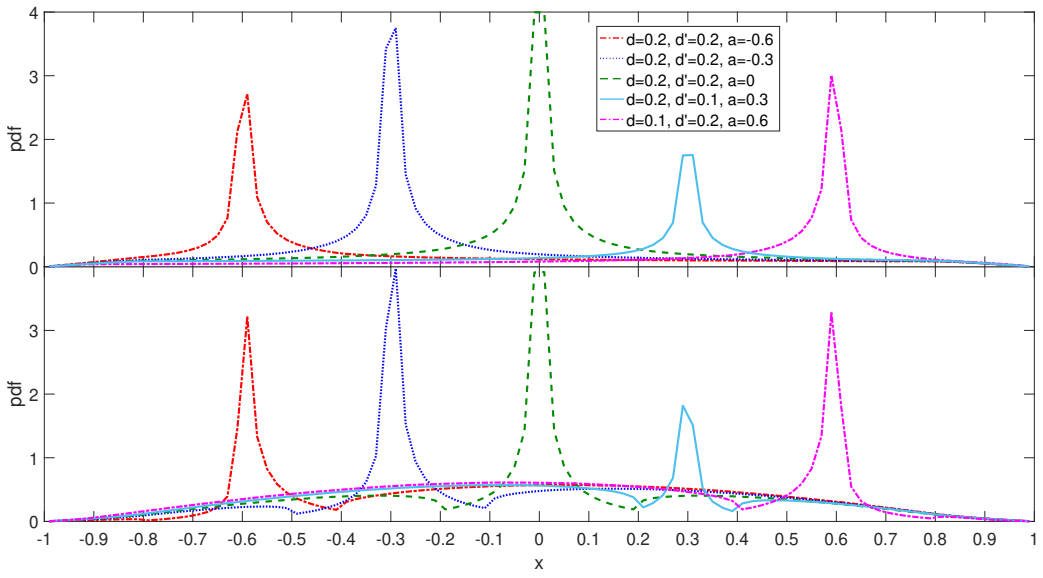

Figure 4.9: Cross-sectional results of mobile distribution from simulation for $d = 0.2, 0.3$, $d' = 0.1, 0.2$, $a = \pm 0.6, \pm 0.3, 0$, and $b = 0$, given the mobile has energy (upper) and is depleted (lower) respecitvely.

a distance d to point F, the mobile would detour from B to the charger c and then the destination D, remaining depleted for the portion F→B→c. The segment B→D is not covered because of the diversion for recharging. By the same token, the mobile, if moving reversely from D to A, would follow the path D→E→G→c→A and remain depleted for E→G→c, with the segment G→A uncovered. By collecting paths of the two directions, we can see gains of density towards the charger but no travel along the chord B↔G. Note that radii like B→c and G→c (with angles rotated) can still contribute density to B↔G, but mainly for its middle part that is closer to the charger. Parts near the endpoints B and G, however, would incur losses of density in the depleted state, resulting in the dips observed. Also, because of the tight space bounded to the west of the charger, the segment D→E is likely to straddle the frontier of the charger's attraction zone, with the depletion point E and detour point G merging with each other. As a consequence, densities of the mobile being in the depleted state would be reduced on both sides of the frontier, lessening the dips to the west, as shown in Figure 4.8 (around $x = -0.8$). Further, the waypoint D can be located within range of the charger (like Figure 4.6),

causing asymmetric distribution in the depleted state with radii B→c and G→c both in the east.

As for the mobile distribution in the operational state, we can examine boundary effects on the segments A→F, c→D, D→E, and c→A in Figure 4.7. Unlike F→B and E→G that are variable in length, A→F and D→E have their lengths unaffected by the boundary as both have to conform with the constant budget d. On the other hand, the segments c→D and c→A suggest that any path involving a detour for recharging would contribute to the density in the operational state *solely* on lines connecting the waypoints and the charger. For paths comprising no detours, only segments covered by the (limited) budget $d = 0.2$ (like A→F and D→E) would count for density in the operational state. All these lead to the mobile distribution shaped as in Figure 4.8(a).

4.5.3 Multiple Chargers Heuristic Approximation

The analysis and simulation so far have illuminated many characteristics of the charging-aware mobility in the presence of a single charger. Often, however, more than one charger may be deployed to increase the opportunity for the mobile to recharge; accordingly, there is also a need to investigate the mobility in n-charger ($n \geq 2$) scenarios. The mobile would still follow the rules of movement in Section 4.2. Note that we assume the chargers are normally scattered (for balanced coverage) such that *no* point in the area is within the attraction ranges of two or more chargers. Instead of rigorous deduction, which is potentially intractable (especially when n is large), we extend the 1-charger result of Theorem 4.4.3.1 *heuristically* to approximate the analytical n-charger mobile distribution. This heuristic approximation approach, which constitutes one of our main contributions, is presented in the form of a remark of Theorem 4.4.3.1:

Remark 5. Suppose a charging-aware mobile with an energy budget $d \geq 0$, a number of $n \geq 2$ chargers situated at $\{c_i \in \Omega \mid i = 1, 2, ..., n\}$ with attraction ranges $d'_i > 0$ respectively, and $d'_i + d \leq 1 - |c_i|$, $|c_i - c_j| > d'_i + d'_j$, for $i, j = 1, 2, ..., n$, $i \neq j$. The stationary pdf $f^{(n)}_{Z(t)}(z)$ of the mobile location $Z(t)$ over the

unit disk Ω can be approximated by

$$\pi^2\alpha^{(n)}\cdot f^{(n)}_{Z(t)}(z) \approx f_{\mathrm{RWP}}(z)+\begin{cases}\sum_{i=1}^{n} g_{0|i}(z) - h_{0|i}(z), & \text{if } z \in \Omega \setminus \bigcup_{i=1}^{n} \overline{\mathcal{D}}(c_i, d'_i)\\ g_{1|i}(z) - h_{1|i}(z) & \\ \quad + \sum_{j\neq i}^{n} g_{0|j}(z) - h_{0|j}(z), & \text{if } \exists i\colon z \in \overline{\mathcal{D}}(c_i, d'_i) \setminus \{c_i\}\\ +\infty, & \text{if } \exists i\colon z \in \{c_i\}\end{cases} \tag{4.73}$$

where the functions $f_{\mathrm{RWP}}(z)$, $h_{0|i}(z)$, $h_{1|i}(z)$, $g_{0|i}(z)$, and $g_{1|i}(z)$ follow the definitions of Equations (4.62)(4.63)(4.65)–(4.67). Besides, $\alpha^{(n)} = \sum_{i=1}^{n} \alpha_i - (n-1)\alpha_{\mathrm{RWP}}$ such that $\int_\Omega f^{(n)}_{Z(t)}(z)\,\mathrm{d}z = 1$, where α_i is the expected travel distance of the mobile in the presence of the ith charger only and α_{RWP} (≈ 0.9054) corresponds to RWP. When $n = 1$, Equation (4.73) would degenerate to Equation (4.53).

Intuitively, Equation (4.73) can be interpreted as the distortion effects of chargers "superimposed iteratively" onto mobile distribution of RWP. The approximation takes *no* account of the interplay among chargers, e.g. the charger located ahead facing the mobile would attract and divert it first, causing fewer visits to other chargers "behind". To understand the efficacy of approximation, we investigate the charging-aware mobility in a scenario of three chargers deployed at $c = (-0.6, 0)$, $(0.6, 0)$, and $(-0.4, -0.3)$ with attraction range $d' = 0.2$, 0.2, and 0.1 respectively. Figure 4.10 displays the corresponding results of mobile distribution from simulation (Figure 4.10(a)) versus approximation as per Equation (4.73) (Figure 4.10(b)), and Figure 4.11(a) gives the cross-sectional plot in the xz-plane.

It can be seen that the actual values of density are well approximated in general. However, as Figure 4.11(a) illustrates, the accuracy of approximation is reduced very close to the charger locations. There, the approximate values of density appear to "upper-bound" the actual ones, with a larger discrepancy noted around the charger location $(-0.6, 0)$ than around the charger located at $(0.6, 0)$, showing the effect of the third charger. This pattern agrees with the aforementioned fact that Equation (4.73) has left out the mutual blocking effect between chargers on attracting the mobile. That is, densities around the location $(-0.6, 0)$, which is in close proximity to the third

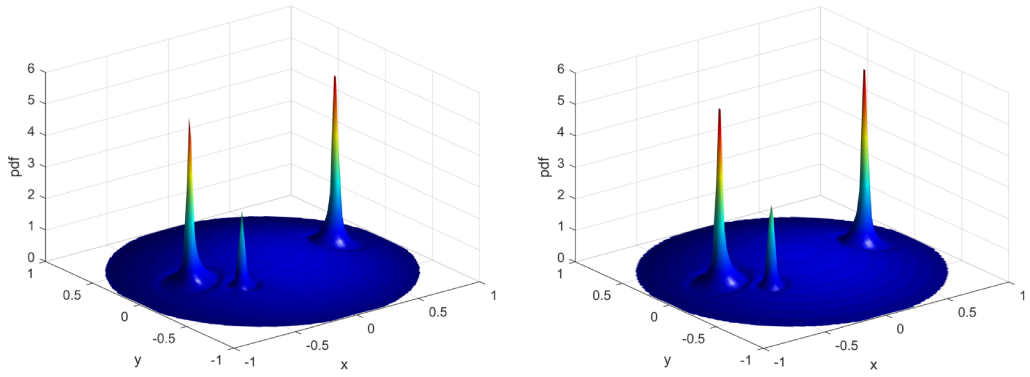

(a) (b)

Figure 4.10: Actual (a) and approximate (b) results of mobile distribution for three chargers with locations $c = (-0.6, 0), (0.6, 0), (-0.4, -0.3)$ and attraction ranges $d' = 0.2, 0.2, 0.1$ respectively.

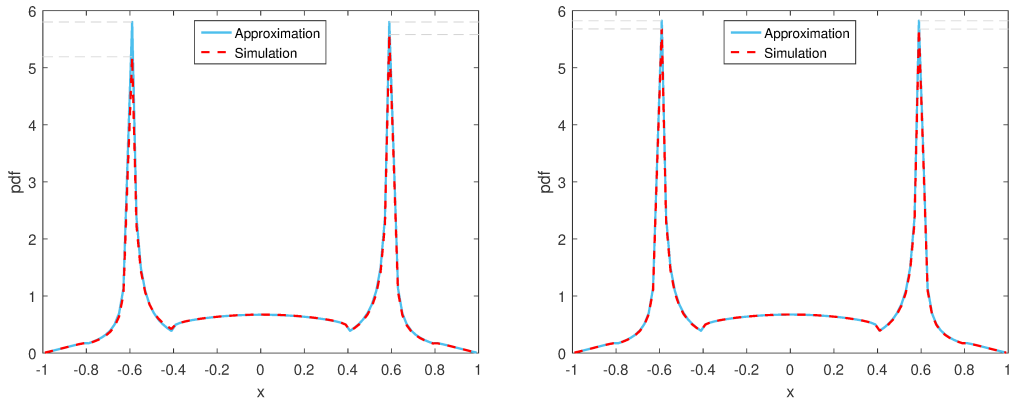

(a) (b)

Figure 4.11: Cross sections of actual and approximate mobile distribution: (a) three chargers with locations $c = (-0.6, 0), (0.6, 0), (-0.4, -0.3)$ and attraction ranges $d' = 0.2, 0.2, 0.1$ respectively; (b) two chargers with locations $c = (-0.6, 0), (0.6, 0)$ and attraction range $d' = 0.2$.

charger at $(-0.4, -0.3)$, tend to be overestimated, more so than around $(0.6, 0)$, which is farther away and thus less affected. In the absence of the charger at $(-0.4, -0.3)$, as shown in Figure 4.11(b), the actual densities around $(-0.6, 0)$ would be higher and match the approximations better, to the same extent of those around $(0.6, 0)$.

4.6 Chapter Summary

In this chapter we conduct a formal analysis of the charging-aware mobility in a (2-dimensional) unit disk and derive an explicit expression for the overall stationary mobile distribution (under the condition $d'+d \leq 1-|c|$). Like Chapter 3, we assume a scenario akin to cellular networks where there is universal cell coverage across the area of interest; hence the mobile can communicate continuously. The numerical results from simulation verify correctness of the analysis and exhibit unique patterns induced by detours. In our model, the charger shows a "quasi-local distortion" effect: while the mobile density spikes high within the charger's attraction range, the values outside are generally thinly reduced from those under no detours. Around the charger we have observed asymmetric concentration enclosed by counterintuitive dips in density around a distance d' to the charger. The former observation can be explained by attraction to the charger overlaid with the boundary effect. The dipped density, on the other hand, is linked to the fact that the frontier of the charger's attraction zone is often where the mobile changes course and starts a diversion for recharging. We also address the approximation for multiple chargers based on 1-charger results. The approximation for a 3-charger deployment shows great accuracy when the chargers are located at sufficient distances from each other.

Chapter 5

Charging-Aware Mobility in Ad Hoc Networks

5.1 Introduction

In Chapter 4 we analyzed the 2-dimensional charging-aware mobility formally and empirically. As a follow-up study, in this chapter we examine the interaction between such mobility and wireless communications in a more practical setting. Specifically, we consider an ad hoc network where the mobiles would communicate and consume energy depending on peers in the neighborhood. This contrasts with the assumption in Chapters 3 and 4 that communication is always possible, like in a cellular network with complete coverage of the whole area. The movement space is assumed to be a grid of square cells to mimic urban scenarios; accordingly, the mobility model from Chapter 4 is discretized to accommodate the Manhattan space. Based on these assumptions (Section 5.2), we investigate the mobility and network performance under three variables, including the network size (Section 5.3), the wireless capacity limit (Section 5.4), and the deployment of multiple chargers (Section 5.5).

5.2 Assumptions

We make the following assumptions about the system for simulation:

- The space is a square grid on the Cartesian plane with its four corner cells centered at coordinates (-1, -1), (1, -1), (1, 1), and (-1, 1) respectively. All the cells have a uniform side length Δ equal to 0.04.

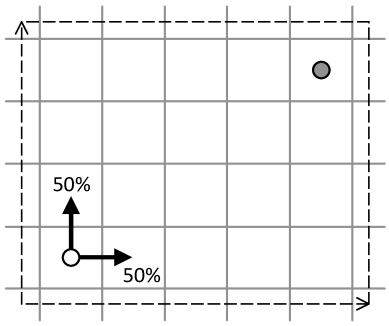

Figure 5.1: Illustration of the Manhattan RWP mobility.

- A charger is situated in a cell $c = (a, b)$ in the grid and is able to recharge any mobile residing in (and only in) cell c to full capacity *instantly*. The charger has an attraction range of $d' \in \mathbb{Z}_{\geq 0}$ (in Manhattan distance), within which any depleted mobile would be attracted and diverted to the charger for replenishment.

- A MANET of m mobiles moves in the grid following a discrete-time Manhattan version of the charging-aware mobility model presented in Chapter 4. Specifically, the movements proceed in *time slots*; at the end of each slot, a mobile can "hop" from the current cell to one of the four adjacent cells that are connected horizontally and vertically (or to one of a smaller set of cells if at boundaries). The mobile still keeps transferring between randomly generated waypoints, like in the Euclidean space, but now would *choose* from the multiple shortest paths (in Manhattan distance) in a *random uniform* manner to travel to a destination, as illustrated in Figure 5.1. Upon arrival at each waypoint, the mobile has its energy renewed to a constant level $d \in \mathbb{Z}_{\geq 0}$ (in Manhattan distance), whose consumption depends on the communication along the path (detailed below). In the case that the mobile falls within the charger's attraction range d' after (and only after) depletion, it would follow an arbitrary shortest path to detour to the charger. After a quick full charge therein to a sufficient level, the mobile would turn to the destination following, again, a random shortest path. The mobile need not recharge again before achieving the current destination.

- The mobiles have continuous data traffic, with queues *never* empty. During a time slot, any two operational mobiles (i.e. having energy to communicate) in the *same* cell can pair up randomly for communication (without interference with neighboring cells), if the wireless capacity $\omega \in \mathbb{Z}_+$ of that cell is unsaturated. A capacity $\omega = 1$ means only one pair of mobiles is allowed communication per cell. Any paired mobile consumes one unit $\Delta = 0.04$ of energy. Note that even the capacity is not exceeded, an operational mobile may still not be able to pair with any peer (thus consuming no energy), because all the other operational mobiles in the cell have already paired up. This occurs if there are an odd number of operational mobiles in that cell.

5.3 Effects of Mobile Numbers

In this section, we investigate the effects of the number of mobiles on their probability density distribution. The objective is to see whether mobile distributions of an ad hoc network in a Manhattan space can be approximated by analytical results especially when the network size is sufficiently large. As we will see, the similarities between the analytical and simulation results show the capacity of our model for more realistic systems. This is one of our main contributions. Throughout the section we assume $\omega = \infty$ to remove the impact of wireless capacity.

First of all, we simulate a special case where there is only a single mobile in the grid. The mobile would consume a unit of energy for communication every slot as long as it has any energy. This corresponds to the ideal models analyzed in Chapters 3 and 4. Since the mobile drains energy at the fastest rate, this setting can provide an upper bound for the charger's attraction effect. Equivalently, we can assume an *infinite* number of mobiles moving in the grid with unlimited capacity and zoom in on the mobility of one mobile. Figure 5.2 shows the simulation results of the mobile's densities, assuming the energy budget $d = 0.2$ (i.e. $\frac{d}{\Delta} = 5$ units of energy), the attraction range $d' = 0.2$, and the charger's location $c = (-0.6, 0)$. Akin to Figures 4.4 and 4.8 (Section 4.5),

the neighborhood of the charger has strikingly high density values, because of the attraction effect. The hotspot with smaller magnitude around the center of the area (Figures 5.2(a)(b)(e)(f)), as previously explained, stems from the *boundary effect* on the component RWP mobility (Figure 2.1); the asymmetry and dips in density also remain around the charger, because of, again, the boundary effect (Section 4.5).

Despite the retained key features, there are two new patterns in Figure 5.2 that are worth noting about the distributions:

- It can be seen that the overall densities around the charger rise markedly towards eight directions, with the operational-state distribution contributing to the diagonal "bumps" (Figures 5.2(c)(d)) and the depleted-state distribution contributing horizontally and vertically (Figures (e)(f)). This comes from the mobility nature of Manhattan RWP: once the mobile has the same x (y resp.) coordinate of the intended destination (i.e. the charger or waypoint) at, say, (x^*, y^*), it would move straight along cells on the line $x = x^*$ ($y = y^*$ resp.) throughout the path afterwards. By the same token, when the mobile heads towards the charger for recharging, it is likely to hit the line $x = a$ or $y = b$ first and then stick to it for the detour. As a result, densities in the horizontal and vertical directions are higher. The diagonal bumps are because the charger is where the mobile started after recharging but its destination waypoint was neither on $x = a$ nor $y = b$. This is not a rare incident. Hence, the possible outgoing paths tend to be diagonal.

- Another interesting observation is the strips of concave density in Figure 5.2(e), as delineated by dashed lines in Figure 5.2(f). The two strips, both of which appear to be d' in width, span the whole area (beyond the charger's locality) and intersect perpendicularly at the charger. The cause behind this shape is explained as follows. Suppose a pair of waypoints, w_0, which is the source waypoint located in the rectangular region $\mathcal{R}_0 = [-0.8, -0.4] \times [-1, -0.2]$, and the destination $w_1 \in \mathcal{R}_1 = [-0.8, -0.4] \times [0.2, 1]$. To reach w_1 the mobile must pass through the

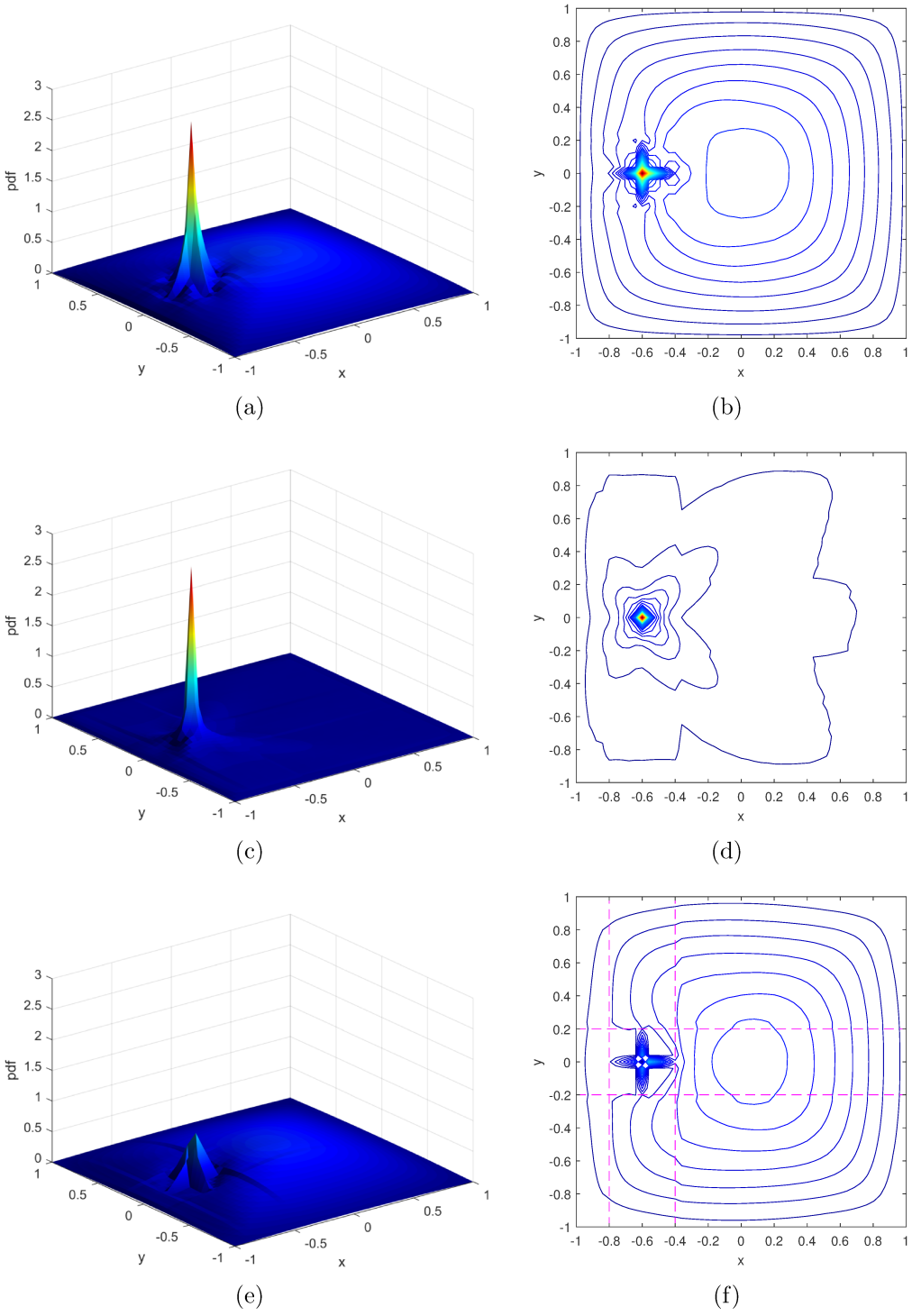

Figure 5.2: Simulation results of mobile distribution for $d = 0.2$, $d' = 0.2$, $c = (-0.6, 0)$, and $\omega = \infty$: (a)(b) surface and contour plots of probability densities irrespective of the mobile's energy state (i.e. having energy or not); (c)(d) plots of densities given that the mobile has energy; (e)(f) densities given that the mobile is depleted.

neighborhood of the charger, which, in the case of a detour for recharging, will guarantee energy sufficiency in the region $\mathcal{R}_1$ for any subsequent path to w_1, hence reducing the depleted-state density therein. Note that this "regional" loss of density can occur even if the source w_0 resides outside the region $\mathcal{R}_0$; it remains as long as the mobile detours to the charger. This also explains the perpendicular strips of convex density in the operational-state distribution of Figure 5.2(c). Additionally, the charger's cell c has zero density when the mobile is depleted, which is unsurprising, since the mobile is assumed to be able to recharge and gain energy sufficiency instantly at the charger.

The mobile distributions of Figure 5.2 showcase the general patterns that apply to various settings. If, instead, a finite number of mobiles consume energy for the pair-wise communication, the overall densities around the charger, especially the maximum value at the cell c, are expected to be lower than those in Figure 5.2. Theoretically, the fewer mobiles there are, the less often they would meet and consume energy for communication, and the less often the charger would be visited for recharging. The energy-wise densities in the charger's neighborhood also vary in sync with the number of mobiles. In view of this, we sample the overall density at the charger cell c to peek into how the number of mobiles affects their distributions over the grid.

Figure 5.3 shows the corresponding probability density values (per mobile) as the population m increases from 500 to 8000, for the case where the attraction range is $d' = 0.2$, the charger cell is at $c = (-0.6, 0)$, and $\omega = \infty$. For the energy budget d, we assume two uniform values, i.e. $d = 0.2$, which accounts for the case of all mobiles being *under-energized*, and $d = 0.6$ (i.e. $\frac{d}{\Delta} = 15$ units of energy), for *highly-energized* ones. It can be seen in Figure 5.3 that for either $d = 0.2$ or $d = 0.6$ the probability density at cell c gradually rises with m towards the upper bound under continuous energy consumption. This demonstrates that the mobiles indeed tend to pay more visits to the charger as they increase in numbers.

Moreover, it is worth discussing the differences in mobility between the two

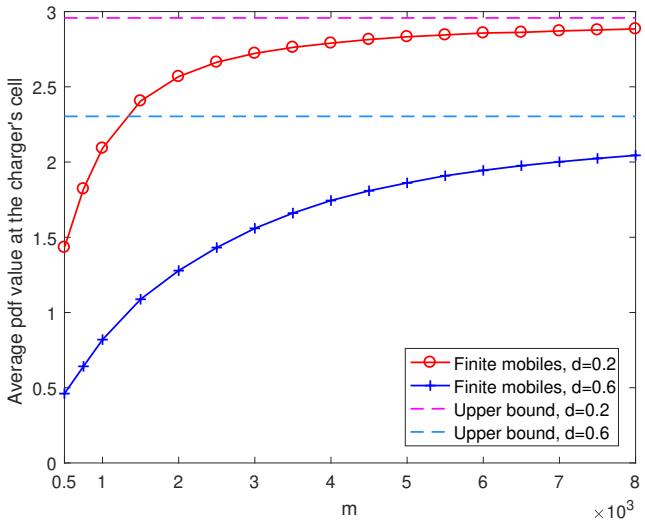

Figure 5.3: Average probability density values (per mobile) at the charger cell c, for the number of mobiles $m = 500, 750, 1000, 1500, \ldots, 8000$, the budget $d = 0.2$ and 0.6, the attraction range $d' = 0.2$, the charger cell $c = (-0.6, 0)$, and the capacity $\omega = \infty$.

energy budgets. Firstly, Figure 5.3 shows that the under-energized ($d = 0.2$) mobiles always pay more visits to the charger than highly-energized ($d = 0.6$) ones for any population m. It reflects the fact that a mobile initialized with a lower budget of energy is more prone to depletion and recharging (Figure 5.4). Secondly, compared to highly-energized mobiles, it takes a smaller population for under-energized mobiles to reach the upper bound of the expected density of the charger. Informally, the bound is a measure of how "attractive" the charger is to mobiles. This is because the increased opportunities for pair-wise communication would increase energy consumption rates and exacerbate the need for recharging more so for under-energized mobiles.

5.4 Effects of Wireless Capacity

In this section we explore the interaction between the charging-aware mobility (denoted MD) and the wireless capacity ω. The interest is in understanding the effects and trade-offs of detours for recharging in the setting of an ad hoc network constrained by different capacities for communications. For comparison, we propose a "detour-free" mobility model, denoted M, which resembles

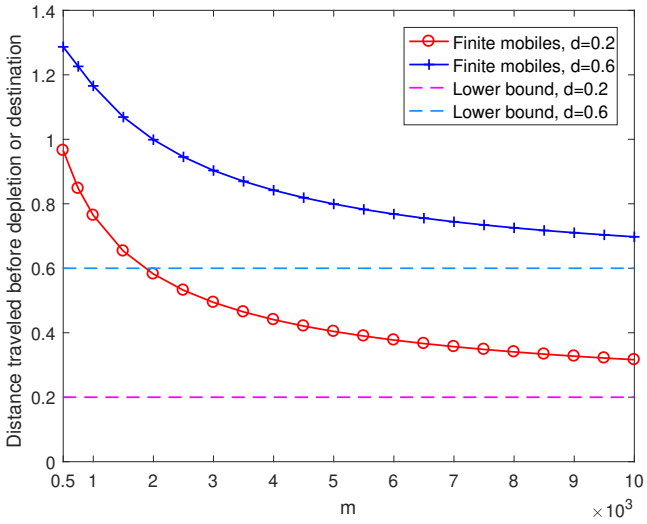

Figure 5.4: Average number of cells reached before depletion or reaching the destination waypoint, for the number of mobiles $m = 500, 750, 1000, 1500, \ldots, 8000$, the budget $d = 0.2$ and 0.6, the attraction range $d' = 0.2$, the charger cell $c = (-0.6, 0)$, and the capacity $\omega = \infty$.

the original model MD, except that the mobile follows (Manhattan) RWP only and *never* initiates a detour to the charger for recharging. In other words, a depleted mobile will recharge at the charger with the rare exception of accidentally passing through the charger's cell c on its path to the destination. In both models, the mobile renews its energy to d upon leaving a waypoint. Like the case of 1-dimensional cellular communications (Section 3.5.3), the investigated interplay between the energy budget d and the congestion level, depending on whether the mobiles are willing to detour to the charger for recharging, makes one of the main contributions of the thesis.

Figure 5.5 displays the (time-average) percentages of mobiles being blocked, communicating, and depleted respectively under the mobility models MD and M,[1] with the number of mobiles $m = 20000$, the budget $d = 0.2$ and 0.6, the attraction range $d' = 0.2$, the charger cell at the center/origin, i.e. $c = (0, 0)$, and the capacity $\omega = 1, 2, \ldots, 5$. In general, the mobiles following MD demonstrate *higher* blocking and *superior* communicating probabilities than mobiles following M. Such differences in performance between the mobility

[1]Recall that a mobile is said to be *blocked* if it has energy but cannot communicate due to exceeding capacity (Section 3.5). An operational mobile that is not blocked is said to be *communicating*.

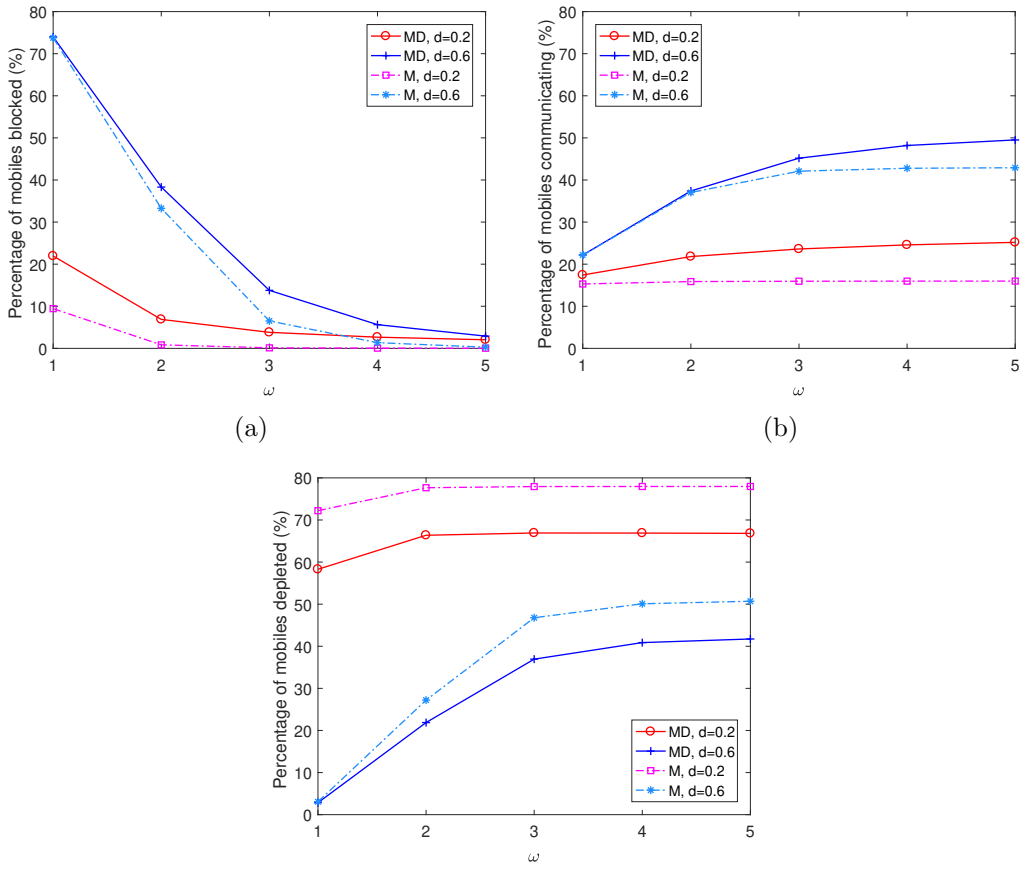

Figure 5.5: Percentages of mobiles blocked (a), communicating (b), and depleted (c) respectively, under the charging-aware mobility model MD and the variant model M, for the number of mobiles $m = 20000$, the budget $d = 0.2$ and 0.6, the attraction range $d' = 0.2$, the charger cell $c = (0, 0)$, and the capacity $\omega = 1, 2, \ldots, 5$.

models are due to two factors.

Firstly, it can be seen in Figure 5.5(c) that the mobiles under MD are always more likely to have energy, because of the ability to detour for recharging, and thus, potentially, have more opportunities for communication (possibly blocked for congestion) than under M. Secondly, the distributions of operational mobiles are supposed to differ between these two models, which can deepen their differences in communication. For this we examine the *conditional* blocking/communicating probabilities *given that* the mobiles have energy, as shown in Figure 5.6. While the higher blocking probabilities of MD are retained in Figure 5.6(a), Figure 5.6(b) shows that the operational mobiles typically have

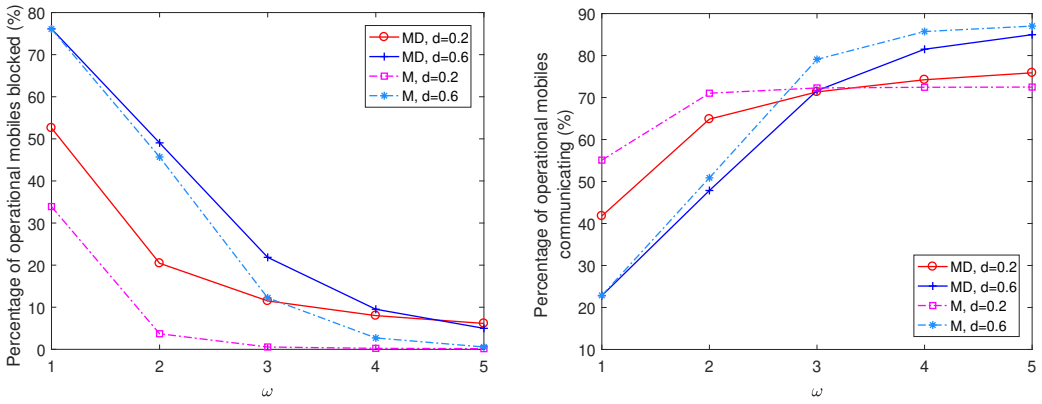

(a) (b)

Figure 5.6: Percentages of operational mobiles being blocked (a) and communicating (b) respectively, under the charging-aware mobility model MD and the variant model M, for the number of mobiles $m = 20000$, the budget $d = 0.2$ and 0.6, the attraction range $d' = 0.2$, the charger cell $c = (0, 0)$, and the capacity $\omega = 1, 2, \ldots, 5$.

lower communicating probabilities under MD than M. This seemingly "counterintuitive" property of MD is believed to be a consequence of the attraction effect of the charger, as elaborated below.

Specifically, for a high energy budget $d = 0.6$ and a highly constrained capacity $\omega = 1$, the mobiles are rarely depleted (Figure 5.5(c)), meaning almost all mobiles in the network are constantly available for pair-wise communication. On the other hand, the mobile distribution would be distorted the least since there is hardly any need for detours and recharging. In effect, in this case, there is little difference in mobility and communication between MD and M.

When the constraint on capacity is relaxed, however, the highly-energized mobiles start to incur less congestion but faster energy consumption. Under MD mobiles will be attracted to the charger and form congregations frequently; despite the gains in energy, this behavior not only increases the chances of being blocked around the charger (Figure 5.6(a)) but also reduces the number of *scattered* mobiles (i.e. those not concentrated at the charger) that can pair up for communication without congestion (Figure 5.6(b)). Nonetheless, regardless of the distortion effect on mobile distribution, the energy sufficiency

characterizing MD still gives the highly-energized mobiles superiority in overall communicating probability (Figure 5.5(b)).

Under a low energy budget ($d = 0.2$), the mobiles exhaust their energy quickly even when the capacity is the lowest ($\omega = 1$). As a result, due to frequent recharging and severe congestion around the charger, the under-energized mobiles that follow MD suffer markedly higher probabilities of being blocked (Figures 5.5(a), 5.6(a)). As the capacity increases, while congestion quickly diminishes under the M model because of its RWP mobility, the mobiles under MD perform more detours to the charger for recharging, gaining energy as well as extra opportunities for communication with peers around the charger (Figure 5.6(b)). Unlike the high-budget case, the under-energized but charging-unaware mobiles that follow M would suffer from persistent depletion and infrequent operational peers with which to communicate.

Lastly, we show in Figure 5.7 the costs of the charging-aware mobility of MD, in terms of delays in reaching waypoints due to detours to the charger (like Figure 3.9 of Section 3.5). Besides $d' = 0.2$, we also show results for attraction range $d' = 0.6$ to allow for possibly long detours. Firstly, it can be seen that the delays are always higher for under-energized mobiles ($d = 0.2$) because of their stronger attraction to the charger. Secondly, when the attraction range is as short as $d' = 0.2$, the delay stays small (less than 5%) with little variation for either energy budget level. By contrast, when $d' = 0.6$, the mobiles can arrive late to the extent of 25%–30% for a budget $d = 0.2$ or 15%–20% for $d = 0.6$, provided the capacity is high enough. We regard these delays as mostly acceptable and the detours for recharging as cost-effective, considering the incidental benefits of more energy and more chances of communication.

5.5 Effect of Multiple Chargers

In this section we investigate the charging-aware mobility MD in the presence of more than one charger. Specifically, we are interested in the communication performance under $n \geq 2$ chargers versus under a single charger. Here we consider $n = 5$ chargers deployed at $c_1 = (0, 0)$, $c_2 = (c^*, c^*)$, $c_3 = (-c^*, c^*)$,

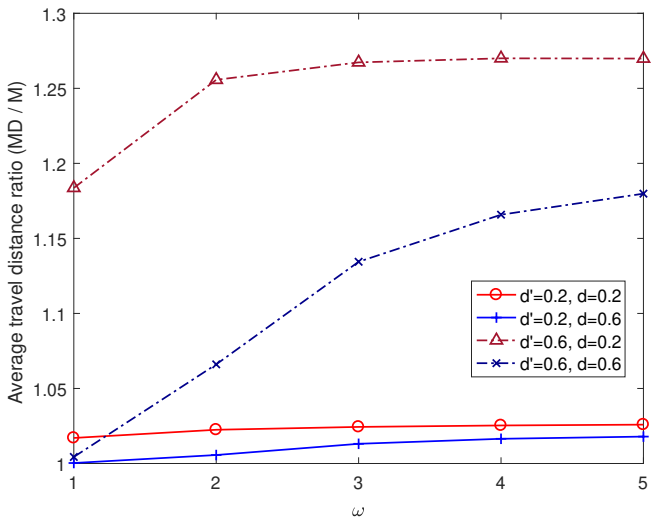

Figure 5.7: Average ratio of travel distance (between waypoints) under the MD model over that under M, for the number of mobiles $m = 20000$, the energy budget $d = 0.2$ and 0.6, the attraction range $d' = 0.2$ and 0.6, the charger cell $c = (0, 0)$, and the capacity $\omega = 1, 2, \ldots, 5$.

$c_4 = (-c^*, -c^*)$, and $c_5 = (c^*, -c^*)$ respectively ($c^* > 0$), with the attraction ranges $d'_1 = 0.12$ (or, 3 cells), $d'_2 = d'_4 = 0.04$ (1 cell), and $d'_3 = d'_5 = 0.08$ (2 cells). Figure 5.8 illustrates a placement of the five chargers with $c^* = 0.6$. In respect of Section 5.4, where the charger has an attraction range $d'_0 = 0.2$, the values of d'_1, d'_2, ..., and d'_n have been configured such that the total attraction areas in the area are *equal* between the 5-charger (D5) and 1-charger (D1) deployments.[2] This assumption allows us to explore the (dis)advantages of multi-charger deployments in connection with different locations of the chargers. Such exploration of multi-charger deployments is a main contribution of the thesis. Note that the value of c^* is supposed to be large enough such that the chargers are scattered with *no overlap* of attraction areas between any two chargers.

Figure 5.9 displays network performance under deployment D5 in comparison with D1, as c^* increases from 0.12 to 0.84, i.e., as the four chargers in the quadrants are gradually moved away from the center. For consistency, the number of mobiles $m = 20000$, the energy budget $d = 0.2$ or 0.6, and

[2]For our specific setting, the five chargers "cover" 61 cells in total that can attract and divert depleted mobiles, the same as that covered by the single charger at $(0, 0)$ with $d'_0 = 0.2$.

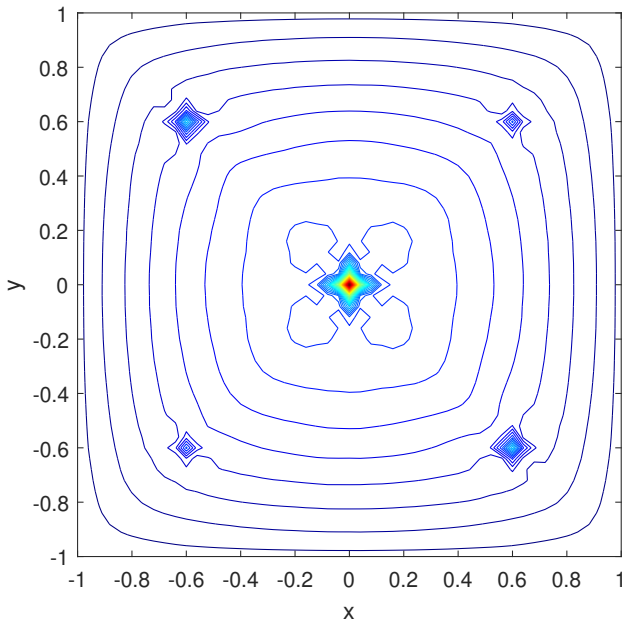

Figure 5.8: A contour plot of overall mobile distribution under the MD model and in the presence of five chargers located at $c_1 = (0, 0)$, $c_2 = (0.6, 0.6)$, $c_3 = (-0.6, 0.6)$, $c_4 = (-0.6, -0.6)$, and $c_5 = (0.6, -0.6)$ respectively, with attraction ranges $d'_1 = 0.12$, $d'_2 = d'_4 = 0.04$, and $d'_3 = d'_5 = 0.08$. The number of mobiles $m = 20000$, the energy budget $d = 0.2$, and the capacity $\omega = 5$.

the capacity $\omega = 2$ or 5. The results of Figure 5.9(c) show that the communication performance of D5 generally outperforms that of D1. The reason behind this superiority of D5 is two-fold: (1) the mobiles have easier access to the distributed chargers for recharging (Figure 5.9(d)); (2) the congestion due to clustering would not be overly exacerbated but even ameliorated when there are multiple chargers (with relatively short attraction ranges) to share the recharging load (Figure 5.9(a)).

As per Figure 5.9(c), when the four corner chargers are placed distantly (i.e. $c^* \geq 0.76$ for $d = 0.2$ and $\omega = 5$), the center charger alone would not attract enough mobiles for good performance. On the other hand, when the chargers are situated too close to each other (e.g. $c^* = 0.12$), D5 begins to resemble D1 and lose its advantage of distributed deployment. The optimal charger locations for maximizing the communication probability generally correspond to around $c^* = 0.28$ and 0.36, leaning towards the center of the area. This is because the mobiles are supposed to visit the center areas more often than

areas near the boundary. Chargers that are close (but not too close) to the center therefore can sustain many mobiles for recharging and communication.

For both energy budgets $d = 0.2$ and $d = 0.6$, the differences in communicating probabilities between D5 and D1 appear larger for a high capacity constraint $\omega = 5$ than for a lower capacity $\omega = 2$. This conforms to the fact that when limited by capacity and unable to transmit, the mobiles would consume energy slowly. Thus they will seldom detour for recharging. In the extreme case of $\omega = 2$ while $d = 0.6$, the rare need for charging leads to almost identical communicating probabilities between the two deployments (Figure 5.9(c)). Also, when $d = 0.2$, the maximum communication performance tends to shift from $c^* = 0.28$ to $c^* = 0.36$ (or 0.44), as the capacity decreases from $\omega = 5$ to $\omega = 2$. The dampened performance at $c^* = 0.28$ under $\omega = 2$ comes from the intense congestion incurred in communication restricted by low capacity (Figure 5.9(a)); hence in this case, as chargers are moved further away from the center, the decrease in their attraction can reduce clustering and produce more opportunities for communication.

Between the two energy budgets $d = 0.2$ and $d = 0.6$, the differences in performance between D5 and D1 are generally larger for $d = 0.2$, because of the corresponding stronger attraction to chargers. This stronger attraction effect under $d = 0.2$ also helps D5 maintain its advantage longer (up to $c^* = 0.76$) as the corner charger locations move away from the center. When the energy budget $d = 0.6$ and the capacity $\omega = 5$, D5 has a higher communicating probability only for $c^* < 0.6$.

In Figures 5.9(a)(d), as mentioned, the probabilities of mobiles being blocked and depleted basically agree with the patterns observed in Figure 5.9(c). In general, when the four corner chargers are deployed properly (e.g. with $c^* = 0.28$), the area would be covered in a balanced manner such that the mobiles can access the chargers easily for recharging (Figure 5.9(d)), meanwhile forming congregations frequently (Figure 5.9(a)). Note that the congregation around multiple chargers is often less harmful than one might think, as shown next. When the capacity constraint is lifted to $\omega = 5$, for instance, the congestion incurred under the deployment D5 is, overall, very close to that under

D1. For $0.36 \leq c^* < 0.76$ while $d = 0.2$, or $c^* = 0.44$ and 0.52 while $d = 0.6$, D5 even has lower blocking probabilities than D1 (Figure 5.9(b)), while still being able to maintain higher communicating probabilities (Figure 5.9(c)). We believe these c^* values (depending on the budget d and capacity ω) have captured certain "sweet spots" of charger locations, in the sense that the extent of clustering around each charger fits the capacity limit well enough to boost communication without causing severer congestion. A similar pattern can be observed for a lower capacity $\omega = 2$. For $c^* = 0.68$ and 0.76 while $d = 0.2$, for instance, the aforementioned "sweet spots" reoccur for D5. Another advantage of multi-charger deployment is the reduced cost of recharging; in the simulation the mobiles are delayed less than 2% under D5 for both energy budgets.

In summary, if the mobiles have a low energy budget and the capacity is highly constrained, the chargers should be deployed slightly distantly from the center (e.g. $c^* = 0.44$) to reduce their attraction and consequent congestion of mobiles. Otherwise, the chargers can be distributed moderately close to the center and each other (e.g. $c^* = 0.28$) for the highest chances of communication.

5.6 Chapter Summary

In this chapter we investigated the performance of charging-aware mobility in a MANET setting. From the plots of stationary mobile distribution we first observe several new patterns particular to the Manhattan space, e.g. "bump" of density sticking out from the charger and convex/concave density in "strips". As the network size grows, the mobiles would encounter each other more often and have their energy drained faster for pair-wise communication; as a result, with concentration intensifying at the charger, the mobile distribution across space tends towards that under the analytical model (or equivalently, under infinite mobiles). This shows that the analytical results can approximate mobile distributions for sufficiently dense networks. On the other hand, by comparing the (detour-enabled) charging-aware mobility MD with a detour-free model M

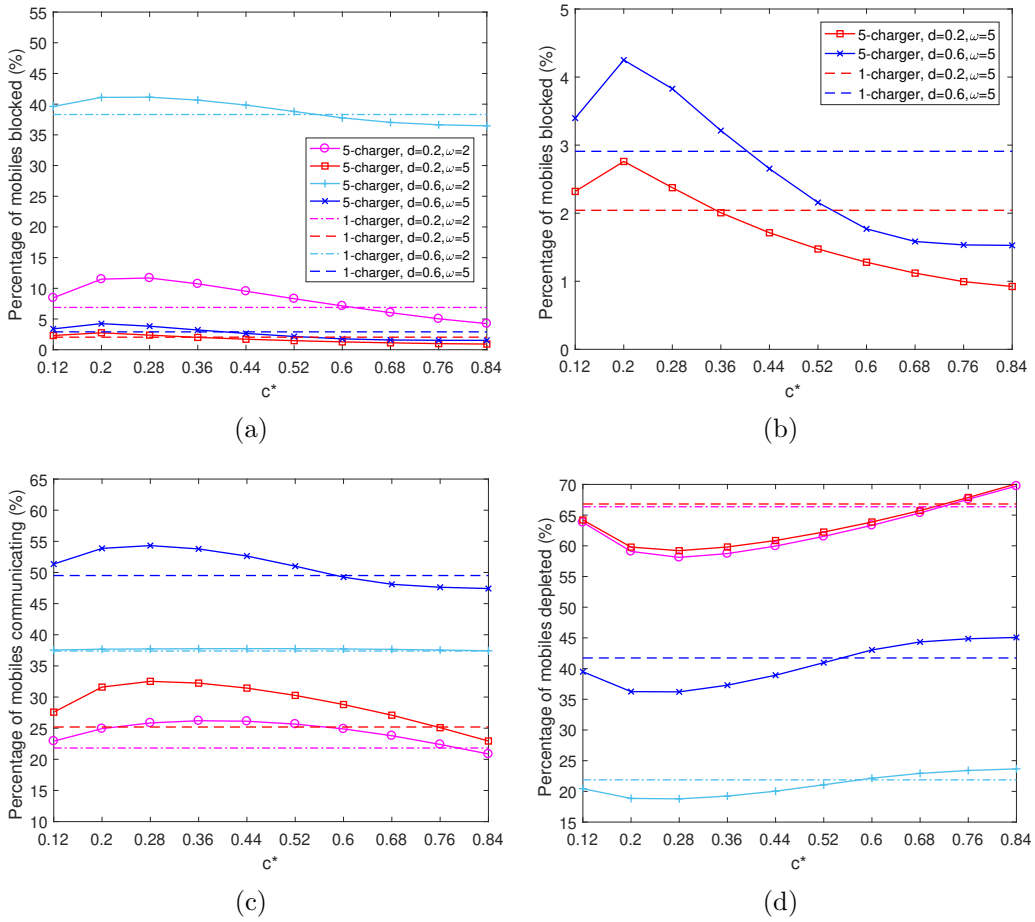

Figure 5.9: Percentages of mobiles blocked (a), communicating (b), and depleted (c) respectively, under the MD model and in the presence of five chargers located at $c_1 = (0, 0)$, $c_2 = (c^*, c^*)$, $c_3 = (-c^*, c^*)$, $c_4 = (-c^*, -c^*)$, and $c_5 = (c^*, -c^*)$ respectively, with $c^* = 0.12, 0.2, 0.28, \ldots, 0.84$, and attraction ranges $d'_1 = 0.12$, $d'_2 = d'_4 = 0.04$, and $d'_3 = d'_5 = 0.08$. The number of mobiles $m = 20000$, the budget $d = 0.2$ or 0.6, and the capacity $\omega = 2$ or 5. The results for comparison assume one charger located at $c_0 = (0, 0)$ with an attraction range $d'_0 = 0.2$. For clearer illustration, we also zoom in on the blocking probabilities with capacity $\omega = 5$ in Figure 5.9(b).

under varied capacity, we find that the detours for recharging not only supply the mobiles with more energy to communicate but also increase the opportunities for communication, provided the mobiles have a lower energy budget ($d = 0.2$) and the communication is not too limited by capacity ($\omega > 3$). For a high energy budget ($d = 0.6$), however, the congregations around the charger appear to reduce the chances of communication across the network. The costs of the benefits, i.e. delays in arrival at destinations, are mostly not signifi-

cant (less than 30%) even when the charger has a fairly large attraction range ($d' = 0.6$). Additionally, the study on multi-charger deployments suggests that it is mostly better to deploy more chargers with shorter attraction ranges than fewer chargers with longer ranges. The rule of thumb is to distribute the chargers not too close to each other and not close to the boundary of the area.

Chapter 6

Conclusion

6.1 Thesis Summary

In this thesis, we have modeled the recharging behavior of mobile nodes in 1-dimensional and 2-dimensional spaces, studied the resultant spatial mobile distributions both analytically and numerically, and explored the interaction between charging-aware mobility and ad hoc wireless communications through simulations. We recap the contributions as follows.

Charging-aware mobility in 1-dimensional space

A 1-dimensional analytical mobility model is proposed to depict a possible pattern of recharging behavior in the presence of a charger. The corresponding stationary distribution of the mobile location is derived, so is the energy-wise mobile distribution (i.e. while the mobile has energy or not). The analytical and simulation results exhibit the impact of boundaries, which creates asymmetry across space and discontinuities at the charger location. Notably, if the charger is located as near as within a distance d (i.e. the distance corresponding to the energy budget) to a boundary, the peak value of mobile density would shift from the charger location.

Insofar the interaction between mobility and wireless capacity is concerned, we have derived two bounds, including an upper bound for the communicating probability (per mobile) and a lower bound for the probability of being blocked due to exceeding capacity. In a comparison between the detour-enabled charging-aware mobility and a variant detour-free mobility model, we

observe the benefits of detours for recharging especially for under-energized mobiles that are more in need of energy supply. The study also indicates the advantages of a centered charger in the space, including the highest chances of communication and the least travel delays in reaching destinations.

Charging-aware mobility in 2-dimensional space

A 2-dimensional charging-aware mobility model is proposed and analyzed first in the setting of a (Euclidean) unit disk. Besides the perfect match between analytical and simulation results, we observe that the charger's impact to the mobile distribution is limited within its attraction range, which we call the "pseudo-local distortion" effect. Another interesting observation induced by the detours is the relatively dipped density at a distance d' (attraction range) to the charger. Based on the analytical results for single chargers, we also approximate the mobile distribution for multiple chargers, finding that the results are most accurate for sparsely distributed chargers.

Extending 2-dimensional analytical models to realistic setups

To understand the interaction between recharging and peer-to-peer communications, we further simulate an ad hoc network of charging-aware mobiles moving in a grid of cells (like in an urban core). When there is only one charger, the simulation results show that the concentration at the charger would increase with the mobile numbers. This is because the energy consumption for pair-wise communication is supposed to be faster when more mobiles are present. Moreover, by varying the limit of capacity and examining the corresponding blocking, communicating, and depletion probabilities of mobiles, we observe that the recharging behavior can indeed improve the network performance, especially for under-energized mobiles, by bringing gains in energy and extra communication opportunities (due to clustering). Meanwhile, the detours for recharging increase the average path time between waypoints by a factor of 1.3 at most, which should be acceptable in many cases. When there are more than one charger to deploy, the simulation results basically match the heuristic: the chargers should be scattered properly so as to cover the area

in a relatively even manner.

6.2 Direct Extensions

The work of this thesis can be extended directly in the following ways:

- As remarked in Section 4.4, the integral-form spatial mobile distribution derived based on the unit disk is generalizable to any 2-dimensional bounded convex area. Hence a direct extension is to apply the results to other (simple) shapes of areas, e.g. rectangles. The crucial part is to redefine the relevant lengths including l_2, l_3, l_{12}, l_{13}, and l_{17}, as well as replacing the factor $\pi^2\alpha$ with $A^2\alpha$, with A being the size of the area.

- Throughout the thesis, we assume the charging process is relatively short and the charging-aware mobiles never pause at any charger (or waypoint). Despite the development of fast charging technologies, this assumption of instantaneous charge may be arguably too idealistic. In effect, according to Equation (2.9), the effect of pauses on mobile distribution can be incorporated as an additive component, provided the pause time follows an independent distribution.

- We can generalize the current models by introducing heterogeneity into mobility, e.g., with respect to the occurrence of destinations across space (like [12, 35]), which is achievable by designating non-uniform distributions for the probability density function of waypoints. Moreover, we can consider mixes of populations with different charging awareness, i.e., a constitution of mobiles who would detour to a charger for recharging plus charging-unaware ones who would not. The expected mobile distribution is supposedly equal to the weighted mean of densities under the charging-aware and RWP mobility. A similar extension applies for a mix of charging-aware populations with differently designated chargers.

- It is conjectured that the modeling of probabilistic energy consumption at mobiles can be well approximated by the weighted mean of mobile

distributions under different constant energy budgets d. Apart from the question of finding proper weights for high accuracy, however, this problem can be prohibitively difficult if the consumption is assumed to be dependent on ad hoc communications between peers.

6.3 Future Work

In this section we propose three directions for future investigation.

Adaptive Energy-Aware Transmission Scheduling

In Chapter 5, we assume a fully greedy communication protocol followed by the mobiles; that is, a mobile is *always* ready to pair with any peer for communication as long as it has energy. A more realistic setting is to assume that an operational mobile is willing to be scheduled for pairing with a certain probability which can be less than 1.0. Or even further, each mobile may adjust its schedule based on energy conditions of it own and of the network. A lesson learned from the study in Chapter 5 is that despite the energy gained from recharging, the clustering resulting from detours to the charger can cause severe congestion especially for low-energy mobiles and highly constrained communication capacity. Given the charging-aware mobility, is there a way to schedule the mobiles optimally such that they can capitalize on energy sufficiency and improved opportunities for communication but at low risk of being blocked? This is a noteworthy question for future exploration.

Optimized Multi-Charger Placement

In Chapter 5, Figure 5.9(b) suggests that there is an optimal deployment (in terms of communicating probability) of five chargers corresponding to c^* valued between 0.2 and 0.44, depending on the energy budget and capacity limit. Note that the optimal charger locations are not fully consistent with the supposedly most balanced coverage, i.e. $c^* = 0.5$, by which the four corner chargers would be centered in their respective quadrants, each covering a unit area. Actually, since there is still a charger at the center, the corner chargers

should be deployed further away with $c^* > 0.5$ so as to yield even coverage across the area. The discrepancy in the optimal value of c^* is conjectured to come from the fact that the center area, which tends to be visited more often than areas near the boundary, correspondingly bears more burden to cover the area with recharging possibilities. Considering this connection, it is noteworthy to formulate the optimal deployment for a given number of chargers under the charging-aware mobility.

Approximation and Bounds of Mobile Distribution

As shown in Equation (4.53) (Chapter 4), the stationary pdf $f_{Z(t)}(z)$ of the mobile location has a non-trivial integral form in the 2-dimensional case. To facilitate its application to further analyses, we can approximate the function $f_{Z(t)}(z)$ by bounding the lengths of relevant line segments through geometric induction. For instance, to bound functions $h_0(z)$ and $h_1(z)$, we can decouple the set of segment lengths including l_2, $l_3 - l_4 - d$, $l_2 + l_3$, and $l_4 + d$, and find their globally admissible ranges (not subject to the integral limits $\theta_5 - \theta_6$ and $\theta_5 + \theta_6$), i.e.

$$\begin{cases} 1 - r \le l_2 \le 1 + r \\ 1 - |c| - d' - d \le l_3 - l_4 - d \le 1 + |c| + d' - d \\ 2\sqrt{1 - r^2} \le l_2 + l_3 \le 2 \\ |z - c| - d' + d \le l_4 + d \le |z - c| \cos\theta_6 + d \end{cases} \tag{6.1}$$

It would be harder to find appropriate bounds for the other two functions $g_0(z)$ and $g_1(z)$. Despite the lack of sophistication and tightness, the above crude method should be generalizable to areas in arbitrary shapes. Further investigation is left for future work.

References

[1] M. Alizadeh et al. "Optimized Path Planning for Electric Vehicle Routing and Charging." In: *Proc. 52nd Annual Allerton Conference on Communication, Control, and Computing (Allerton '14)*. Sept. 2014, pp. 25–32. 25

[2] C. M. Angelopoulos et al. "Traversal Strategies for Wireless Power Transfer in Mobile Ad-Hoc Networks." In: *Proc. 18th ACM International Conference on Modeling, Analysis and Simulation of Wireless and Mobile Systems (MSWiM '15)*. Nov. 2015, pp. 31–40. 25

[3] N. Aschenbruck, A. Munjal, and T. Camp. "Trace-based Mobility Modeling for Multi-Hop Wireless Networks." In: *Computer Communications* 34.6 (2011), pp. 704–714. 7

[4] F. Ashtiani, J. A. Salehi, and M. R. Aref. "Mobility Modeling and Analytical Solution for Spatial Traffic Distribution in Wireless Multimedia Networks." In: *IEEE Journal on Selected Areas in Communications* 21.10 (Dec. 2003), pp. 1699–1709. 8

[5] S. Bae and A. Kwasinski. "Spatial and Temporal Model of Electric Vehicle Charging Demand." In: *IEEE Transactions on Smart Grid* 3.1 (Mar. 2012), pp. 394–403. 24

[6] M. Balazinska and P. Castro. "Characterizing Mobility and Network Usage in a Corporate Wireless Local-area Network." In: *Proc. 1st ACM International Conference on Mobile Systems, Applications, and Services (MobiSys '03)*. 2003, pp. 303–316. 7

[7] N. Banerjee, M. D. Corner, and B. N. Levine. "An Energy-Efficient Architecture for DTN Throwboxes." In: *Proc. 26th IEEE International Conference on Computer Communications (INFOCOM '07)*. May 2007, pp. 776–784. 3

[8] W. Bao and B. Liang. "Stochastic Geometric Analysis of User Mobility in Heterogeneous Wireless Networks." In: *IEEE Journal on Selected Areas in Communications* 33.10 (Oct. 2015), pp. 2212–2225. 8

[9] I. S. Bayram et al. "Electric Power Allocation in a Network of Fast Charging Stations." In: *IEEE Journal on Selected Areas in Communications* 31.7 (July 2013), pp. 1235–1246. 24

[10] C. Bettstetter. "Mobility Modeling in Wireless Networks: Categorization, Smooth Movement, and Border Effects." In: *ACM SIGMOBILE Mobile Computing and Communications Review* 5.3 (July 2001), pp. 55–66. 15, 16

[11] C. Bettstetter, G. Resta, and P. Santi. "The Node Distribution of the Random Waypoint Mobility Model for Wireless Ad Hoc Networks." In: *IEEE Transactions on Mobile Computing* 2.3 (July 2003), pp. 257–269. 15–17, 70

[12] C. Bettstetter and C. Wagner. "The Spatial Node Distribution of the Random Waypoint Mobility Model." In: *Mobile Ad-Hoc Netzwerke, 1. deutscher Workshop über Mobile Ad-Hoc Netzwerke (WMAN '02)*. GI, 2002, pp. 41–58. 8, 99

[13] C. Boldrini and A. Passarella. "HCMM: Modelling Spatial and Temporal Properties of Human Mobility Driven by Users' Social Relationships." In: *Computer Communications* 33.9 (2010), pp. 1056–1074. 9, 13, 14

[14] V. Borrel et al. "SIMPS: Using Sociology for Personal Mobility." In: *IEEE/ACM Transactions on Networking* 17.3 (June 2009), pp. 831–842. 9

[15] E. Bulut and B. K. Szymanski. "Mobile Energy Sharing through Power Buddies." In: *Proc. IEEE Wireless Communications and Networking Conference (WCNC '17)*. Mar. 2017, pp. 1–6. 27

[16] T. Camp, J. Boleng, and V. Davies. "A Survey of Mobility Models for Ad Hoc Network Research." In: *Wireless Communications and Mobile Computing* 2.5 (2002), pp. 483–502. 9

[17] C. J. E. Castle and A. T. Crooks. "Principles and Concepts of Agent-based Modelling for Developing Geospatial Simulations." In: *Working Paper 110, Centre for Advanced Spatial Analysis, UCL* (Sept. 2006). 3

[18] A. Chaintreau et al. *Pocket Switched Networks: Real-World Mobility and its Consequences for Opportunistic Forwarding*. Tech. rep. UCAM-CL-TR-617. University of Cambridge, Computer Laboratory, Feb. 2005. 14

[19] C. Chau, K. Elbassioni, and C. Tseng. "Drive Mode Optimization and Path Planning for Plug-In Hybrid Electric Vehicles." In: *IEEE Transactions on Intelligent Transportation Systems* 18.12 (Dec. 2017), pp. 3421–3432. 25

[20] T. Chiu et al. "Mobility-Aware Charger Deployment for Wireless Rechargeable Sensor Networks." In: *Proc. 14th Asia-Pacific Network Operations and Management Symposium (APNOMS '12)*. Sept. 2012, pp. 1–7. 21, 24

[21] H. Dai et al. "SCAPE: Safe Charging With Adjustable Power." In: *IEEE/ACM Transactions on Networking* 26.1 (Feb. 2018), pp. 520–533. 21, 24

[22] L. De Nardis and M.-G. Di Benedetto. "MoMo: A Group Mobility Model for Future Generation Mobile Wireless Networks." In: *arXiv preprint arXiv:1704.03065* (2017). 9

[23] A. Einstein. "On the Movement of Small Particles Suspended in Stationary Liquids Required by the Molecular-Kinetic Theory of Heat." In: *Annalen der Physik* 17 (1905), pp. 549–560. 8

[24] *Energous WattUp® - Wireless Charging 2.0 Technology*. `http://energous.com/`. 2019. 20

[25] L. M. Feeney and M. Nilsson. "Investigating the Energy Consumption of a Wireless Network Interface in an Ad Hoc Networking Environment." In: *Proc. 20th IEEE International Conference on Computer Communications (INFOCOM '01)*. Vol. 3. Apr. 2001, pp. 1548–1557. 3

[26] W. Gao and J. Harms. "Charging-Aware Mobility Modeling for Wirelessly Chargeable Intermittently Connected MANETs." In: *Proc. 28th IEEE Annual International Symposium on Personal, Indoor, and Mobile Radio Communications (PIMRC '17)*. Oct. 2017, pp. 1–7. 2

[27] W. Gao, I. Nikolaidis, and J. Harms. "On the Interaction of Charging-Aware Mobility and Wireless Capacity." In: *IEEE Transactions on Mobile Computing* (2019), pp. 1–1. iii

[28] M. Gorlatova, A. Wallwater, and G. Zussman. "Networking Low-Power Energy Harvesting Devices: Measurements and Algorithms." In: *IEEE Transactions on Mobile Computing* 12.9 (Sept. 2013), pp. 1853–1865. 20

[29] I. S. Gradshteyn and I. M. Ryzhik. *Table of Integrals, Series, and Products*. Academic Press, 2014. 109

[30] M. Grossglauser and D. N. C. Tse. "Mobility Increases the Capacity of Ad Hoc Wireless Networks." In: *IEEE/ACM Transactions on Networking* 10.4 (Aug. 2002), pp. 477–486. 27

[31] P. Gupta and P. R. Kumar. "The Capacity of Wireless Networks." In: *IEEE Transactions on Information Theory* 46.2 (Mar. 2000), pp. 388–404. 27, 28

[32] S. He et al. "Energy Provisioning in Wireless Rechargeable Sensor Networks." In: *Proc. 30th IEEE International Conference on Computer Communications (INFOCOM '11)*. Apr. 2011, pp. 2006–2014. 21, 23, 24

[33] X. Hong et al. "A Group Mobility Model for Ad Hoc Wireless Networks." In: *Proc. 2nd ACM International Workshop on Modeling, Analysis and Simulation of Wireless and Mobile Systems (MSWiM '99)*. Aug. 1999, pp. 53–60. 9, 10

[34] *How Can Quick Charge™4+ Turbocharge Your Mobile Device*. `https://www.qualcomm.com/news/onq/2018/02/23/how-can-quick-charge-4-turbocharge-your-mobile-device`. 2019. 3

[35] W.-J. Hsu et al. "Weighted Waypoint Mobility Model and its Impact on Ad Hoc Networks." In: *ACM SIGMOBILE Mobile Computing and Communications Review* 9.1 (Jan. 2005), pp. 59–63. 9–11, 99

[36] W.-J. Hsu et al. "Modeling Spatial and Temporal Dependencies of User Mobility in Wireless Mobile Networks." In: *IEEE/ACM Transactions on Networking* 17.5 (Oct. 2009), pp. 1564–1577. 9, 11, 13

[37] K. Huang and V. K. N. Lau. "Enabling Wireless Power Transfer in Cellular Networks: Architecture, Modeling and Deployment." In: *IEEE Transactions on Wireless Communications* 13.2 (Feb. 2014), pp. 902–912. 21, 22, 27, 28

[38] E. Hyytia, P. Lassila, and J. Virtamo. "A Markovian Waypoint Mobility Model with Application to Hotspot Modeling." In: *Proc. IEEE International Conference on Communications (ICC '06)*. Vol. 3. June 2006, pp. 979–986. 9, 12, 13, 15, 19

[39] E. Hyytia, P. Lassila, and J. Virtamo. "Spatial Node Distribution of the Random Waypoint Mobility Model with Applications." In: *IEEE Transactions on Mobile Computing* 5.6 (June 2006), pp. 680–694. 15, 18, 19

[40] M. Janssen and E. Ostrom. "Empirically based, Agent-based Models." In: *Ecology and Society* 11.2 (2006). 3

[41] D. B. Johnson and D. A. Maltz. "Dynamic Source Routing in Ad Hoc Wireless Networks." In: *Mobile Computing*. Springer US, 1996, pp. 153–181. 3, 8

[42] H. Ju and R. Zhang. "Throughput Maximization in Wireless Powered Communication Networks." In: *IEEE Transactions on Wireless Communications* 13.1 (Jan. 2014), pp. 418–428. 21

[43] S. Ko and S. Kim. "Impact of Node Speed on Energy-Constrained Opportunistic Internet-of-Things with Wireless Power Transfer." In: *Sensors* 18.7 (2018). 28

[44] S. Ko, S. Yu, and S. Kim. "The Capacity of Energy-Constrained Mobile Networks with Wireless Power Transfer." In: *IEEE Communications Letters* 17.3 (Mar. 2013), pp. 529–532. 25, 27, 28

[45] I. Krikidis. "Simultaneous Information and Energy Transfer in Large-Scale Networks with/without Relaying." In: *IEEE Transactions on Communications* 62.3 (Mar. 2014), pp. 900–912. 28

[46] A. Kurs et al. "Wireless Power Transfer via Strongly Coupled Magnetic Resonances." In: *Science* 317.5834 (2007), pp. 83–86. 20

[47] J.-Y. Le Boudec. "Understanding the Simulation of Mobility Models with Palm Calculus." In: *Performance Evaluation* 64.2 (Feb. 2007), pp. 126–147. 15, 16, 18, 19, 32, 54, 67

[48] J.-Y. Le Boudec. *Performance Evaluation of Computer and Communication Systems*. EPFL Press, 2011. 15

[49] J.-Y. Le Boudec and M. Vojnovic. "The Random Trip Model: Stability, Stationary Regime, and Perfect Simulation." In: *IEEE/ACM Transactions on Networking* 14.6 (Dec. 2006), pp. 1153–1166. 8, 15, 16, 18

[50] A. Madhja, S. Nikoletseas, and T. P. Raptis. "Efficient, Distributed Coordination of Multiple Mobile Chargers in Sensor Networks." In: *Proc. 16th ACM International Conference on Modeling, Analysis and Simulation of Wireless and Mobile Systems (MSWiM '13)*. Nov. 2013, pp. 101–108. 25, 26

[51] A. Madhja, S. Nikoletseas, and A. A. Voudouris. "Mobility-Aware, Adaptive Algorithms for Wireless Power Transfer in Ad Hoc Networks." In: *Algorithms for Sensor Systems*. Springer International Publishing, 2019, pp. 145–158. 21–23

[52] A. Madhja et al. "Peer-to-Peer Energy-Aware Tree Network Formation." In: *Proc. 16th ACM International Symposium on Mobility Management and Wireless Access (MobiWac'18)*. 2018, pp. 1–8. 27

[53] B. B. Mandelbrot. *The Fractal Geometry of Nature*. 3rd ed. W. H. Freeman and Company, 1983. 8, 12

[54] A. Mei and J. Stefa. "SWIM: A Simple Model to Generate Small Mobile Worlds." In: *Proc. 28th IEEE International Conference on Computer Communications (INFOCOM '09)*. Apr. 2009, pp. 2106–2113. 9, 13, 14

[55] F. Morlot, S. E. Elayoubi, and F. Baccelli. "An Interaction-Based Mobility Model for Dynamic Hot Spot Analysis." In: *Proc. 29th IEEE International Conference on Computer Communications (INFOCOM '10)*. Mar. 2010, pp. 1–9. 13

[56] A. Munjal, T. Camp, and W. C. Navidi. "SMOOTH: A Simple Way to Model Human Mobility." In: *Proc. 14th ACM International Conference on Modeling, Analysis and Simulation of Wireless and Mobile Systems (MSWiM '11)*. 2011, pp. 351–360. 9, 12

[57] M. Musolesi and C. Mascolo. "A Community Based Mobility Model for Ad Hoc Network Research." In: *Proc. 2nd International Workshop on Multi-Hop Ad Hoc Networks: From Theory to Reality (REALMAN '06)*. ACM, May 2006, pp. 31–38. 9, 13, 14

[58] *New Discovery Makes Fast-Charging, Better Performing Lithium-Ion Batteries Possible*. `https://phys.org/news/2019-04-discovery-fast-charging-lithium-ion-batteries.html`. 2019. 3

[59] N. Nigam et al. "Control of Multiple UAVs for Persistent Surveillance: Algorithm and Flight Test Results." In: *IEEE Transactions on Control Systems Technology* 20.5 (Sept. 2012), pp. 1236–1251. 25

[60] S. Nikoletseas, T. P. Raptis, and C. Raptopoulos. "Radiation-Constrained Algorithms for Wireless Energy Transfer in Ad Hoc Networks." In: *Computer Networks* 124 (2017), pp. 1–10. 24

[61] Y. Peng et al. "Prolonging Sensor Network Lifetime Through Wireless Charging." In: *Proc. 31st IEEE Real-Time Systems Symposium (RTSS '10)*. Nov. 2010, pp. 129–139. 25, 26

[62] M. Piórkowski, N. Sarafijanovic-Djukic, and M. Grossglauser. "On Clustering Phenomenon in Mobile Partitioned Networks." In: *Proc. 1st ACM SIGMOBILE Workshop on Mobility Models (MobilityModels '08)*. 2008, pp. 1–8. 9, 11

[63] *Powercast®*. `http://www.powercastco.com/`. 2019. 20

[64] W. H. Press et al. *Numerical Recipes 3rd Edition: The Art of Scientific Computing*. Cambridge University Press, 2007. 68

[65] *Qi®*. `https://www.wirelesspowerconsortium.com/`. 2018. 20

[66] A. Rojas, P. Branch, and G. Armitage. "Experimental Validation of the Random Waypoint Mobility Model Through a Real World Mobility Trace for Large Geographical Areas." In: *Proc. 8th ACM International Symposium on Modeling, Analysis and Simulation of Wireless and Mobile Systems (MSWiM '05)*. 2005, pp. 174–177. 7

[67] E. M. Royer, P. M. Melliar-Smith, and L. E. Moser. "An Analysis of the Optimum Node Density for Ad hoc Mobile Networks." In: *Proc. IEEE International Conference on Communications (ICC '01)*. Vol. 3. June 2001, pp. 857–861. 8, 9

[68] A. H. Sakr and E. Hossain. "Cognitive and Energy Harvesting-Based D2D Communication in Cellular Networks: Stochastic Geometry Modeling and Analysis." In: *IEEE Transactions on Communications* 63.5 (May 2015), pp. 1867–1880. 21, 28

[69] M. Sánchez and P. Manzoni. "ANEJOS: a Java based Simulator for Ad Hoc Networks." In: *Future Generation Computer Systems* 17.5 (2001). I: Best of Websim99. II: Traffic Simulation, pp. 573–583. 9, 10

[70] J. Scherer and B. Rinner. "Persistent Multi-UAV Surveillance with Energy and Communication Constraints." In: *Proc. 12th IEEE International Conference on Automation Science and Engineering (CASE '16)*. Aug. 2016, pp. 1225–1230. 25

[71] C. Tuduce and T. Gross. "A Mobility Model Based on WLAN Traces and its Validation." In: *Proc. 24th IEEE International Conference on Computer Communications (INFOCOM '05)*. Vol. 1. Mar. 2005, pp. 664–674. 7

[72] G. Wang et al. "Traffic-Constrained Multiobjective Planning of Electric-Vehicle Charging Stations." In: *IEEE Transactions on Power Delivery* 28.4 (Oct. 2013), pp. 2363–2372. 25

[73] *WiTricity®*. `http://witricity.com/`. 2019. 20

[74] P. Worgan et al. "PowerShake: Power Transfer Interactions for Mobile Devices." In: *Proc. 2016 CHI Conference on Human Factors in Computing Systems (CHI '16)*. ACM, 2016, pp. 4734–4745. 27

[75] L. Xie et al. "On Traveling Path and Related Problems for a Mobile Station in a Rechargeable Sensor Network." In: *Proc. 14th ACM International Symposium on Mobile Ad Hoc Networking and Computing (MobiHoc '13)*. July 2013, pp. 109–118. 25, 26

[76] Y.-C. Chen, J. Kurose, and D. Towsley. "A Mixed Queueing Network Model of Mobility in a Campus Wireless Network." In: *Proc. 31st IEEE International Conference on Computer Communications (INFOCOM '12)*. Mar. 2012, pp. 2656–2660. 8

Appendix A

Proof of Theorem 3.4.1.1

We detail the proof only for the case where $d \leq \frac{1}{2}$ and $c \in [d, 1-d]$, considering that given other settings of d and c (Table 3.3) the pdf can be derived following similar steps. Firstly, we have the following lemma for Case I (i.e. movements following direct paths), provided $d \leq \frac{1}{4}$ and $c \in [2d, 1-2d]$.

Lemma 1. *Suppose $c \in [2d, 1-2d]$ while $d \leq \frac{1}{4}$, and the waypoints are such that the mobile travels directly without detours. Then the stationary pdf, $f^{\mathrm{I}}_{X(t)}(x)$, of the mobile location $X(t)$ is*

$$\alpha f^{\mathrm{I}}_{X(t)}(x) = \begin{cases} h(x,c), & \text{if } x \in [0, d) \\ h(x,c) + \frac{(x-d)^2}{2}, & \text{if } x \in [d, c-d] \\ d^2 + x + c - d - \frac{(x+c)^2}{2}, & \text{if } x \in (c-d, c+d) \\ h(x,c) - x + c - d + \frac{(x+d)^2}{2}, & \text{if } x \in [c+d, 1-d] \\ h(x,c) + c - \frac{1}{2}, & \text{if } x \in (1-d, 1] \end{cases} \tag{A.1}$$

where

$$h(x,c) = 2x - \frac{3x^2}{2} - cx.$$

Proof. Supposing $w_0 \leq w_1$, then we can make substitutions as follows:

$$\begin{cases} \rho = \frac{l_0}{l_0 + l_1} \\ w_0 = x - l_0 \\ w_1 = x + l_1 \end{cases}$$

where l_0 (l_1 resp.) is the distance from the mobile's current location x to waypoint w_0 (w_1 resp.). The Jacobian of such transformation is given by [29]

$$\det\left[\mathbf{J}(x, l_0, l_1)\right] = \begin{vmatrix} 0 & \frac{l_1}{(l_0+l_1)^2} & -\frac{l_0}{(l_0+l_1)^2} \\ 1 & -1 & 0 \\ 1 & 0 & 1 \end{vmatrix} = -\frac{1}{l_0 + l_1}.$$

Then we have for Equation (3.3) that

$$
\begin{aligned}
&\int_{\mathcal{W}_0^{w_0\le w_1}}\int_{\mathcal{W}_1^{w_0\le w_1}} |w_0-w_1| \int_0^1 [(1-\rho)w_0+\rho w_1]\,\mathrm{d}\rho\,\mathrm{d}w_1\,\mathrm{d}w_0 \\
&\quad= \int_0^d x\int_0^x\int_0^{d-l_0} 1\,\mathrm{d}l_1\,\mathrm{d}l_0\,\mathrm{d}x + \int_d^{1-d} x\int_0^d\int_0^{d-l_0} 1\,\mathrm{d}l_1\,\mathrm{d}l_0\,\mathrm{d}x \\
&\qquad+ \int_{1-d}^1 x\int_0^{1-x}\int_0^{d-l_1} 1\,\mathrm{d}l_0\,\mathrm{d}l_1\,\mathrm{d}x + \int_0^d x\int_0^x\int_{d-l_0}^{1-x} 1\,\mathrm{d}l_1\,\mathrm{d}l_0\,\mathrm{d}x \\
&\qquad+ \int_d^{c-d} x\int_0^d\int_{d-l_0}^{1-x} 1\,\mathrm{d}l_1\,\mathrm{d}l_0\,\mathrm{d}x + \int_d^{c-d} x\int_d^x\int_0^{1-x} 1\,\mathrm{d}l_1\,\mathrm{d}l_0\,\mathrm{d}x \\
&\qquad+ \int_{c-d}^c x\int_{x-(c-d)}^d\int_{d-l_0}^{1-x} 1\,\mathrm{d}l_1\,\mathrm{d}l_0\,\mathrm{d}x + \int_{c-d}^c x\int_d^x\int_0^{1-x} 1\,\mathrm{d}l_1\,\mathrm{d}l_0\,\mathrm{d}x \\
&\qquad+ \int_c^1 x\int_{x-(c-d)}^x\int_0^{1-x} 1\,\mathrm{d}l_1\,\mathrm{d}l_0\,\mathrm{d}x \\
&\quad= \int_0^d x\cdot\left(dx-\frac{x^2}{2}\right)\mathrm{d}x + \int_d^{1-d} x\cdot\frac{d^2}{2}\,\mathrm{d}x \\
&\qquad+ \int_{1-d}^1 x\cdot\left(d(1-x)-\frac{(1-x)^2}{2}\right)\mathrm{d}x + \int_0^d x\cdot\left[(1-d)x-\frac{x^2}{2}\right]\mathrm{d}x \\
&\qquad+ \int_d^{c-d} x\cdot\left(x(1-x)-\frac{d^2}{2}\right)\mathrm{d}x + \int_{c-d}^c x\cdot\left(c-d(1-x)-\frac{x^2}{2}-\frac{c^2}{2}\right)\mathrm{d}x \\
&\qquad+ \int_c^1 x\cdot(c-d)(1-x)\,\mathrm{d}x
\end{aligned}
\tag{A.2}
$$

Likewise, when $w_0 > w_1$, there is

$$
\begin{aligned}
&\int_{\mathcal{W}_0^{w_0>w_1}}\int_{\mathcal{W}_1^{w_0>w_1}} |w_0-w_1| \int_0^1 [(1-\rho)w_0+\rho w_1]\,\mathrm{d}\rho\,\mathrm{d}w_1\,\mathrm{d}w_0 \\
&\quad= \int_0^d x\cdot\left(dx-\frac{x^2}{2}\right)\mathrm{d}x \;+ \int_d^{1-d} x\cdot\frac{d^2}{2}\,\mathrm{d}x \\
&\qquad+ \int_{1-d}^1 x\cdot\left(d(1-x)-\frac{(1-x)^2}{2}\right)\mathrm{d}x \\
&\qquad+ \int_{1-d}^1 x\cdot\left[(x-d)(1-x)+\frac{(1-x)^2}{2}\right]\mathrm{d}x + \int_{c+d}^{1-d} x\cdot\left(x(1-x)-\frac{d^2}{2}\right)\mathrm{d}x \\
&\qquad+ \int_c^{c+d} x\cdot\left[(1-d)x-\frac{x^2}{2}-\frac{c^2}{2}\right]\mathrm{d}x + \int_0^c x\cdot(1-c-d)x\,\mathrm{d}x
\end{aligned}
\tag{A.3}
$$

We can then obtain Equation (A.1) by combining Equations (A.2)(A.3). □

Now we consider Case II, i.e. movements involving detours, and still $c \in [2d, 1-2d]$.

Lemma 2. *Suppose $c \in [2d, 1-2d]$ while $d \le \frac{1}{4}$, and the waypoints are such that the mobile always needs to detour for charging. Then the stationary pdf of location, $f^{\mathrm{II}}_{X(t)}(x)$, is*

$$\alpha f^{\mathrm{II}}_{X(t)}(x) = \begin{cases} \frac{x^2}{2} + cx, & \text{if } x \in [0, d) \\ dx - \frac{d^2}{2} + cx, & \text{if } x \in [d, c-d] \\ x - c + d - d^2 + \frac{(x+c)^2}{2} - x^2, & \text{if } x \in (c-d, c) \\ 1 - x - c + d - d^2 + \frac{(x+c)^2}{2} - x^2, & \text{if } x \in [c, c+d) \\ d(1-x) - \frac{d^2}{2} + (1-x)(1-c), & \text{if } x \in [c+d, 1-d] \\ \frac{(1-x)^2}{2} + (1-x)(1-c), & \text{if } x \in (1-d, 1] \end{cases} \tag{A.4}$$

Proof. Firstly, suppose $w_0 \le w_1$, then we can derive for Equation (3.4) that

$$\begin{aligned} &\int_{\mathcal{U}_0^{w_0 \le w_1}} \int_{\mathcal{U}_1^{w_0 \le w_1}} \psi(w_0, w_1)\, \mathrm{d}w_1\, \mathrm{d}w_0 \\ &\quad = \int_{c-d}^{1-d} d(1 - w_0 - d)\phi_1(w_0, w_0 + d)\, \mathrm{d}w_0 \\ &\qquad + \int_{c-d}^{1-d} (1 - w_0 - d)(w_0 + d - c)\phi_2(w_0 + d, c)\, \mathrm{d}w_0 \\ &\qquad + \int_{c-d}^{1-d} \int_{w_0+d}^{1} (w_1 - c)\phi_3(c, w_1)\, \mathrm{d}w_1\, \mathrm{d}w_0 \\ &\quad = \int_{c-d}^{c} x \int_0^{x-(c-d)} (1 - x + l_2 - d)\, \mathrm{d}l_2\, \mathrm{d}x + \int_c^{1-d} x \int_0^{d} (1 - x + l_2 - d)\, \mathrm{d}l_2\, \mathrm{d}x \\ &\qquad + \int_{1-d}^{1} x \int_{x-(1-d)}^{d} (1 - x + l_2 - d)\, \mathrm{d}l_2\, \mathrm{d}x + \int_c^1 x \int_0^{1-x} (1 - x - l_3)\, \mathrm{d}l_3\, \mathrm{d}x \\ &\qquad + \int_c^1 x \int_0^{1-x} \int_c^{x+l_4} 1\, \mathrm{d}w'\, \mathrm{d}l_4\, \mathrm{d}x \\ &\quad = \int_{c-d}^{c} x \cdot \left(x - c + d + \frac{c^2}{2} - \frac{(x+d)^2}{2} \right) \mathrm{d}x + \int_c^{1-d} x \cdot \left(d(1-x) - \frac{d^2}{2} \right) \mathrm{d}x \\ &\qquad + \int_{1-d}^{1} x \cdot \frac{(1-x)^2}{2}\, \mathrm{d}x + \int_c^1 x \cdot (1-x)(1-c)\, \mathrm{d}x \end{aligned} \tag{A.5}$$

where

$$\begin{aligned} \phi_1(w_0, w_0 + d) &= \int_0^1 [(1 - \varrho_1)w_0 + \varrho_1(w_0 + d)]\, \mathrm{d}\varrho_1 \\ \phi_2(w_0 + d, c) &= \int_0^1 [(1 - \varrho_2)(w_0 + d) + \varrho_2 c]\, \mathrm{d}\varrho_2 \\ \phi_3(c, w_1) &= \int_0^1 [(1 - \varrho_3)c + \varrho_3 w_1]\, \mathrm{d}\varrho_3 \end{aligned}$$

and for $w_0 > w_1$,

$$
\begin{aligned}
&\int_{\mathcal{U}_0^{w_0>w_1}} \int_{\mathcal{U}_1^{w_0>w_1}} \psi(w_0, w_1)\,\mathrm{d}w_1\,\mathrm{d}w_0 \\
&\quad= \int_d^{c+d} d(w_0-d)\varphi_1(w_0, w_0-d)\,\mathrm{d}w_0 \\
&\qquad+ \int_d^{c+d} (w_0-d)(c-w_0+d)\varphi_2(w_0-d, c)\,\mathrm{d}w_0 \\
&\qquad+ \int_d^{c+d} \int_0^{w_0-d} (c-w_1)\varphi_3(c, w_1)\,\mathrm{d}w_1\,\mathrm{d}w_0 \\
&\quad= \int_c^{c+d} x \int_0^{c+d-x} (x+l_2-d)\,\mathrm{d}l_2\,\mathrm{d}x + \int_d^c x \int_0^d (x+l_2-d)\,\mathrm{d}l_2\,\mathrm{d}x \qquad \text{(A.6)} \\
&\qquad+ \int_0^d x \int_{d-x}^d (x+l_2-d)\,\mathrm{d}l_2\,\mathrm{d}x + \int_0^c x \int_0^x (x-l_3)\,\mathrm{d}l_3\,\mathrm{d}x \\
&\qquad+ \int_0^c x \int_0^x \int_{x-l_4}^c 1\,\mathrm{d}w'\,\mathrm{d}l_4\,\mathrm{d}x \\
&\quad= \int_c^{c+d} x \cdot \left[\frac{c^2}{2} - \frac{(x-d)^2}{2}\right]\mathrm{d}x + \int_d^c x \cdot \left(dx - \frac{d^2}{2}\right)\mathrm{d}x \\
&\qquad+ \int_0^d x \cdot \frac{x^2}{2}\,\mathrm{d}x + \int_0^c x \cdot cx\,\mathrm{d}x
\end{aligned}
$$

where

$$
\begin{aligned}
\varphi_1(w_0, w_0-d) &= \int_0^1 [(1-\varrho_1)w_0 + \varrho_1(w_0-d)]\,\mathrm{d}\varrho_1 \\
\varphi_2(w_0-d, c) &= \int_0^1 [(1-\varrho_2)(w_0-d) + \varrho_2 c]\,\mathrm{d}\varrho_2 \\
\varphi_3(c, w_1) &= \phi_3(c, w_1)
\end{aligned}
$$

Combining Equations (A.5)(A.6), proves the lemma. □

Finally, by joining Equations (A.1)(A.4), we can obtain the piecewise $f_{X(t)}(x)$ of Equation (3.5) with sub-domains $x \in [0, c)$ and $x \in [c, 1]$. A similar procedure can be followed to derive the pdf for $c \in [d, 2d)$ and $c \in (1-2d, 1-d]$ respectively. It turns out the location $c-d$ ($c+d$ resp.) relative to d ($1-d$ resp.) has no effect on the form of Equation (3.5) and the according sub-domains, as long as $c \in [d, 1-d]$ and $d \leq \frac{1}{2}$.

Appendix B

Proof of Theorem 3.4.2.1

The complete proof of Theorem 3.4.2.1 consists of six lemmas accounting for the distributions under different settings of d and c (Table 3.5). For the sake of brevity, and because of the symmetry in all sub-cases, we provide complete proofs for two lemmas (Lemma 3 and 6); the rest can be verified in a likewise fashion.

Lemma 3. *Assuming $d \leq \frac{1}{2}$ and $c \in [d, 1-d]$, the stationary pdf of location, $f_{X(t),U(t)=1}(x)$, is*

$$\alpha f_{X(t),U(t)=1}(x) = \begin{cases} \frac{x^2}{2}, & \text{if } x \in [0, d) \\ \frac{x^2}{2} + (1-x)(x-d), & \text{if } x \in [d, c) \\ \frac{(1-x)^2}{2} + (1-d-x)x, & \text{if } x \in [c, 1-d] \\ \frac{(1-x)^2}{2}, & \text{if } x \in (1-d, 1] \end{cases} \tag{B.1}$$

Proof. If $d \leq \frac{1}{2}$ and $c \in [d, 1-d]$, then Equation (3.8) (normalized by α^{-1}) can be expanded as

$$\begin{aligned} &\frac{\lambda}{\alpha^{-1}} \mathbb{E}_{\mathrm{I}}^{0} \left(\int_{T'}^{T_1} X(\tau)\, \mathrm{d}\tau + \int_{T'}^{T_c} X(\tau)\, \mathrm{d}\tau \right) \\ &\quad = \int_{d}^{c} x \int_{0}^{x-d} \int_{0}^{1-x} 1\, \mathrm{d}l_1\, \mathrm{d}l_0'\, \mathrm{d}x + \int_{c}^{1-d} x \int_{0}^{1-d-x} \int_{0}^{x} 1\, \mathrm{d}l_1\, \mathrm{d}l_0'\, \mathrm{d}x \\ &\quad = \int_{d}^{c} x \cdot (1-x)(x-d)\, \mathrm{d}x + \int_{c}^{1-d} x \cdot (1-d-x)x\, \mathrm{d}x \end{aligned} \tag{B.2}$$

while for Equation (3.9) there is

$$\begin{aligned}
&\frac{\lambda}{\alpha^{-1}}\mathbb{E}^0_{\mathrm{II}}\left(\int_{T'}^{T_c} X(\tau)\,\mathrm{d}\tau\right) \\
&\quad=\int_c^1 x\int_0^{1-x}(1-x-l_3)\,\mathrm{d}l_3\,\mathrm{d}x+\int_0^c x\int_0^x(x-l_3)\,\mathrm{d}l_3\,\mathrm{d}x \\
&\quad=\int_c^1 x\cdot\frac{(1-x)^2}{2}\,\mathrm{d}x+\int_0^c x\cdot\frac{x^2}{2}\,\mathrm{d}x
\end{aligned} \tag{B.3}$$

Combining Equations (B.2)(B.3) we derive Equation (B.1). □

Lemma 4. *Assuming $d \le \frac{1}{2}$ and $c \in [0, d)$, the stationary pdf of location, $f_{X(t),U(t)=1}(x)$, is*

$$\alpha f_{X(t),U(t)=1}(x)=\begin{cases}\frac{x^2}{2}, & \text{if } x\in[0,c)\\ \frac{(1-d)^2}{2}+(1-d-x)x, & \text{if } x\in[c,d)\\ \frac{(1-x)^2}{2}+(1-d-x)x, & \text{if } x\in[d,1-d]\\ \frac{(1-x)^2}{2}, & \text{if } x\in(1-d,1]\end{cases} \tag{B.4}$$

Lemma 5. *Assuming $d \le \frac{1}{2}$ and $c \in (1-d, 1]$, the stationary pdf of location, $f_{X(t),U(t)=1}(x)$, is*

$$\alpha f_{X(t),U(t)=1}(x)=\begin{cases}\frac{x^2}{2}, & \text{if } x\in[0,d)\\ \frac{x^2}{2}+(1-x)(x-d), & \text{if } x\in[d,1-d]\\ \frac{(1-d)^2}{2}+(1-x)(x-d), & \text{if } x\in(1-d,c]\\ \frac{(1-x)^2}{2}, & \text{if } x\in(c,1]\end{cases} \tag{B.5}$$

Lemma 6. *Assuming $d > \frac{1}{2}$ and $c \in (1-d, d)$, the stationary pdf of location, $f_{X(t),U(t)=1}(x)$, is*

$$\alpha f_{X(t),U(t)=1}(x)=\begin{cases}\frac{x^2}{2}, & \text{if } x\in[0,1-d]\\ \frac{(1-d)^2}{2}, & \text{if } x\in(1-d,d)\\ \frac{(1-x)^2}{2}, & \text{if } x\in[d,1]\end{cases} \tag{B.6}$$

Proof. In this case, since $\mathcal{V}_0 = \mathcal{V}_1 = \mathcal{V}_1' = \emptyset$ when $d > \frac{1}{2}$ and $c \in (1-d, d)$, we

only need to expand Equation (3.9) as

$$\begin{aligned}
&\frac{\lambda}{\alpha^{-1}}\mathbb{E}^0_{\mathrm{II}}\left(\int_{T'}^{T_c} X(\tau)\,\mathrm{d}\tau\right) \\
&\quad= \int_d^1 x\int_0^{1-x}(1-x-l_3)\,\mathrm{d}l_3\,\mathrm{d}x + \int_c^d x\int_{d-x}^{1-x}(1-x-l_3)\,\mathrm{d}l_3\,\mathrm{d}x \\
&\qquad+ \int_0^{1-d} x\int_0^{x}(x-l_3)\,\mathrm{d}l_3\,\mathrm{d}x + \int_{1-d}^{c} x\int_{x-(1-d)}^{x}(x-l_3)\,\mathrm{d}l_3\,\mathrm{d}x \\
&\quad= \int_0^{1-d} x\cdot\frac{x^2}{2}\,\mathrm{d}x + \int_d^1 x\cdot\frac{(1-x)^2}{2}\,\mathrm{d}x + \int_{1-d}^{d} x\cdot\frac{(1-d)^2}{2}\,\mathrm{d}x
\end{aligned} \tag{B.7}$$

□

Lemma 7. *Assuming $d > \frac{1}{2}$ and $c \in [0, 1-d]$, the stationary pdf of location, $f_{X(t),U(t)=1}(x)$, is*

$$\alpha f_{X(t),U(t)=1}(x) = \begin{cases} \frac{x^2}{2}, & \text{if } x \in [0,c) \\ \frac{(1-d)^2}{2} + (1-d-x)x, & \text{if } x \in [c,1-d] \\ \frac{(1-d)^2}{2}, & \text{if } x \in (1-d,d) \\ \frac{(1-x)^2}{2}, & \text{if } x \in [d,1] \end{cases} \tag{B.8}$$

Lemma 8. *Assuming $d > \frac{1}{2}$ and $c \in [d, 1]$, the stationary pdf of location, $f_{X(t),U(t)=1}(x)$, is*

$$\alpha f_{X(t),U(t)=1}(x) = \begin{cases} \frac{x^2}{2}, & \text{if } x \in [0,1-d] \\ \frac{(1-d)^2}{2}, & \text{if } x \in (1-d,d) \\ \frac{(1-d)^2}{2} + (1-x)(x-d), & \text{if } x \in [d,c] \\ \frac{(1-x)^2}{2}, & \text{if } x \in (c,1] \end{cases} \tag{B.9}$$

Appendix C

Charging-Aware Mobility on a Circle

To demonstrate the impact of removing the boundary effect on the mobile distribution, we simulate the charging-aware mobility on a circle (1-torus), as illustrated in Figure C.1 (where the two ends of the line segment $\mathcal{S} = [0, 1]$ are conjoined). The mobile still follows the rules of movement as modeled in Section 3.2 (Figure 3.1), except that it may now cross the boundaries so as to travel along a *shorter path* to any target location (be it the destination or the charger).

Figure C.2 shows the simulation results of charging-aware mobiles (depleted or not) on the circle, with the charger location c at 0.1, 0.3, 0.5, and 0.7, and energy budget d of 0.2, 0.4, and 0.6, respectively. It can be seen that the charging-aware mobility would degenerate to what is expected of RWP and yield a uniform mobile distribution over the circle when $d = 0.6$ (≥ 0.5). This is because of the absence of boundaries that enables access to any destination within a distance of 0.5. More importantly, in contrast to the results of Figure 3.2, the discontinuities of distributions around the charger have disappeared for any given values of c and d. Additionally, the hotspot around the charger persists and is symmetric, regardless of where the charger is placed, i.e., even if $c = 0.1 < d = 0.2$. These notable differences compared to the model with boundaries confirm the important impact of the boundaries.

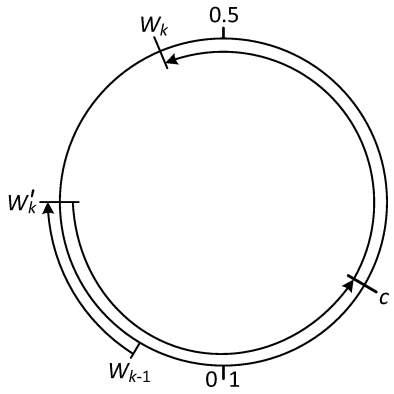

Figure C.1: A trajectory of the charging-aware mobility on a circle. The mobile can cross the 1/0 boundary for a shorter detour to the charger at c.

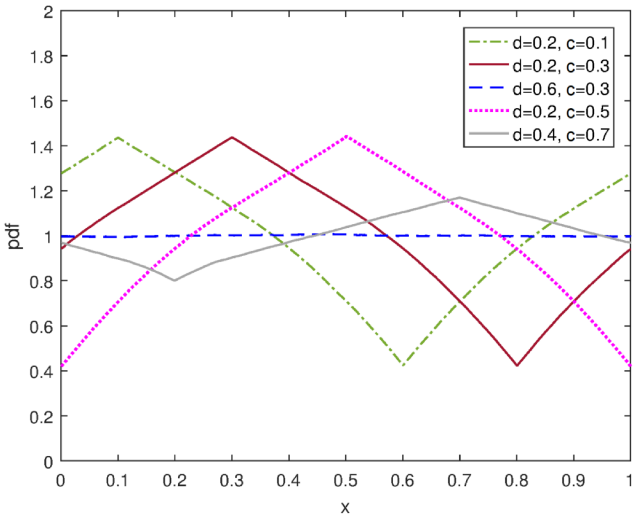

Figure C.2: Frequency histogram (for 10^3 subintervals) of simulated charging-aware mobility on the circle, for $c = 0.1, 0.3, 0.5, 0.7$, and $d = 0.2, 0.4, 0.6$.